1993

Interstitially stabilized phases in the zirconium-nickel system

Richard Alan Mackay
Iowa State University

Order Number 9334997

Interstitially stabilized phases in the zirconium-nickel system

Mackay, Richard Alan, Ph.D.

Iowa State University, 1993

U·M·I
300 N. Zeeb Rd.
Ann Arbor, MI 48106

Interstitially stabilized phases in the zirconium - nickel system

by

Richard Alan Mackay

A Dissertation Submitted to the

Graduate Faculty in Partial Fulfillment of the

Requirements for the Degree of

DOCTOR OF PHILOSOPHY

Department: Chemistry
Major: Inorganic Chemistry

Approved:

Signature was redacted for privacy.

In Charge of Major Work

Signature was redacted for privacy.

For the Major Department

Signature was redacted for privacy.

For the Graduate College

Iowa State University
Ames, Iowa

1993

TABLE OF CONTENTS

1. INTRODUCTION

The investigation of metal rich sulfides of the early transition metals has led to the discovery of several new compounds and has necessitated new explanations in the theory of bonding in extended solids. To illustrate this point, a report published in 1964 stated the compound Ti_2S would be thermodynamically unstable with respect to disproportionation to the elements or to TiS and Ti, and hence would not form [1]. The thermodynamic calculations were based on the Kapustinskii equation [3] for an ionic model of bonding. Shortly afterwards, the crystal structure of Ti_2S was solved [2]. The structure of Ti_2S is very different from an ionic compound where Coulombic interactions between the metal and nonmetal provide the significant stabilizing force. The high coordination of titanium and the short titanium-titanium distances are evidence of the strong metal-metal interactions involved in this metal-rich sulfide and these interactions are not accounted for by considering only Coulombic interactions. The ability to calculate properties and predict the chemistry in this class of metal rich compounds depends on the ability to determine the effect of the presence of extensive metal-metal bonding, a factor not included in the ionic model . While the ability to predict new compounds and structures still lies in the future, the discovery of so many new materials with extensive regions of metal-metal bonding has motivated chemists to explain the electronic and structural features in these compounds. Before proceeding further, the term metal-rich should be defined more clearly. For any compound M_xX_y, where M is a metal atom and X is a nonmetal atom, one can quickly determine if $x > y$, however, this criterion tells nothing about the extent of metal-metal bonding or coordination environment of the metal. As it is the strength of this metal-metal bonding that is essential for the formation of these phases, a better criterion is the condition $\Sigma\, n(M\text{-}M) / \Sigma\, n(M\text{-}X) > 1$, where n is the Pauling bond order [4], as determined by the equation $d(n) = d(1) - 0.6 \log n$. Because of the empirical nature of this equation the individual bond orders calculated mean little by themselves, but the bond orders scale as indications of bond

strengths, and the comparison of the sum of all the metal-metal interactions with the sum of all the metal-nonmetal interactions does yield a meaningful definition of metal-rich compounds. With this in mind, the new oxygen stabilized phases found in this research are viewed as oxidized intermetallics rather than reduced metal oxides.

A number of metal-rich compounds have been discovered in this lab alone. Considering just the binary sulfides of the Group 4 and Group 5 elements, they include Ti_2S [2], Ti_8S_3 [5], Zr_2S [6], $Zr_{21}S_8$ [6], Zr_9S_2 [7], Hf_2S [8], $Nb_{21}S_8$ [9], $Nb_{14}S_5$ [10], Ta_2S [11], α-Ta_6S [12], β-Ta_6S [13]. Other groups in other laboratories have contributed to this work, synthesizing additional new compounds, such as a low temperature binary phase, Ta_3S_2 [14], and carrying out theoretical band energy calculations [15]. The results are immensely interesting and surprising. For example, for a given stoichiometry, M_2S, the phases Ti_2S, Zr_2S, Hf_2S, Ta_2S exist. Within Group 4, the titanium and zirconium phases have the same structure, roughly based on bcc units in the metal framework. Dihafnium sulfide has a unique hexagonal structure, with close packed layers in the order ABACBC for Hf-S-Hf-Hf-S-Hf layers. In Group 5, the structure of the tantalum phase is different from either of those in Group 4, being built of chains of interpenetrating icosahedra. No phases of this stoichiometry form at all for vanadium or niobium. All of the phases are characterized by high sulfur coordination, often with capped trigonal prismatic coordination, and with sulfur occuring as a substituent on metal sites in bcc fragments. The tantalum sulfides have distinctive icosahedral chains. The zirconium and niobium phases are built up of bcc units. The compounds formed by the elements grouped together within a column of the Periodic Table are distinguished as much by their differences as by their similarities, if not more so. Naturally, it is these differences that are of interest to the chemist.

Exploiting the differences between the tantalum sulfides and the niobium sulfides, X.Yao discovered several new ternary metal rich compounds in the Ta/Nb/S system [16-19]. These

compounds form only in the ternary system and form structures stabilized entropically by a mixing of tantalum and niobium on the metal sites. The results of band calculations on two of these phases indicate also the importance of the relative strength of the metal-metal and the metal-nonmetal bonds in determining the ordering of niobium and tantalum on the mixed metal sites [19]. This result has been generalized to include several mixed-metal phosphides and sulfides [20]. Similarly, an investigation of mixed-metal sulfides of mixed Group 4 and Group 5 metals has yielded exciting results. A new structure $Hf_{10}Ta_3S_3$ is related to the gamma brass structure, with sulfur filling large channels. Other phases, such as $Zr_9Ta_4S_{4-x}$, are new examples of kappa phases, with metal frameworks made up of early transition metals [21]. In a like manner, there are investigations on the mixing of sulfur and selenium in metal rich systems. That is to say, Ta_2S and Ta_2Se have different structures, so the ternary Ta/S/Se system is not necessarily expected to contain large solid solubility regions, and the ternary system may include interesting new phases [22].

The formation of these metal-rich compounds has always involved the early transition metals. The specific examples cited so far have been from Groups 4 and 5. Binary metal-rich compounds are not known to form for the later transition metals [23]. The ability of the early transition metals to fill vacant d-orbitals in forming metal-nonmetal bonds through interactions with the nonmetal, and maintain significant metal-metal bonding seems a necessary condition for the formation of these compounds. As the late transition metals have few vacant orbitals they do not meet this condition and binary metal rich sulfides of late transition metals do not form.

The question arises of what might happen in ternary compounds with mixed early transition metal-late transition metal frameworks. Although initially begun as an effort to place iron group metals in the sulfur - lined channels of the Ta_2S structure, the discovery of $M_2Ta_9S_6$ (where M = Fe, Co, Ni) suggested new possibilities in structures and properties of metal rich compounds [24,25]. Significantly, the structure contains only M-Ta, Ta-Ta, and Ta-S interactions, but no M-S

interactions. The structure consists of a hexagonal metal network, with large channels lined by sulfur atoms, a feature similar to Ta_2S. A theoretical band structure calculation suggests that filling the sulfur-lined channels of $M_2Ta_9S_6$ with metal atoms might be energetically favorable [26]. This suggestion neglects the inference that these channels are not void regions at all; they contain nonbonding, lone pair orbitals of sulfur. The sulfur atoms are separated by van der Waals' contacts within the channels. Presumably that is why the addition of the metal M atoms to Ta_2S caused a rearrangement of the structure, rather than a filling of the channels. Additional new ternary phases include $Nb_9Ni_{2-x}S_{3+x}$[27] and $M_2Ta_{11}Se_8$ (where M = Fe, Co, Ni) [28]. These results in the ternary systems of mixed early and late transition metals again confirm the differences that exist in chemical behaviour between niobium and tantalum, as was found in the binary sulfides.

The research project described in this dissertation began as an investigation of the ternary system of mixed early-late transition metal compounds involving zirconium rather than niobium or tantalum as the early transition metal. Based on the known binary phases of metal-rich sulfides, and the observed differences between the Group 4 and Group 5 compounds, as well as the novel features in the ternary phases, there was no way of predicting what phases might form, but it was highly probable new phases would form.

This research has in fact led to the discovery of several new phases. The results, however, have taken a somewhat different path than the work previously described. Several new phases have been discovered, but rather than new sulfides, these phases are all new oxides. The presence of oxygen, adventitious or not, is a well documented problem in the synthesis of solid state compounds. Modern instrumentation has increased the solid-state scientists' capability of detecting the presence of small impurity atoms in samples. For example, the intensity of X-ray diffraction depends on the amount of electron density within the unit cell of the crystal, and the geometrical distribution of the electron density. Light elements such as oxygen have less electron density than transition elements

and are less easily observed by single crystal X-ray diffraction techniques. The increased intensity in X-ray beams available with a rotating anode as the X-ray source enables sufficient collection of even the weak data points to satisfactorily refine the light atom positions in the structure. This has been an important factor in the success of this research. Neutron diffraction, although not a common procedure, is now a standard procedure, and is in a number of cases inherently better for locating light atoms since it does not depend on electron density. In addition, elemental analysis of bulk samples, such as by Energy Dispersive X-ray Spectroscopy or EDS, can help identify the presence of impurity atoms.

Techniques have also been improved so as to eliminate, or reduce, the likelihood of oxygen contamination in solid state reactions. Whether the oxygen comes from surface oxides on the starting material, or from residual gaseous oxygen in the reaction chamber, or from reaction with the container, the end result is the same - an oxide phase forms. Each source of oxygen must be eliminated to form oxygen free samples. The presence of surface oxides can be reduced by using foils, with less surface than powders, which are etched or cleaned before using. This use has the disadvantage of providing less surface area for reaction with the desired reactants. This is of no consequence in arc-melting, but is important for diffusion-limited reactions. Alternately, bulk metals can be converted to the hydride, and subsequently dehydrided. Sample containers can also be a source of oxygen. Samples heated in fused silica ampoules, SiO_2, are susceptible to reaction directly with the container, which contains oxygen, as well as with oxygen in the form of water, absorbed within the walls of the glass, which degasses at temperatures above 1000°C. Of course, if the sample melts it may react with the container whether the container is silica, alumina, zirconia or any other refractory material. A common technique now in use is to carry out reactions in inert metal containers. These containers can be sealed under an inert gas, and subsequently sealed in an evacuated silica tube. Another technique, used exclusively in this research, is the use of tungsten

crucibles and heating of the samples under a dynamic vacuum in an induction furnace. The Knudsen cell design of the tungsten crucibles actually creates a condition within the cell that is more reducing than the residual atmosphere that can be achieved by pumping [30]. Tungsten oxides are volatile and pumped out. As noted by previous workers in the zirconium sulfide system, reaction with the crucible can result in the formation of W_2Zr [29].

The effectiveness of these techniques for the careful exclusion of oxygen is evident in the number of new compounds which have been discovered, and which would not form in the presence of oxygen. The early transition metals have a high affinity towards oxygen, and the formation of oxides is often thermodynamically favorable to the formation of oxygen - free compounds. Thus, although the metal - rich sulfides are often quite stable with respect to oxidation under ambient conditions, they do not form in the presence of oxygen. The exclusion of oxygen has been so effective it has perhaps led chemists to believe the interesting phases do not contain oxygen. The results of this research certainly show the interesting aspects of oxygen - stabilized phases, that is, phases which form only in the presence of small amounts of oxygen. Subtleties in the structural chemistry of these oxygen - stabilized phases are more clearly understood with the single crystal X-ray diffraction studies carried out and the improved ability to detect the light elements by X-ray crystallography.

At first glance, there is not an obvious connection between the sulfides described earlier, and the oxides studied in this research. Indeed, the differences between the sulfides and the oxides in the metal rich compounds are readily apparent. First, sulfur is larger than oxygen. That is to say, sulfur occupies larger crystallographic sites, and can be more highly coordinated. Second, oxygen is more electronegative than sulfur; the energy levels of oxygen 2p orbitals lie at lower energies than do those of sulfur 3p. The bonding overlaps will be different in oxides than in sulfides, and the nature of the bonding will be different. The sulfur in binary metal - rich sulfides has been described

as having directional, delocalized bonds [31]. Oxygen orbital overlaps are more localized. The results of these differences are twofold. First, because of the size difference, oxygen can often occupy small vacant so-called interstitial sites within a metal framework, without significant structural distortion of the framework. Hence, many oxygen stabilized compounds are called after a parent structure type, i.e. Zr_3NiO has the filled Re_3B type structure, and Zr_4Ni_2O has the filled Ti_2Ni type structure. Sulfur, on the other hand, is larger, and occupies larger interstitial sites, or can occupy smaller vacant sites only by making the site larger, with a corresponding expansion in the metal framework, as observed for the new sulfur-containing kappa phases and stuffed gamma brasses [21]. The second effect is seen in the ability of sulfur to, in essence, become part of the metal framework, i.e. substitute on a metal atom position in the bcc units in the niobium sulfides, or the layered compounds of mixed niobium/tantalum sulfides, with an accompanying distortion in the framework. The metallic character of sulfur becomes apparent in these phases - that is, the ability of the sulfur orbitals to be involved in delocalized bonding in the conduction band. The corollary to this, then, is the substitution of a metal atom on a sulfur site, as in $Nb_9Ni_{2-x}S_{3+x}$ [27], and in the kappa phase $Zr_9W_4(S,Ni)O_3$ [80]. One might object to describing the sulfur in these metal-rich sulfides as interstitial atoms. The metal-rich sulfides are novel structures, and the metal frameworks within these structures are also novel. To avoid overextending the use of the term "interstitial", rather than characterizing the sulfur as interstitial sulfur, the mixed tantalum/niobium sulfides and mixed early-late transition metal sulfides are here referred to as sulfur-stabilized intermetallics. The presence of small amounts of sulfur (up to 6 metal atoms for each sulfur atom) enables the formation of new phases which do not exist in the binary intermetallic phases. In a similar way, by calling the new phases oxygen stabilized, it is recognized that the phases do not form in the binary zirconium-nickel intermetallic system. By calling them interstitially stabilized one notes the oxygen atoms occupy small sites which are known to be vacant in some intermetallic compounds

with the same local structural arrangement. Whether considering sulfides or oxides, the structural chemistry is dominated by the fact that the presence of either of these nonmetal atoms effects the metal-metal bonding in intermetallics. The resulting balance of metal-metal and metal-nonmetal interactions results in new phases, and gives clues about the nature of the bonding.

Specifically, to note the change in the bonding that results from interstitial oxygen, consider the binary zirconium - nickel system. There are eight known phases in this system: Zr_2Ni, ZrNi, Zr_9Ni_{11}, Zr_7Ni_{10}, Zr_8Ni_{21}, $ZrNi_3$, Zr_2Ni_7, $ZrNi_5$ [32]. The phase diagram is complex, and the variation in structure and stoichiometry is striking. Classical chemical concepts, such as oxidation numbers, are not useful in intermetallic systems. Oxidation numbers, such as Zr^{+1} and Ni^{-1} for ZrNi, that would have any meaning throughout the series of phases, or even for that particular phase cannot be simply assigned. Intermetallic compounds characteristically fill space efficiently, and the atoms have correspondingly high coordination numbers. The bonding cannot be interpreted as containing two-centered - two-electron bonds. Rather, the bonding within these compounds involves extensive delocalization of electrons.

Today, band calculations can give quantitative analysis of bonding in many known solids. Earlier interpretations of intermetallic compounds were more qualitative. One prevalent concept was the radius ratio rule. This was based on a model of packing of hard spheres. Crystal structures of intermetallics could be generalized, as Laves did, as arrangements of spheres which pack to exhibit high symmetry, fill space most efficiently, and have the greatest number of connections between the atoms [33]. In a general sense this was useful because certain structure types appear over and over in intermetallic systems. There are two weaknesses of this model, however. The idea of hard sphere packing gives no chemical understanding to the structures. Atoms are not hard spheres. A completely nondirectional nature of bonding results. It also led to a proliferation of tables of radii to be used which would satisfy the radius ratio rules for the new structures constantly being

discovered. Tables for radii take into account all possible factors influencing interatomic distances, including atomic charge and coordination number [34-38]. One result of the use of this model was the rationalization of the reported nonoccurrence of the Ti_2Ni type structure in the Zr/Ni/O system [39], a phase this study shows does indeed exist. A recent study has successfully classified the structures that form for all binary, ternary and quaternary compounds [110]. This method also depends on the size differences of the constituent atoms, but uses this parameter along with the electronegativity differences of the atoms, and the sum of the valence electrons. The consideration of these three parameters together, rather than individually, increases the success and usefulness of the classification.

While the radius-ratio rules and structural classification are based on purely structural considerations, and no chemical considerations, the concept of Lewis acid - base behavior as it relates to the interactions among the transition metals does not explain structures of intermetallics. Late transition metals have paired electrons in d orbitals unavailable for bonding. Early transition metals have empty d orbitals. The sharing of electrons between late transition metals, acting as Lewis bases, and early transition metals, acting as Lewis acids, increases the total number of electrons available for bonding, and increases bond strength. This concept explains why compounds such as $HfPt_3$ have such favorable enthalpies of formation [40-41]. In the binary zirconium/nickel system one would expect strong zirconium - nickel bonds according to the their Lewis acid - base properties. From the crystal structures of the phases that form in this system, one can indeed see the high coordination of zirconium by nickel, and of nickel by zirconium, as well as zirconium - zirconium and nickel - nickel contacts.

The Brewer-Engel theory relies heavily on the concept of Lewis acid-base interactions and gives a structural component to the concept. The qualitative aspects have been highly successful in predicting the structure and properties of new compounds [42-43]. The structure, or long range

electronic ordering is determined by the number of s and p electrons. The electrons in the d orbitals are involved in short range interactions. To count the electrons in the s and p orbitals correctly one must consider the electronic configuration of the atom as it is in the compound, not in the electronic ground state of the gaseous atom. For those phases that form, according to the theory, the energy necessary for promotion of electrons from the ground state is more than offset by the bonding energy gained.

One deficiency of this method is the treatment of interstitial elements. They are considered in this model, if at all, only as electron acceptors or electron donors. They are not considered to have an influence on bonding within the network. They are hard spheres which fill space. The effect of adding interstitial atoms is only to possibly change the number of electrons in the s and p orbitals, which may then favor a structure different than that adopted by the interstitial-free compound. A more chemically sound explanation in terms of bonding comes from band theory. In the rigid band approach the addition of oxygen to an intermetallic system provides energetically low-lying core levels, which are filled by electrons from the conduction band, thus the number of electrons in the conduction band changes, and a corresponding change in structure may be energetically favorable. Furthermore, the addition of oxygen, and the donation of electrons from the conduction band implies the formation of metal-oxygen bonds, and as these bonds form, there is a simultaneous change in the metal-metal bonding within the metal framework, which may favor formation of a new phase.

The idea of electron counts is an important one. Hume-Rothery suggested certain electron concentrations as being important for formation of certain phases. Several systems have been studied in which structural changes corresponding to modification of electron counts by substitution of more or less electron rich elements, or by addition of interstitials, have been observed. This conceptual understanding of electron count and the role of interstitials in intermetallics is being

supported by recent band energy calculations [44,45].

Typically, when an interstitial element reacts with a binary early-late transition metal compound to form a ternary compound, the compound crystallizes in a common structure type. In fact, only a limited number of structure types are known for interstitially - stabilized phases of mixed early and late transition metals [46]. These phases are: 1) the filled Ti_2Ni type, 2) the kappa phase type, 3) the filled Re_3B type, 4) the filled Mn_5Si_3 type (known for Nb-M-O where M = Ir, Pt), and 5) the cubic Laves phase observed in the Zr-Ni-O system [47,48]. The first three of these types are found in the zirconium - nickel system with the addition of interstitial atoms, and make up the body of this research. In order of appearance in this dissertation, a single crystal study of the previously reported Zr_3NiO phase, of the filled Re_3B type structure, is presented first. Following this is a discussion of a series of compounds of the filled Ti_2Ni type, involving the early transition metals zirconium and niobium, and mixed zirconium/titanium and niobium/tantalum. A discussion of the results of band calculations for this phase is included. New zirconium kappa phases have been found and are reported next. Finally, a new structure type has been found for an interstitially stabilized phase made up of a ternary metal framework of zirconium - titanium - nickel. The ternary metal system, Zr-Ti-Ni, contains phases which do not occur in either of the binary systems Zr-Ni or Ti-Ni (i.e. the hexagonal Laves phase ZrTiNi [9,10], and the $BaPb_3$ type structure $ZrTi_2Ni_9$ [11,12]). It is natural to expect that interstitials in this ternary system may stabilize new compounds, with respect to the ternary intermetallics and interstitially stabilized binary compounds.

2. EXPERIMENTAL TECHNIQUES

Synthesis

This section contains information on experimental techniques common to all the experiments performed in this work. Specific details will be included in the individual sections. The experiments were designed to take advantage of the equipment available in the lab. Specifically, the synthetic procedure of metal rich compounds generally consists of arc melting of the initial reactants, followed by annealing the samples.

Arc melting was performed with a CENTORR Model 5SA Single Arc Furnace, powered by a Hanovia Model 28151 Compact Arc Lamp Power System. Samples of between 0.5 and 1.5 grams were placed on a water cooled copper hearth, and melted under argon by an arc formed between the sample and a thoriated non-consumable tungsten electrode. Depending on the sample, current output was between 50-100 Amps D.C. There has been no indication of contamination by copper in arc melted samples in any of the previous work done in this lab. Likewise, there has been no evidence of copper contamination in any of the samples in this work, either by the formation of copper containing phases, or as detected by elemental analysis. A more significant source of contamination is atmospheric oxygen. The chamber is pumped by a mechanical pump, and backfilled with argon. This pump/purge cycle is repeated 3-5 times, and the chamber is left with a positive pressure of argon (~ 3 atm). A safety valve releases pressure at 6 atm. To remove residual oxygen in the chamber prior to melting the sample, a zirconium metal piece is melted first for 30-60 seconds as an oxygen getter. The calculated collision frequency is sufficiently high that the high reactivity of zirconium towards oxygen is expected to be effective in reducing the amount of oxygen present which may contaminate the sample. This has been true for work done on sulfides, and holds true for this work with oxides. After the initial discovery of the oxides as minor phases, it was desirable

to find a way of controlling the amount of oxygen present in the sample and thus synthesize bulk samples of the desired phases. This was accomplished by preparing samples, by arc melting, using a stoichiometric amount of a metal oxide. Other sources of oxygen were reduced to a minimum. Surface oxides on the metals were reduced by using metal foils rather than powders. The surface oxides were removed by cleaning with acid solutions immediately prior to use. This was most important for compounds containing titanium and zirconium, both of which are very reactive towards oxygen. The reactivity of these metals to oxygen indicates the high stability of the oxides with respect to the elements. The fact that these metal oxides can be used as reactants in these reactions indicates the high stability of the products with respect to the oxides and the competing intermetallic phases. A problem can arise in the reaction of oxides in that it is difficult to arc melt insulating materials. They often splatter, or fly apart when the arc comes in contact with them. A generally successful technique was to place the oxide powder between layers of metal foils. The arc was brought in contact with the edge of the foil and slowly moved toward the center. In this way the small amount of oxide present dissolved and reacted with the molten metal and the sample maintained its conductive, metallic properties. Typically a sample was arc melted three times, for approximately one minute each time, the sample being turned over each time to increase homogeneity.

Despite this procedure, the arc melted samples are generally not homogeneous due to the large difference in cooling rate between the part of the sample in contact with the water cooled copper hearth and the top of the sample. All of the samples prepared were between 0.5 and 1.5 grams, and within this range sample size had no apparent affect on homogeneity. The arc melting procedure was often very clean, with little mass loss due to vaporization. The most volatile species was nickel, and if samples were arc melted for longer times the loss of nickel was detected by mass loss as well as by formation of ZrO_2 from the excess zirconium.

The samples show no evidence of decomposition or reactivity with air or moisture, and all subsequent handling was done in air. The homogeneity of the samples could be improved by annealing samples after arc melting. Two types of furnaces were available for annealing. The Marshall/Thermcraft and Astro furnaces are tube furnaces with capabilities of reaching 1200°C. Samples were placed in fused silica tubes, 10 mm I.D., 12 mm O.D., and evacuated to 10^{-5}-10^{-6} torr using an oil diffusion pump backed by a mechanical rough pump. Sometimes the samples were annealed as a button resulting from the arc melt. However, greater homogeneity resulted from first crushing the arc-melted button to a powder in a diamond mortar and cold pressing the powder to form a pellet for annealing. When samples were placed in the silica tube, the tubes were heated while they were being evacuated to try to eliminate as much moisture from the walls of the silica as possible, and finally sealed under vacuum. Sealed tubes were typically 120-150 mm in length. To ensure the vacuum was not lost in the sealing step each tube was gently heated. If the walls slowly collapsed, this was taken as evidence that the tube was still under vacuum. A single sample was placed in each tube, but several tubes could be placed in the furnace at once. Samples were annealed at varying temperatures, as low as 800°C, but generally not above 1000°C where reaction with oxygen from moisture degassed from the walls of the silica container is more likely.

Annealing at higher temperatures was performed in a Lepel High Frequency Induction Heating Unit. This unit contained a Lepel High Frequency Generator T-20 with Thyratron Regulator T-660. A quarter inch copper tube carried the high frequency field, and surrounded the water cooled quartz jacket which in turn surrounded the sample. The sample chamber was under a dynamic vacuum maintained by an oil diffusion pump backed by a mechanical pump. The sample was not heated until the pressure within the chamber, measured by an ion gauge, was 10^{-6} torr. The pressure within the chamber could become as low as 10^{-8} torr. The samples were placed in tungsten crucibles. Tungsten is a suitable container for annealing several intermetallics and oxides, as long

as the sample does not melt. Samples containing zirconium that melted in the crucible often form W_2Zr. Surprisingly, the new kappa phase $Zr_9W_4(S,Ni)O_3$ was formed because of reaction between the sample and container. Melting the sample is to be avoided exactly for this reason. It is much easier to include tungsten in the starting material than to use the container as a reactant. The presence of a low melting phase, melting below 1000°C, presumably the cubic Laves phase in the Zr-Ni-O system [47,48], often resulted in reaction of the sample with the container. To avoid melting samples some were heated in the crucible without a lid. Thus, it could be visually determined whether or not the sample had melted during the annealing procedure. However, this procedure is not without consequence. The temperature of the sample in the induction furnace is determined by optical pyrometry. Each tungsten crucible is made with a hole in the bottom from which nearly black body radiation is emitted. The sample temperature within a closed crucible is higher than the sample temperature within an open crucible, without a lid, when the temperatures read by the pyrometer in the two cases are equal. For this reason, temperatures as measured were used for comparison between samples, and are not to be taken as actual temperatures. No attempt was made to calibrate these measurements. No corrections are applied to pyrometer readings for loss of intensity from passing through the quartz windows or reflectance from the mirror. Actual temperatures within a closed crucible are believed to be at least 50°C higher than the temperature read at this temperature range.

Except for the foils, all chemicals were used as received. Foils were placed in acid cleaning solutions just prior to use in order to remove surface oxides. They were immediately rinsed with distilled water and subsequently with alcohol (methanol or ethanol) and air dried. The acid cleaning solution for zirconium was made from the volume percents of the following - 10% HF, 45% HNO_3, 45% H_2O. The titanium cleaning solution was made from 60% by volume of H_2O_2 (30%), 10% HF, 30% H_2O; for niobium the solution contained 50 volume % HF, and 50% HNO_3. Nickel was

Table 2.1 Chemicals used in synthesis of new materials

Chemical	Source	Purity	Comments
Zr	Alfa	99.9%	0.25 mm foil
Zr	Alfa	99+%	powder
Zr	Johnson Matthey	99.9%	-20+60 mesh[a]
ZrO_2	Johnson Matthey Puratronic	99.9975%	
Ti	Ames Laboratory		foil
Ti_2O_3	Johnson Matthey	99+%	
Ni	Inco	99.99%	foil[b]
Ni	Fisher Scientific	purified	powder
NiO	Johnson Matthey Puratronic	99.998%	
Nb	Alfa	99.8%	-325 mesh
Ta	Johnson Matthey	99.98%	-60 mesh
Mo	Alfa	99.9+%	-200 mesh
W	Alfa	99.98%	-100 mesh
Cu	J.T. Baker Chemical Co.	99.98%	ribbons
Co	Alfa	99.5%	pieces
Si	Johnson Matthey	99.999%	zone refined
S	Fisher Scientific		lab grade

a This powder contained 10 atomic % Ti, according to quantitative analysis by XPS.

b Nickel received from Inco was arc-melted under argon and rolled into a foil. Elemental analysis was performed after this treatment.

cleaned in concentrated HNO_3. The materials used are listed in the following table, Table 2.1.

Characterization

Sample characterization and phase identification was routinely performed by X-ray diffraction techniques. X-ray powder diffraction was used to identify phases present in a sample. Powder patterns were recorded photographically using vacuum Guinier cameras, Enraf-Nonius, Delft Model FR552. The cameras are equipped with quartz monochromators and adjusted to select diffraction from CuKα1 radiation (λ=1.54056 Å). With the X-ray generator power set at 20 mA and 45 kV, exposure time was typically two hours for powder samples. Samples were mounted on clear adhesive tape and placed on a rotating holder to eliminate effects of preferred orientation. The films were interpreted by measurement of line positions relative to an internal silicon standard (NIST, a=5.43088 Å). These measurements were done automatically on a KEJ Instruments Line Scanner LS-20.

Single crystals were examined by oscillation and Weissenberg photographs on a Charles Supper Company Weissenberg Camera 9000ST. A nickel filter reduced CuKβ radiation. Photographic techniques are useful for determining lattice parameters and possible space groups.

A Rigaku AFC6R diffractometer, with a rotating anode, was used to collect single crystal diffraction data. This diffractometer was set up to run with MoKα radiation (λ= 0.71069 Å) at 50 kV and 140 mA. The high intensity of the X-ray beam obtained with this diffractometer made it possible to collect enough weak intensity peaks to solve the structures from very small crystals.

Qualitative elemental analysis was performed by electron spectroscopy for chemical analysis (ESCA) on a Perkin Elmer 5500 multitechnique system, and by energy dispersive spectroscopy with X-rays (EDS) on a Cambridge S-200 scanning tunneling microscope fitted with a Northern Tracor Micro Z-II X-ray detector. Quantitative analysis was done by EDS on polished samples on a JEOL

JSM-840 electron microscope with KEVEX EDX system.

Magnetic measurements and tests for superconductivity were done on a Quantum Design SQUID magnetometer.

Calculations

Many of the calculations are performed routinely and quickly on the computer. A list of the programs used is presented in Table 2.2. A brief description of the programs follows. All the calculations were done on a VAX system, except the extended Hückel band calculations, which were carried out on the Iowa State University Project Vincent system.

The first analysis of a sample is often a powder X-ray diffraction experiment. Powder patterns are very useful in identifying the phases present in a sample. The films are scanned automatically in the Line Scanner LS-20. The positions and intensities of the lines are converted to d-spacings, 2θ values, and relative intensities by the program SCANPI. The d-spacings of the observed pattern can be compared to the values corresponding to known phases, or patterns calculated for new phases, as calculated by the program PWDR. Visual comparison of calculated powder patterns and observed powder patterns is possible by plotting the calculated patterns with the PLOT program. If the phase is positively identified, the *hkl* indices can be assigned to the appropriate lines and the LATT program will do a least squares refinement of the lattice parameters based on the observed d-spacings, or 2θ values, and the assigned *hkl* values. The lattice parameters of the powdered samples obtained from this calculation are those used in the reports of structural information.

The Rigaku AFC6R X-ray single crystal diffractometer is fully automated for data collection. While several options exist in the data collection procedure, in a successful structural determination the diffractometer will search for several diffraction peaks, and index them. The cell is reduced to

a standard cell by the Delauney subroutine. The Laue symmetry is checked before intensity data are actually collected. Data collection often extends to 50-60° in 2θ. Following the data collection, the lattice parameters are refined based on the position of several high-angle reflections (although parameters from powder samples are reported). Finally, a psi scan is collected for absorption correction purposes. The data are processed and refined by full matrix least squares refinement using the accompanying TEXSAN package. The SHELXS direct methods program is used to obtain a starting model for the structure solution. The graphic generation of crystal structures is done with the ORTEP program.

Energy band calculations based on the extended Hückel method were performed on the Project Vincent workstation. The calculations performed gave total energies, Fermi energies, orbital populations and overlap populations. Results could be plotted as DOS curves and COOP curves. Starting parameters for H_{ii} values were obtained by using a charge iteration program.

Table 2.2 Computer programs used in this research

Program	Calculations performed	Reference
Charge iteration	Charge iteration	49,50
Extended Hückel	Energy band calculations	51-54
LATT	Least squares refinement of lattice parameters	55
PLOT	Plot calculated powder patterns	56
PWDR	Calculate powder patterns	57
ORTEP	Graphical display of crystal structures	58
SCANPI	Calculate d-spacings in observed powder patterns	59-61
SHELXS	Direct methods structural solution for X-ray diffraction data	62
TEXSAN	X-ray single crystal structural least squares refinement	63

3. SINGLE CRYSTAL X-RAY STUDY OF Zr_3NiO

Introduction

A good starting place for the study of interstitially stabilized phases in the zirconium-nickel system is with the only previously reported Zr/Ni/O ternary phase, Zr_3NiO. This compound crystallizes in the filled Re_3B type structure. It was first identified in a study of the zirconium-rich corner of both the Zr/Co/O and Zr/Ni/O ternary systems at 950°C [39]. The structure for this phase was not known until a single crystal solution was published for Zr_3Co [64]. Subsequently, the phases Zr_3MO_x (M = Fe, Co, Ni) were examined by powder diffraction data to determine the range and extent of oxygen occupancy, with related changes in lattice parameters [65]. The iron compound is reported to occur as a binary intermetallic, with no oxygen solubility ($x = 0$). The cobalt compound is found to exhibit a full range of oxygen occupancy ($0 \leq x \leq 1$), forming as a binary and with full filling of octahedral sites by oxygen. The nickel compound exists only as an oxide, and does not occur as a binary phase ($0.2 \leq x \leq 1.0$). The single crystal X-ray study confirms the previously reported results [66].

Experimental Details

A crystal for X-ray study was selected from a sample which had undergone a number of experimental treatments. Initially, zirconium, nickel and sulfur in the molar ratios 6:4:5 were heated in an evacuated silica tube at temperatures up to 690°C. The resulting mixture was arc melted. Additional zirconium and nickel were added to the sample to bring the final metal ratio to n(Zr):n(Ni)=3:1. The sample was repeatedly crushed, pelletized, and inductively heated to temperatures of 1050-1230°C for 12-18 hours. The sample was soaked in concentrated HCl for a week to remove a binary sulfide phase, Zr_3S_2, and subsequently heated to 1130°C for 5 days. The

crystal studied here was picked from this final sample, although the oxide phase, as identified by X-ray diffraction films of the powder, was present before the sample was placed in the acid.

Intensity data for this crystal were collected using a Rigaku AFC6R single crystal diffractometer and monochromated MoKα radiation, employing the ω-2θ scan technique up to 55°(2θ). From a total of 422 reflections (±*h*,*k*,*l*), 162 independent reflections with $F_o^2 > 3\sigma(F_o^2)$ were obtained and used for structure analysis. The observed intensities were corrected for Lorentz polarization and absorption effects with the maximum to minimum transmission factor ratio of 1 to 0.768. No significant decay was observed during the data collection. The crystal data are tabulated in Table 3.1.

Results and Discussion

The atomic coordinates and thermal parameters for Zr_3NiO are reported in Table 3.2, and Table 3.3, respectively. This phase has been shown to exist with variable oxygen content. The fractional oxygen occupancy ranges from 0.2 to 1.0, and the variation of the lattice parameters as a function of oxygen occupancy has been measured [65]. Full oxygen occupancy in this crystal was indicated by agreement in lattice parameters (a = 3.33 Å, b = 10.99 Å, c = 8.77 Å [65], cf Table 3.1) as well as the single crystal refinement.

The structure may be viewed as being built up from two polyhedral units - trigonal prisms of zirconium centered by nickel atoms, and octahedra of zirconium centered by oxygen atoms (Figure 3.1). The trigonal prisms share triangular faces, forming chains in the a direction. Adjacent chains are offset from each other by x=1/2. Oxygen atoms occupy the interstitial octahedral site formed by the zirconium atoms from adjacent chains. The octahedra form a zig-zag chain sharing corners in the c direction, and they share edges with adjacent octahedra in the a direction.

The interatomic distances less than 3.5 Å are listed in Table 3.4. The zirconium-zirconium

Table 3.1 Crystal data for Zr_3NiO

Formula	Zr_3NiO
Space Group	Cmcm(#64)
a (Å)	3.353(1)
b (Å)	11.013(4)
c (Å)	8.755(7)
V (Å^3)	323.3(3)
Z	4
d_{calc}, (g/cm^3)	7.153
Crystal size, (μm^3)	60x30x20
μ(MoKα), (cm^{-1})	147.71
Data collection instrument	Rigaku AFC6R
Radiation (monochromated in incident beam)	MoKα (λ=0.71069 Å)
Temperature, °C	23
No. unique data, total with $F_o^2 > 3\sigma(F_o^2)$	162
No. parameters refined	20
Secondary ext. coeff. (10^{-7})	8(1)
R[a], R_w[b], GOF[c]	0.025, 0.033, 1.149
Largest difference peak (Å^3)	+1.50
Largest negative diff. peak (Å^3)	-1.40

[a] $R = \Sigma||F_o| - |F_c|| / \Sigma|F_o|$

[b] $R_w = [\Sigma w(|F_o| - |F_c|)^2 / \Sigma w|F_o|^2]^{1/2}$; $w = 1/\sigma^2|F_o|$

[c] $GOF = (\Sigma(|F_o| - |F_c|)/\sigma_i) / (N_{obs\ refl} - N_{parameters})$

Table 3.2 Atomic parameters for Zr_3NiO

Atom	Site	*x*	*y*	*z*	B_{eq}[a]($Å^2$)
Zr1	8*f*	0	0.3645(1)	0.5601(1)	0.65(5)
Zr2	4*c*	0	0.9338(2)	1/4	0.69(8)
Ni	4*c*	0	0.2460(2)	1/4	1.2(1)
O	4*a*	0	0	0	0.9(6)

[a] $B_{eq} = 8\pi^2/3\ \Sigma_i^3\Sigma_i^3 U_{ij} a_i^* a_j^* \vec{a}_i^* \vec{a}_j^*$

Table 3.3 Anisotropic thermal parameters for Zr_3NiO

Atom	U_{11}	U_{22}	U_{33}	U_{12}	U_{13}	U_{23}
Zr1	0.0082(7)	0.0071(7)	0.0093(7)	0	0	-0.0016(5)
Zr2	0.005(1)	0.012(1)	0.010(1)	0	0	0
Ni	0.022(2)	0.014(1)	0.010(1)	0	0	0
O	0.010(7)	0.018(7)	0.007(6)	0	0	0.006(6)

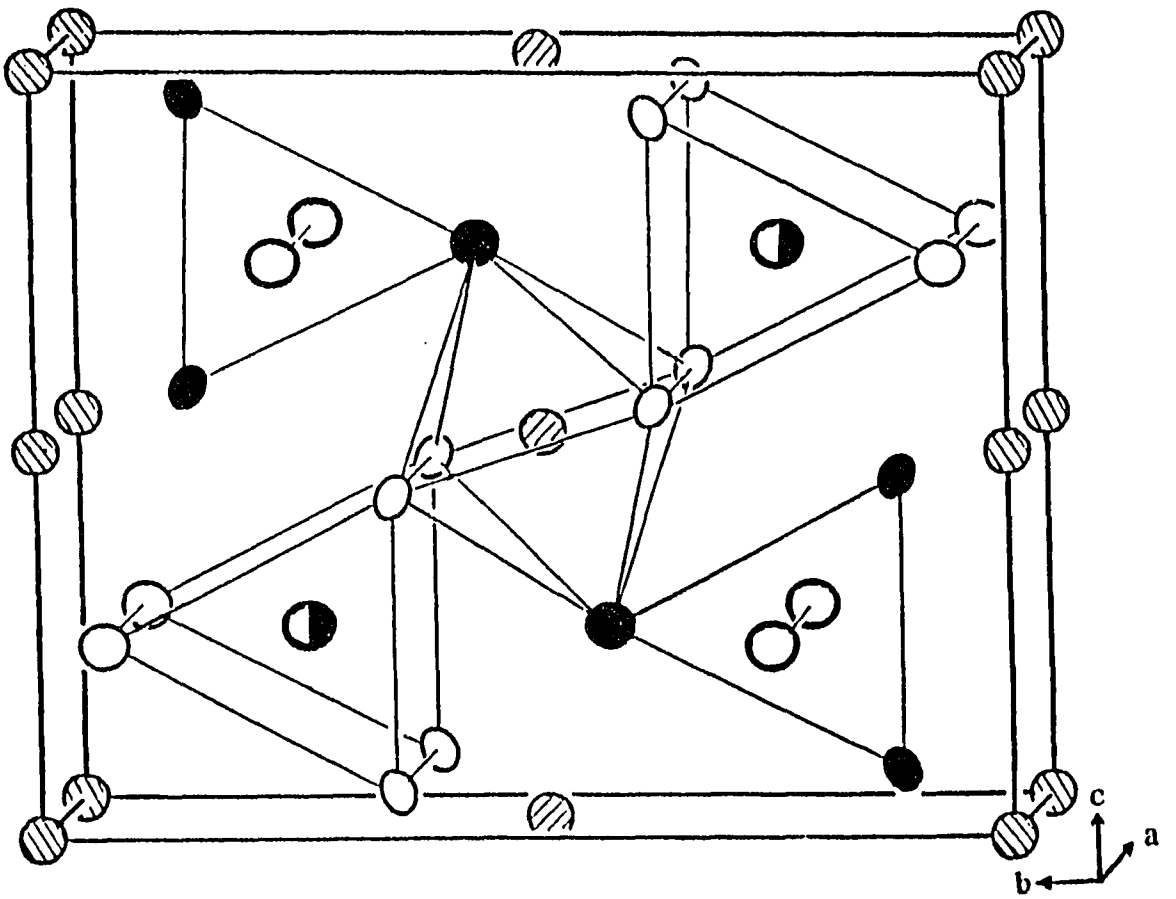

Figure 3.1 Unit cell of Zr_3NiO showing ocahedral coordination of oxygen and trigonal prismatic coordination of nickel

Table 3.4 Interatomic distances less than 3.5 Å in Zr_3NiO

Zr1	- O	2.305(1) x 2	Zr2	- O	2.307(2) x 2
	- Ni	2.657(2) x 2		- Ni	2.662(3) x 2
	- Ni	3.012(3) x 1		- Zr1	3.242(2) x 4
	- Zr1	3.165(3) x 1		- Zr1	3.281(2) x 4
	- Zr1	3.206(2) x 2		- Zr2	3.353(1) x 2
	- Zr2	3.242(2) x 2		- Ni	3.439(4) x 1
	- Zr2	3.281(2) x 2			
	- Zr1	3.325(4) x 1	Ni	- Zr1	2.657(2) x 4
	- Zr1	3.353(1) x 2		- Zr2	2.662(3) x 2
				- Zr1	3.012(3) x 2
O	- Zr1	2.305(1) x 4		- Ni	3.353(1) x 2
	- Zr2	2.307(2) x 2		- Zr2	3.439(1) x 1

distances between the zirconium atoms in adjacent trigonal prisms are short compared to those distances within the prism, suggesting zirconium-zirconium interactions are stronger between the trigonal prisms than within the prism. All the zirconium-zirconium distances in the trigonal prism are greater than 3.3 Å. In fact, the Zr1-Zr2 distance on the triangular face of the prism is 3.682 Å. This is significantly larger than the 3.23 Å separation in elemental zirconium and the 3.165 Å separation within the octahedra here, as well as other zirconium-zirconium separations in this oxide (Table 3.4). Although the zirconium-zirconium linkages around the prism are outlined in Figure 3.1, the important interactions within the prism are between the nickel and the zirconium atoms. This is expected on the basis of the behavior of early transition metals and late transition metals, where strong Lewis acid - base interactions are involved. The zirconium-nickel separation here is 2.66 Å. This is shorter than the zirconium-nickel distances in ZrNi (d = 2.68-2.77 Å) and Zr_2Ni (d = 2.76 Å) [67].

The role of oxygen in the compounds Zr_3MO_x (M = Fe, Co, Ni) is that of an electron acceptor. In terms of so-called electron compounds, where a certain electron per atom ratio is necessary for a given phase, the binary Zr_3Fe is taken to have an ideal composition. Then in moving from iron to cobalt, and then to nickel, the electron/atom ratio increases until the phase becomes unstable with respect to neighboring intermetallic phases. When the metal atoms have more electrons the oxygen acts as an electron sink to maintain the proper electron/atom ratio in the metal framework, enabling the phase to form. In terms of energy band arguments, if the Fermi level in Zr_3Fe lies at the energy at which all bonding levels are occupied, additional electrons would fill antibonding orbitals. Oxygen, octahedrally coordinated by zirconium atoms, provides low lying orbitals for the additional electrons in the cobalt and nickel compounds.

The magnetic susceptibility of a single phase sample, prepared by arc melting and annealing at 1000°C, was measured in a field of 3 Tesla, over a temperature range of 6 - 298 K.

The sample was also checked for superconductivity, but none was detected. The lattice parameters of this sample were a = 3.3238(4)Å, b = 10.974(1)Å, and c = 8.7982(9)Å. By Boller's plot [65], this corresponds to a stoichiometry of $Zr_3NiO_{0.6}$. Figure 3.2 shows paramagnetic behavior for this compound. The very low apparent magnetic moment may actually be caused by a very small amount of nickel in the sample. The figure is not corrected for core diamagnetism, which would increase the molar susceptibility by 0.5 x 10^{-4} emu/mole [111]. See also Figure 4.7.

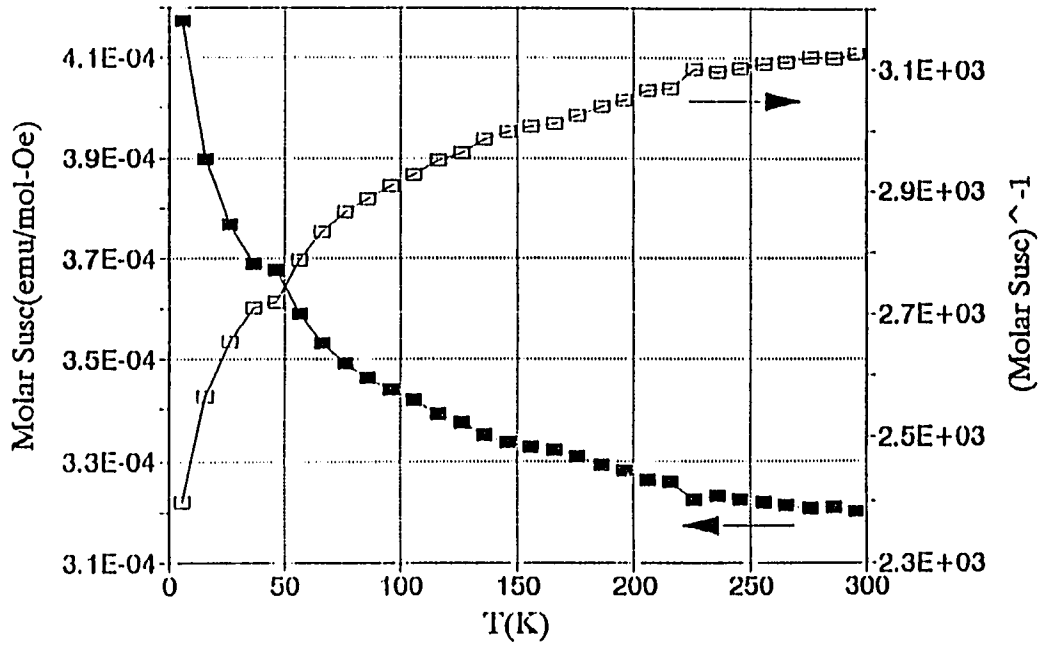

Figure 3.2 Magnetic susceptibility of $Zr_3NiO_{0.6}$

4. NEW OXIDES OF THE FILLED Ti_2Ni TYPE STRUCTURE

Introduction

The study of new phases of the filled Ti_2Ni type structure is but one of many potentially fruitful areas of investigation in intermetallics and in interstitially stabilized intermetallics. The chemistry of intermetallics in general is not well understood. The commercial world benefits greatly from the technologically important uses of intermetallic compounds, while scientists continue to incrementally increase their knowledge and understanding of these materials. One area of increasing interest in recent years is the role of interstitials in intermetallics. Many known structures may include undetected interstitials. Discoveries in this field are being made because the interstitials are being specifically looked for. Also, the ability to detect the presence of interstitials has increased. The precision of Guinier cameras makes measurements of lattice parameters from powder data very sensitive to changes in composition, either from changes in metal composition or from the presence of light interstitial atoms. Single crystal diffractometers can provide X-ray beam intensity sufficient to detect and refine light elements present in the intermetallic. Although over 150 compounds with this structure have been reported, only now, with the discovery of new phases and the reinvestigation of reported phases, are the structural details being investigated and clarified.

The metal-atom ordering and oxygen occupancy of four compounds of the filled-Ti_2Ni type structure have been determined by single crystal X-ray diffraction studies. Three additional phases have been identified and indexed from powder X-ray diffraction data. All the phases crystallize in space group $Fd\bar{3}m$ with the following compositions: Zr_4Ni_2O (a=12.1970(9) Å), $Zr_6Ni_4Ti_2O_{0.6}$ (a=12.0299(9) Å), Nb_6Ni_6O (a=11.2117(5) Å), and $Nb_6Ni_4Ta_2O_2$ (a=11.5813(3) Å). Phases identified using powder data are Nb_4Ni_2O (a=11.5933(3) Å), Zr_4Cu_2O (a=12.2659(7) Å), and $Zr_6Co_4Ti_2O$ (a=11.8649(9) Å). A comparison of the structures and oxygen occupancies, as well as

tentative explanations, are presented based on extended Hückel calculations. The role of interstitial oxygen as an electron acceptor and its affect on metal-metal bonding will be considered.

The Ti_2Ni, the filled Ti_2Ni, and the related η carbide type structures have been known for some time [68]. Much of the earlier work revealed the variety of combinations of metals which adopt this framework to make it the most frequently found structure of binary intermetallics of stoichiometry A_2B [69]. The simplicity of the formula conceals the subtleties and complexities in the chemistry of these phases. Many of the binary intermetallics may incorporate light interstitial elements [69]. Many more phases form only in the presence of these interstitial atoms, commonly C [67,70-72], N [73,74], O [46,75,76], and even H [77], and these are the interstitially stabilized phases. Structural reports indicate the interstitial atoms, not considering H, occupy one of two possible octahedral sites, but not both. An additional feature is the possible deviation from an A_2B stoichiometry to an AB stoichiometry. In some systems both ratios are observed, not as a wide solid solution, but as two distinct phases. A review of the literature and list of reported phases suggests there is no general explanation for the variability in compositions, nor is there any correlation to interstitial atom site occupancy and metal/metal ratio. Although much of the work was done a number of years ago, significant recent reports in the literature prompt further investigation of these phases [46,72,77,78]. Many reports are based on X-ray powder diffraction data, with the inherent difficulty in refining parameters for light interstitial elements. Some neutron diffraction work has been reported [72,77-79]. Single crystal work has not been previously reported for the oxides or carbides. Presumably this is because of the difficulty in forming single crystals suitable for diffraction experiments. The crystals examined here were all very small, and the successful refinements were possible because of the high X-ray beam intensity obtained from using a diffractometer with a rotating anode X-ray generator.

The filled Ti_2Ni type structure crystallizes in space group $Fd\bar{3}m$, and the unit cell contains

96 metal atoms. Adopting the notation by Newsam et. al.[72], the general formula for the oxides is written $M_6^f M_4^e M_2^d O_2^c O_1^a$. The superscript letters are those of the Wyckoff symbol for the crystallographic site occupied by the superscripted atoms. The subscripts are based on the unit cell formula with Z=8. For a ternary compound M^f and M^e are different transition metals. M^d may either be the same as M^f or M^e, depending on the system being considered. The transition metal M^f is always to the left of the M^e metal atom on the periodic table. The M^f atoms form an octahedral network. The M^e atoms have a tetrahedral arrangement. The M^d atoms cap the faces of the tetrahedra formed by the M^e atoms. When the *f* and *d* sites are occupied by the same metal the metal:metal ratio is 8:4, or 2:1. When the *e* and *d* sites are occupied by the same metal the metal:metal ratio is 6:6, or 1:1. There is no mixing reported on the M^d site, and this explains the two ratios reported as distinct phases, and not as a single phase with a large range of homogeneity. The assumption is made that the interstitial oxygen atoms occupy only one of the two possible sites. They occupy either the 16*c* site, in which they fill distorted octahedra, or the 8*a* site, in which they fill regular octahedra. Thus for a given ternary system the four possible compositions reported are $M_8M'_4O$, $M_8M'_4O_2$, $M_6M'_6O$, and $M_6M'_6O_2$. Examples of each have been reported.

The Ti_2Ni structure contains ninety-six metal atoms in the unit cell. When interstitial atoms are present there are up to 104 or 112 atoms in the unit cell. It is hard to visualize or depict a cell this size. It is easiest to consider the building blocks in the unit cell and see how they order. Consider first a large cubic cell divided into two alternating subunits, as in Figure 4.1. Each subunit is one - eighth of the total cell, and the alternating pattern extends in all three directions in space. Figure 4.2 is a projection of one layer of the unit cell depicted in Figure 4.1, and contains four subunits. The subunits in the lower left and upper right are centered by an octahedron. The lower right and upper left subunits are centered by a tetrahedron. The octahedron - centered subunits and

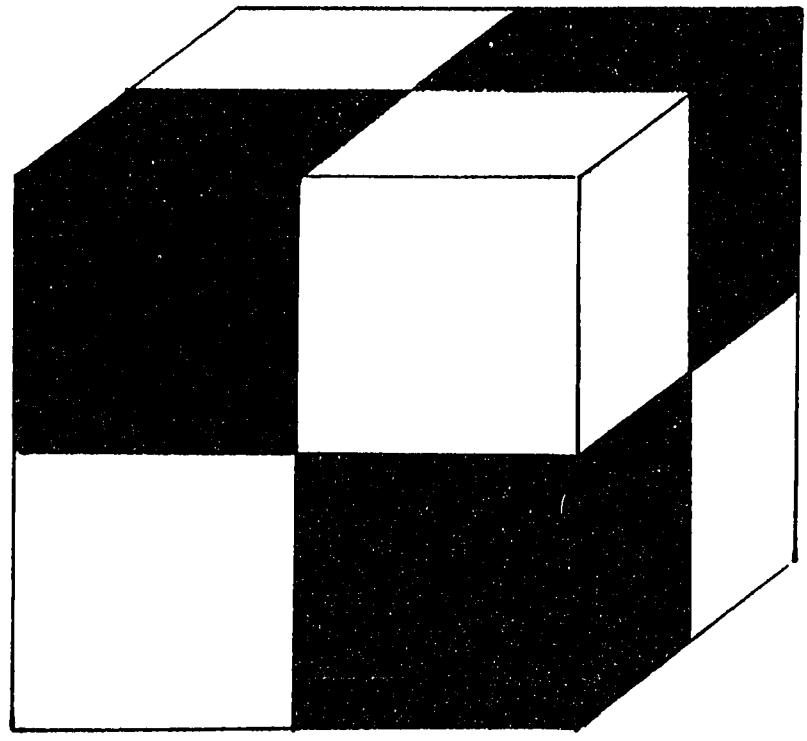

Figure 4.1 A large cubic cell divided into two alternating subunits

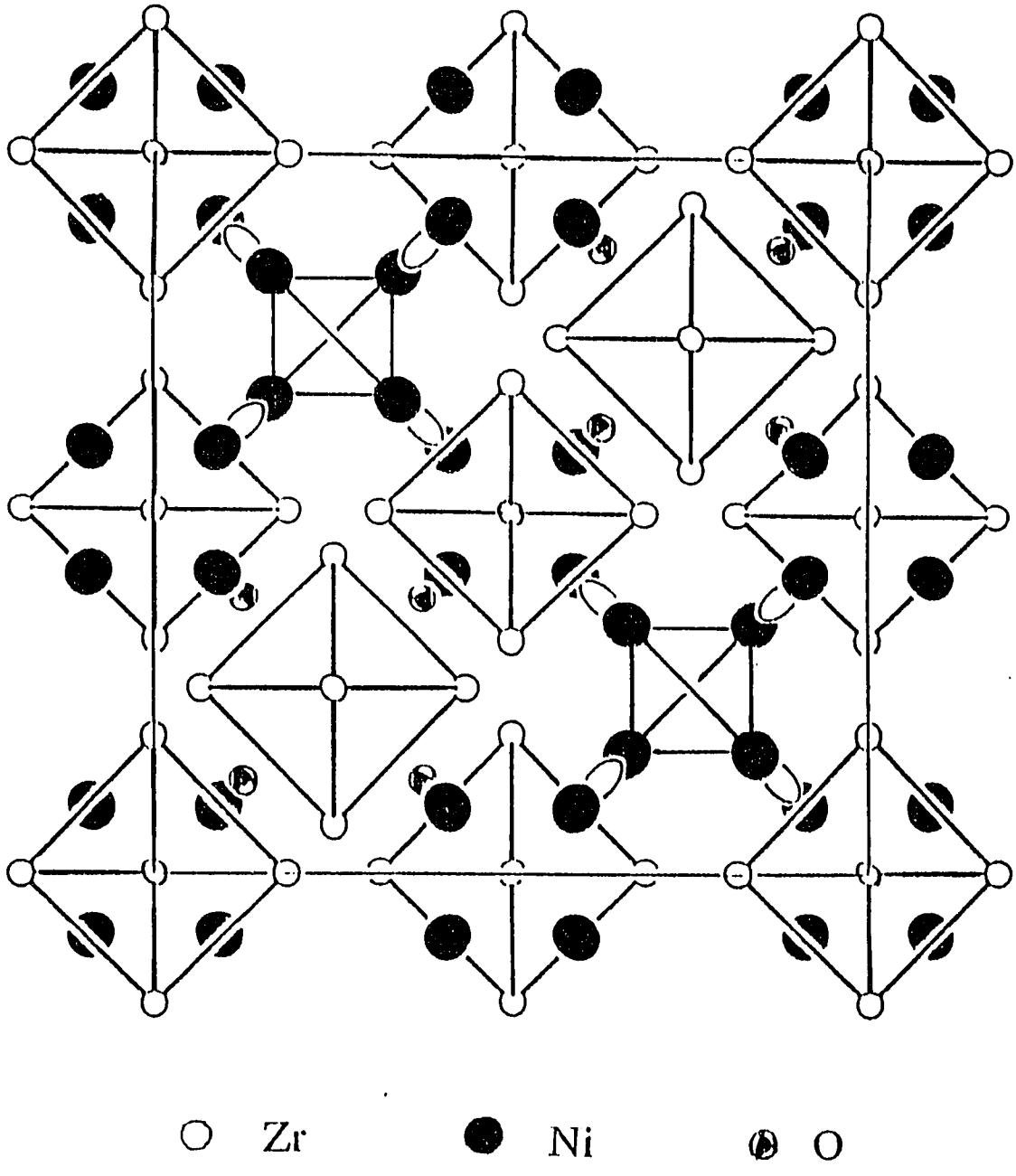

Figure 4.2 Projection of one half the unit cell, in the direction of projection axis, of Zr_4Ni_2O.

tetrahedron - centered subunits pack in an alternating pattern in all three dimension. Each subunit is displayed individually in Figure 4.3. Figure 4.3 (a) shows the subunit centered by an octahedron in which the central octahedron is surrounded by four more octahedra arranged tetrahedrally at the corners of the subunit. It is also surrounded by four tetrahedra, arranged tetrahedrally at the other four corners of the subunit. Figure 4.3 (b) is centered by a tetrahedron, and is similarly surrounded by four octahedra and four tetrahedra. Note that these two subunits adjoin one another, so that the octahedron at the lower right of Figure 4.3 (a) is the same octahedron at the lower left of Figure 4.3 (b), and so on for the other polyhedra on the shared face.

The diagram for Figure 4.3 is made for the compound Zr_4Ni_2O, where the M^d atom is the same metal as the M^f atom, which is zirconium in this case. The M^d zirconium atom is seen capping the faces of the central tetrahedron in Figure 4.3 (b). The interstitial oxygen in the 16*c* site is seen in Figure 4.3 (a), capping four faces of the central octahedron. This atom is actually six coordinated, in a distorted octahedral arrangement, where opposite faces of the distorted octahedron share faces with the regular octahedra outlined. Thus, rather than looking at isolated polyhedra, consider a network built up of these face - sharing octahedra. The subunit in Figure 4.3 (a) viewed as a section of such a network is drawn in Figure 4.4. The central octahedron shares four faces with four other octahedra. Each of these four octahedra, shown shaded and centered by oxygen, share just two opposite faces. The network, then, consists of face - sharing octahedra which alternately share two and four faces. The octahedra shown are alternately centered by oxygen and empty. The face - sharing octahedra form rings made up of 12 octahedra. The void spaces within and between these rings are filled by an interpenetrating network consisting of the tetrahedra and the capping atoms, forming stella quadrangulea. This network is depicted in Figure 4.5. The structure has been described in the literature by both schemes outlined here; as made up of alternating subunits, and as two interpenetrating networks. Additional comments about the structure

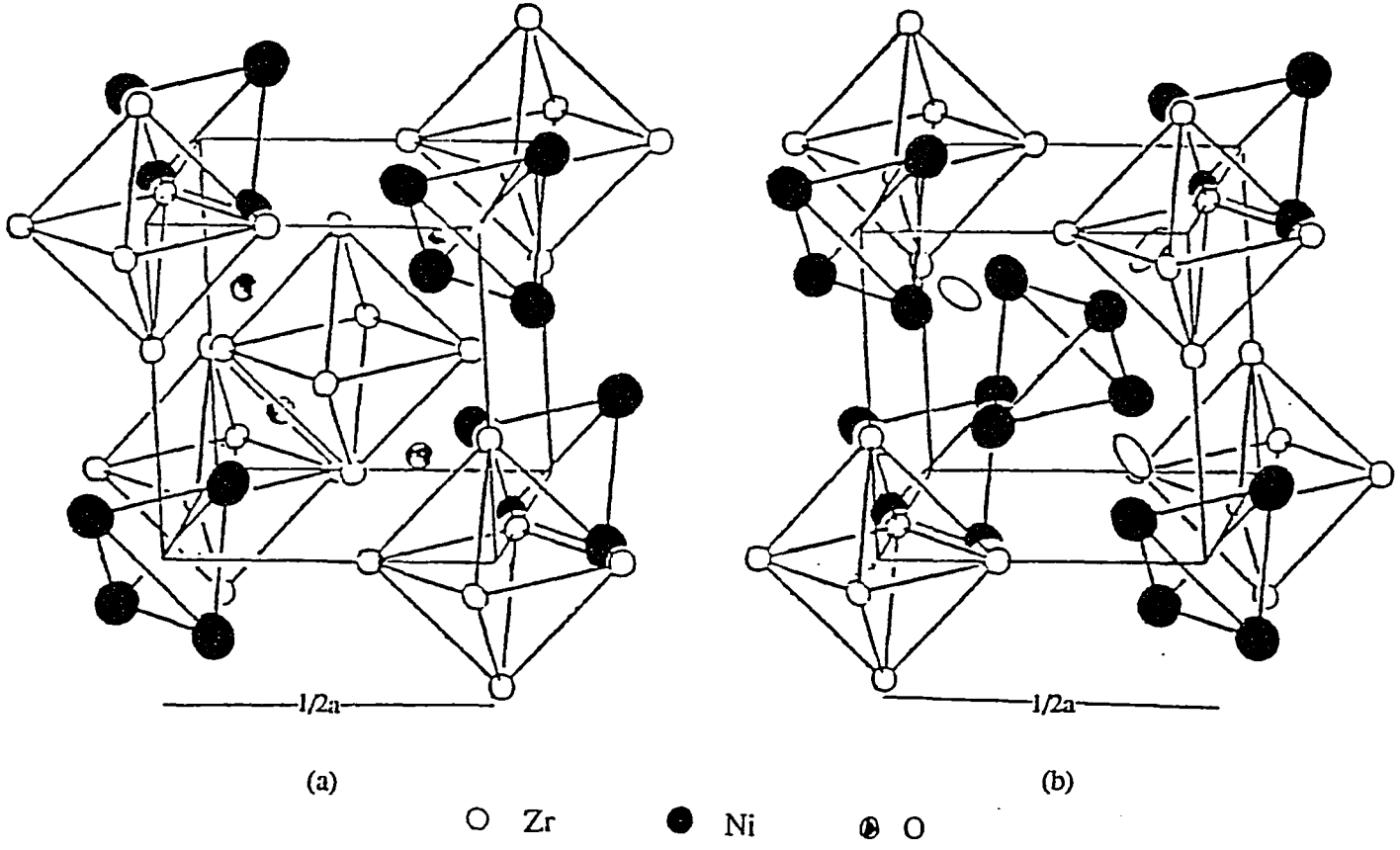

Figure 4.3 View of individual subunits making up the unit cell of Zr_4Ni_2O
(a) subunit centered by zirconium octahedron
(b) subunit centered by nickel tetrahedron

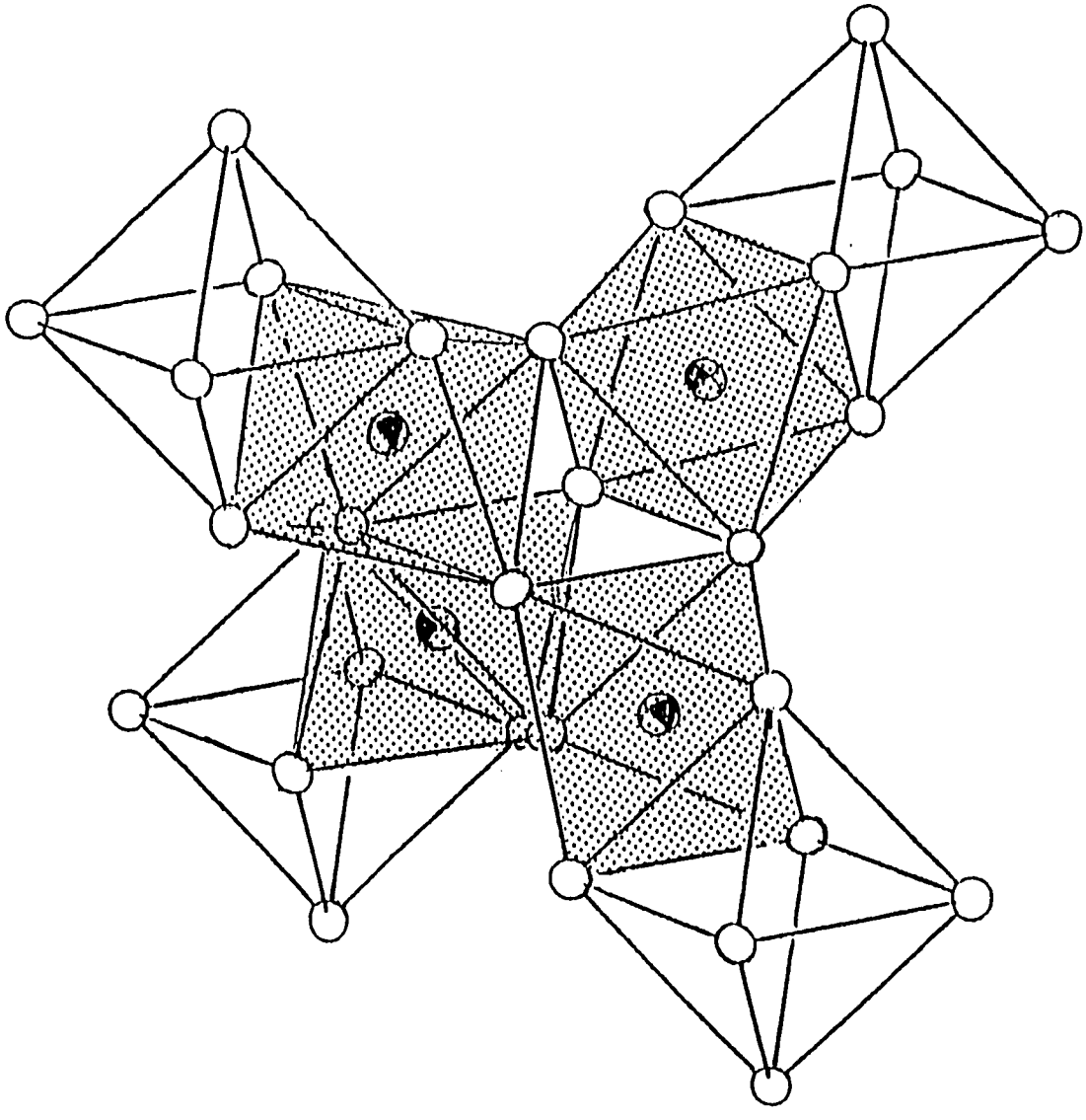

Figure 4.4 Network of face-sharing zirconium octahedra in Zr_4Ni_2O. Shaded octahedra are centered by oxygen, unshaded octahedra are empty.

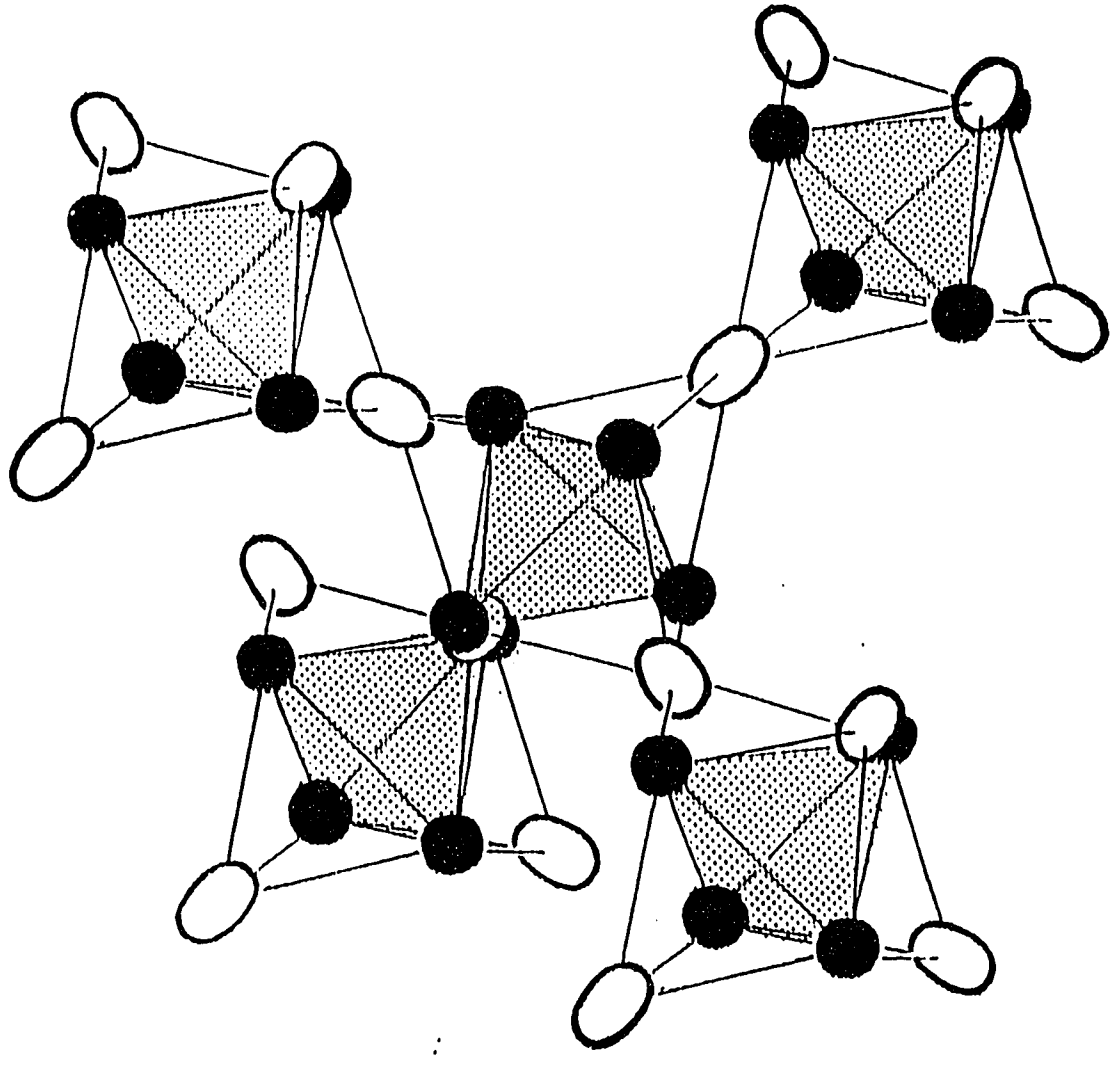

Figure 4.5 Network of stella quadrangulae in Zr_4Ni_2O. Nickel tetrahedra are shaded.

will be made later, at which point structural features are considered in terms of chemical interactions.

Experimental Details

All chemicals were used as they were received from the supplier, except as noted in the experimental section earlier. Samples were prepared by two general techniques. The first technique consisted of arc melting the metals and the oxide of either zirconium or nickel. The samples were then annealed under vacuum in an induction furnace. This technique often resulted in a mixture of phases. ZrO_2 was always present as a minor phase. Other minor phases present in various samples were Zr_3NiO and the cubic Laves phase. Apparently, the Laves phase has a low melting point (less than 1000°C) and the presence of this phase masks the refractory nature of this family of compounds. Samples free of this phase remained solid when annealed at 1250-1275°C. Samples containing niobium all had NbO as a minor phase, and some also had Nb_7Ni_6 present. The desired phase was present upon annealing as low as 1000°C, but most samples were annealed at 1250°C. The melting point of Nb_7Ni_6 is 1290°C.

A second method was used successfully for the preparation of a nearly single phase sample of Zr_4Ni_2O. Only the two strongest lines of ZrO_2 were barely visible in the powder X-ray diffraction pattern of this phase. A sample of Zr and Ni was arc-melted, as before, then ground to small pieces. The metal and an appropriate amount of oxidizing agent, $NaClO_4$, were sealed in an evacuated fused silica tube. Upon heating to 600°C for 4 days in a tube furnace the perchlorate decomposed, and crystals of NaCl formed at the cool end of the tube. The resulting oxide was crushed to a fine powder and pressed into a pellet before annealing as before.

Single crystal X-ray diffraction data collection was done on a Rigaku AFC6R diffractometer, with MoKα radiation (λ=0.71069 Å). All crystals were refined in space group $Fd\bar{3}m$. Details of

crystal data are listed in Table 4.1.

A Quantum Design SQUID magnetometer was used to check for superconductivity and to measure magnetic behavior at a field of 3T over the temperature range of 6 - 298 K.

A JEOL JSM-840 electron microscope was used to examine the zirconium nickel oxides.

Results

Interest in the Ti_2Ni type structures initially arose from a study of the interstitially stabilized intermetallic phases that form in the Zr-Ni system [66,80,81]. Two curious results deserved attention. First, previous work on the Zr-Ni-O phase diagram in an intentional search for this phase indicated that it does not exist in equilibrium at 950°C [39]. It does exist, however, at 1275°C, the annealing temperature used in these experiments. This is thus an example of a high temperature solid phase which decomposes at lower temperature, in this case probably to Zr_3NiO and Ni. Second, there was a noticeable shift in lattice parameters for this phase in several of the samples, as observed in the films of the powder diffraction patterns taken on a Guinier camera. A single crystal was chosen from both a sample with the larger lattice parameter, and a sample with the smaller lattice parameter. The results for the data refinement of the larger cell correspond to the data reported for Zr_4Ni_2O in Table 4.2. The preliminary solution for the smaller cell was also based on a Zr/Ni/O ternary system, and required Ni vacancies on the 16*d* site for a suitable refinement, giving a stoichiometry of $Zr_6Ni_{6-x}O$. This solution was corrected when elemental analysis revealed the presence of titanium, which could be detected in samples prepared with a zirconium starting material which unexpectedly contained significant amounts of titanium. Placing Ti in the 16*d* site in the structure solution improved the refinement significantly, and the final refinement showed full occupancy on all the metal sites. The results for $Zr_6Ni_4Ti_2O_{0.6}$ are also in Table 4.2. Efforts to synthesize a compound of stoichiometry Zr_6Ni_6O, without titanium, were unsuccessful.

Table 4.1 Single crystal data of new filled - Ti_2Ni type phases

Formula	Zr_4Ni_2O	$Zr_6Ni_4Ti_2O_{0.6}$	Nb_6Ni_6O	$Nb_6Ni_4Ta_2O_2$
a Å	12.1970(9)	12.0299(9)	11.2117(5)	11.5813(3)
V $Å^3$	1814.5(4)	1740.9(4)	1409.3(2)	1553.4(1)
Z	16	8	8	8
d_{calc}, g/cm^3	7.295	6.747	8.742	10.390
Crystal size, μm^3	40x50x70	50x50x100	40x40x40	30x40x50
μ(MoKα), cm^{-1}	167	169	246	494
Data collection range, 2θ	0-60	0-55	0-55	0-60
No. refl. measured	768	579	482	1253
No. unique data, total with $F_o^2 > 3\sigma(F_o^2)$	112	87	79	101
No. parameters refined	13	15	11	15
Trans. factors, max./min.	1.116	1.168	1.146	1.179
R^a	0.020	0.029	0.017	0.022
$R_w{}^b$	0.024	0.031	0.023	0.029
GOF[c]	1.019	0.995	0.980	1.026
Largest peak, $e/Å^3$	1.59	1.20	0.88	1.54
Largest negative peak, $e/Å^3$	-1.17	-1.31	-1.04	-3.19

[a] $R = \Sigma||F_o|-|F_c||/\Sigma|F_o|$

[b] $R_w = [\Sigma w(|F_o|-|F_c|)^2/ \Sigma w|F_o|^2]^{1/2}$; $w = 1/\sigma^2(|F_o|)$

[c] $GOF = (\Sigma(|F_o|-|F_c|)/ \sigma_i)/ (N_{obs\ refl} - N_{parameters})$

Table 4.2 Final atomic parameters from single crystal refinement

Atom	Site	*x*	*y*	*z*	$B_{eq}(Å^2)$[a]
			Zr_4Ni_2O		
Zr1	48*f*	0.18517(8)	0.0	0.0	0.51(1)
Ni	32*e*	0.8396(1)	0.8396	0.8396	1.2716(5)
Zr2	16*d*	0.625	0.625	0.625	1.5990(5)
O	16*c*	0.125	0.125	0.125	0.562(2)
			$Zr_6Ni_4Ti_2O_{0.6}$		
Zr	48*f*	0.1901(1)	0.0	0.0	0.73(4)
Ni	32*e*	0.8326(2)	0.8326	0.8326	1.1795(7)
Ti	16*d*	0.625	0.625	0.625	1.430(1)
O[b]	16*c*	0.125	0.125	0.125	1.17(3)
O[b]	8*a*	0.0	0.0	0.0	0.98(3)
			Nb_6Ni_6O		
Nb	48*f*	0.1996(1)	0.0	0.0	0.47(2)
Ni1	32*e*	0.8317(1)	0.8317	0.8317	0.3289(4)
Ni2	16*d*	0.625	0.625	0.625	0.4602(6)
O	8*a*	0.0	0.0	0.0	0.497(4)
			$Nb_6Ni_4Ta_2O_2$		
Nb[c]	48*f*	0.1867(1)	0.0	0.0	0.48(4)
Ni	32*e*	0.8311(1)	0.8311	0.8311	0.422(1)
Ta[d]	16*d*	0.625	0.625	0.625	0.3491(6)
O	16*c*	0.125	0.125	0.125	1.154(5)
			Idealized Metal Positions[e]		
M1	48*f*	0.1875	0.0	0.0	
M2	32*e*	0.8250	0.8250	0.8250	

[a] $B_{eq} = 8\pi^2/3 \sum_i^3 \sum_j^3 U_{ij} a_i^* a_j^* \vec{a}_i^* \vec{a}_j^*$

[b] Refinement of the oxygen occupancy gave results of the 16*c* site being 18(6)% occupied and the 8*a* site 24(6)% occupied.

[c] Refined with mixed Nb/Ta occupancy; Nb 82(2)%, Ta 18(2)%.

[d] Refined with mixed Ta/Nb occupancy; Ta 61(3)%, Nb 39(3)%.

[e] [84]

A systematic check for a solid solution between Zr_4Ni_2O and Ti_4Ni_2O was not performed but for low concentrations of titanium, the titanium preferentially substitutes on the 16*d* site. Furthermore, the oxygen partially occupies both interstitial sites in the sample containing titanium, with total oxygen occupancy given by the formula $Zr_6Ni_4Ti_2O_{0.6}$. The refinement was carried out considering the possible solutions: $Zr_6Ni_4Ti_2$ (no oxygen), $Zr_6Ni_4Ti_2O_{1-x}$ (variable oxygen occupancy on the 8*a* site only), $Zr_6Ni_4Ti_2O_{2-x}$ (variable oxygen occupancy on the 16*c* site only), and $Zr_6Ni_4Ti_2O_{3-x}$ (variable oxygen occupancy on both the 8*a* and the 16*c* sites). By careful comparison of each of the refinement solutions, according to Hamilton's test [82], the solution with both sites partially occupied is correct with a 95% level of confidence. This result raises the question of whether a small amount of oxygen is required for the formation of the phase with a small addition of Ti (these samples were all made with intentional inclusion of oxygen). The binary intermetallic Ti_2Ni can reportedly accommodate oxygen to completely occupy of the 16*c* site, forming Ti_4Ni_2O [79]. The corresponding zirconium compound reported here has complete occupation of the 16*c* site.

Conflicting reports exist for the Zr_4Co_2O phase. Nevitt and Downey [39] did not find this phase in determining the 950°C isothermal section of this ternary system. Hollock and Thümmler [74] include Zr_4Co_2O (a=12.18 Å) in a list of phases observed. Attempts to synthesize this phase at 1100°C were unsuccessful. However, it was observed that this phase formed in samples prepared with the titanium-contaminated zirconium. By analogy with the substitution of Ti in Zr_4Ni_2O, this is formulated as $Zr_6Co_4Ti_2O$ (a=11.8649(9) Å), with undetermined oxygen occupancy.

The Zr/Cu/O system was also investigated. The synthesis of both Zr_4Cu_2O and Zr_6Cu_6O was attempted. With the Zr:Cu starting ratio of 2:1, the powder pattern indicated the presence of the desired phase as well as binary Zr_2Cu as a minor phase. When the starting Zr:Cu ratio was 1:1 the products were the cubic phase and the binary Zr_3Cu_8. The lattice parameters of the Ti_2Ni type

phase differed only slightly in all of the samples made. For the nearly single phase sample made with a 2:1 starting metal ratio, a=12.2659(7) Å. The smallest cell edge measured for the cubic phase with the 1:1 starting ratio was a=12.2615(6) Å. This leads to the conclusion there is only the one phase, Zr_4Cu_2O, with perhaps a slightly varying oxygen content accounting for the differences in observed cell lengths. Characterization of these phases was done by film data from X-ray powder diffraction experiments. The oxygen is assumed to occupy the 16*c* site. A significant shortening in the unit cell is observed when Ti is added to form $Zr_6Cu_4Ti_2O$ (a=12.16(2)Å).

The existence of the two distinct phases in the Nb/Ni/O system reported previously is confirmed [74]. Single crystal X-ray diffraction data for Nb_6Ni_6O (a=11.2117(5) Å) was used to determine oxygen occupancy in this phase, which had been reported as Nb_3Ni_3O (a=11.20 Å). Nb_4Ni_2O has lattice parameter a=11.5933(3) Å (previously reported as 11.58 Å). Comparison of oxygen occupancies in the Nb/Ni/O samples is incomplete because single crystals of Nb_4Ni_2O have not been found. The difference in lattice parameters clearly indicates the existence of two distinct phases. This contrasts with the Nb/Ni/C system for which only the Nb_4Ni_2C phase appears in the 1100°C isothermal section of the ternary phase diagram [83]. Samples of the oxides have been prepared which contain both phases in an equilibrium mixture. The existence of two distinct phases shows the 16*d* site is occupied either entirely by niobium or by nickel, but not by both in a solid solution on this metal site.

Ta_4Ni_2O is reported by Holleck & Thümmler [74], but Kotyk & Stadelmaier [73] find this phase only exists with nitrogen present, as either Ta_4Ni_2N or the mixed $Ta_4Ni_2(O,N)$, but not as the pure oxide. Efforts to synthesize both Ta_4Ni_2O and Ta_6Ni_6O, annealing at temperatures between 1430-1550°C, resulted in mixtures of binary phases. However, noting the effect of titanium in the zirconium compounds, the synthesis of mixed Ta/Nb compounds was attempted. Both of the starting compositions $Ta_6Ni_4Nb_2O_2$ and $Nb_6Ni_4Ta_2O_2$ were tried. Only the latter formed the cubic

phase, at 1550°C, with $(Ta,Nb)_7Ni_6$ present as a minor phase. A single crystal was selected for study by X-ray diffraction. A psi - scan suitable for absorption correction in the refinement process was not collected. As an empirical absorption correction (DIFABS) did not improve the refinement, no correction was applied in the final refinement. The Nb and Ta occupancies were allowed to mix in the refinement, resulting in a final stoichiometry of $(Nb_{0.82}Ta_{0.18})_6Ni_4(Ta_{0.61}Nb_{0.39})_2O_2$, or $Nb_{5.7}Ni_4Ta_{2.3}O_2$.

Crystal data for all the single crystal refinements are listed in Table 4.1. Positional and thermal parameters for the four single crystal refinements are listed in Table 4.2. Table 4.3 contains anisotropic thermal parameters. Interatomic distances are shown in Table 4.4. Table 4.5 summarizes all of the phases identified in this study and corresponding lattice parameters.

Zr_4Ni_2O, $Nb_6Ni_4Ta_2O_2$, Nb_4Ni_2O, and Nb_6Ni_6O were checked for superconductivity down to 6 K. None was detected. Magnetic measurements of the Zr_4Ni_2O and $Nb_6Ni_4Ta_2O_2$ phases from 6 - 297 K at a field of 3 Tesla show they are both paramagnetic (Figure 4.6). Figure 4.6 (a) shows a peculiar rise in susceptibility with temperature for Zr_4Ni_2O. Note the expanded scale on this figure. The sample contained an estimated 5% impurity phase of ZrO_2. A correction for the diamagnetism of the impurity phase and the core diamagnetism increases the molar susceptibility by $0.7x10^{-4}$ emu/mole from that shown in the figure. The source of the glitch at 225 K in Figure 4.6 (b) for $Nb_6Ni_4Ta_2O_2$ is unknown. When the temperature was cycled the glitch shifted to 240K, but did not disappear. This sample contained approximately 10% of an impurity phase of the Nb_7Ni_6 type. No magnetic measurements of Nb_7Ni_6 or Ta_7Ni_6 have been reported, and as it is possible this phase is paramagnetic also, no correction is made to the measured values. Figure 4.7 contains the results of the magnetic measurements on all the samples measured on the same scale.

Table 4.3 Anisotropic thermal parameters[a] for new phases of filled Ti_2Ni type

Atom	U_{11}	U_{22}	U_{12}	U_{23}
		Zr_4Ni_2O		
Zr1	0.0066(3)	0.0064(3)	0	0.0010(4)
Ni	0.02025(5)	0.02025	0.002(1)	0.002
Zr2	0.01611(5)	0.01611	0.009(1)	0.009
O	0.00712(3)	0.00712	0.0000(1)	0.0
		$Zr_6Ni_4Ti_2O_{0.6}$		
Zr	0.009(1)	0.0094(6)	0	0.0000(8)
Ni	0.01494(1)	0.01494	0.0003(8)	0.0003
Ti	0.01812(2)	0.01812	0.008(2)	0.008
O	0.0148(4)	0.0148	-0.01(3)	-0.01
O[b]	0.0125(3)			
		Nb_6Ni_6O		
Nb	0.0073(5)	0.0053(4)	0	0.0005(4)
Ni1	0.004167(5)	0.004167	0.0006(4)	0.0006
Ni2	0.005830(7)	0.005830	-0.0010(6)	0.0010
O[b]	0.00630(5)			
		$Nb_6Ni_4Ta_2O$		
Nb	0.0070(8)	0.0055(6)	0	-0.0002(5)
Ni	0.00534(1)	0.00534	0.0001(6)	0.0001
Ta	0.004421(7)	0.004421	-0.0007(3)	-0.0007
O	0.01461(6)	0.01461	-0.005(6)	-0.005

[a] Symmetry requirements for atoms listed first are $U_{22} = U_{33}$, and $U_{12} = U_{13} = 0$. For all other atoms, $U_{11} = U_{22} = U_{33}$, and $U_{12} = U_{13} = U_{23}$. U_{33} and U_{13} values are not explicitly included on table.

[b] Isotropic refinement

Table 4.4 Interatomic distances in new filled-Ti_2Ni type phases

		Zr_4Ni_2O	$Zr_6Ni_4Ti_2O$	Nb_6Ni_6O	$Nb_6Ni_4Ta_2O_2$
M1[a] -	O1 x1	--	2.287(2)	2.238(1)	--
	O2 x2	2.2776(7)	2.266(2)	--	2.162(1)
	Ni x2	2.7832(9)	2.861(2)	2.691(1)	2.774(1)
	Ni x2	3.152(1)	3.075(2)	2.773(1)	2.9912(6)
	M2 x2	3.164(1)	3.078(1)	2.7920(8)	2.999(1)
	M1 x4	3.194(1)	3.175(1)	2.915(1)	3.058(1)
	M1 x4	3.248(1)	3.234(1)	3.165(1)	3.075(1)
Ni -	M2 x3	2.688(1)	2.600(1)	2.4170(6)	2.4928(6)
	Ni x3	3.0910(9)	2.811(5)	2.591(1)	2.657(1)
	M1 x3	2.7832(9)	2.861(2)	2.691(1)	2.774(1)
	M1 x3	3.152(1)	3.075(2)	2.773(1)	2.999(1)
	O1 x1	--	3.488(3)	3.268(2)	--
	O2 x3	3.534(1)	3.590(2)	--	3.388(1)
M2[b] -	Ni x6	2.6878(8)	2.600(1)	2.4170(6)	2.4928(6)
	M1 x6	3.164(1)	3.078(1)	2.7920(8)	2.9912(6)
O1[c]	M1 x6	--	2.287(2)	2.238(1)	--
	Ni x4	--	3.488(3)	3.268(2)	--
O2[d]	M1 x6	2.2776(7)	2.266(2)	--	2.162(1)
	Ni x6	3.534(1)	3.590(2)	--	3.388(1)

[a]M1 = Zr or Nb in 48*f*

[b]M2 = Zr, Ti, Ni, or Ta in 16*d*

[c]O1 = O in 8*a*

[d]O2 = O in 16*c*

Table 4.5 Lattice Parameters for all new filled-Ti_2Ni type phases found

Composition	a (Å)
Zr_4Cu_2O	12.2659(7)
Zr_4Ni_2O	12.1970(9)
$Zr_6Ni_4Ti_2O_{0.6}$	12.0299(9)
$Zr_6Co_4Ti_2O$	11.8649(9)
Nb_4Ni_2O	11.5933(3)
$Nb_6Ni_4Ta_2O_2$	11.5813(3)
Nb_6Ni_6O	11.2117(5)

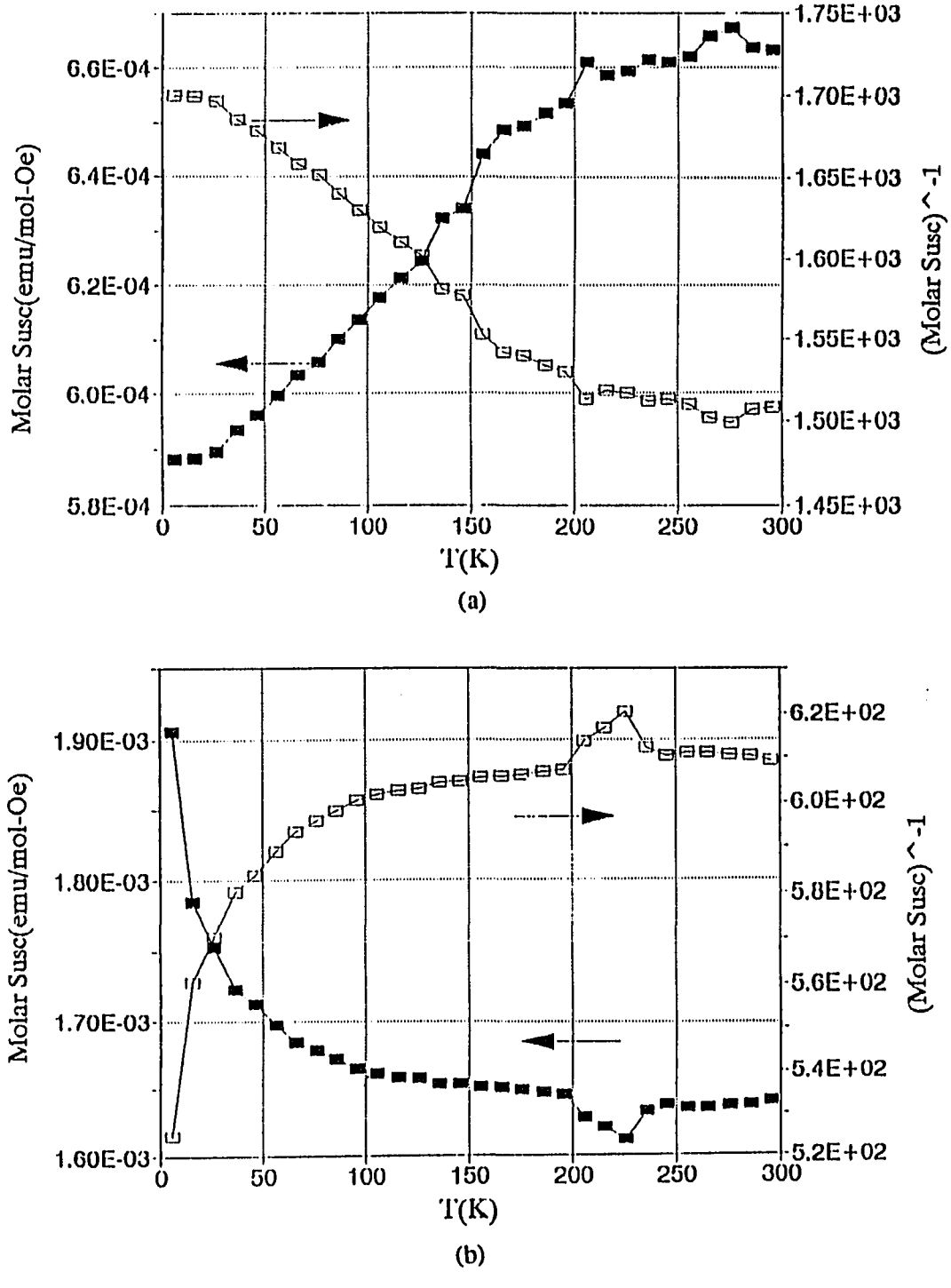

Figure 4.6 (a) Magnetic susceptibility of Zr_4Ni_2O. (b) Magnetic susceptibility of $Nb_6Ni_4Ta_2O_2$.

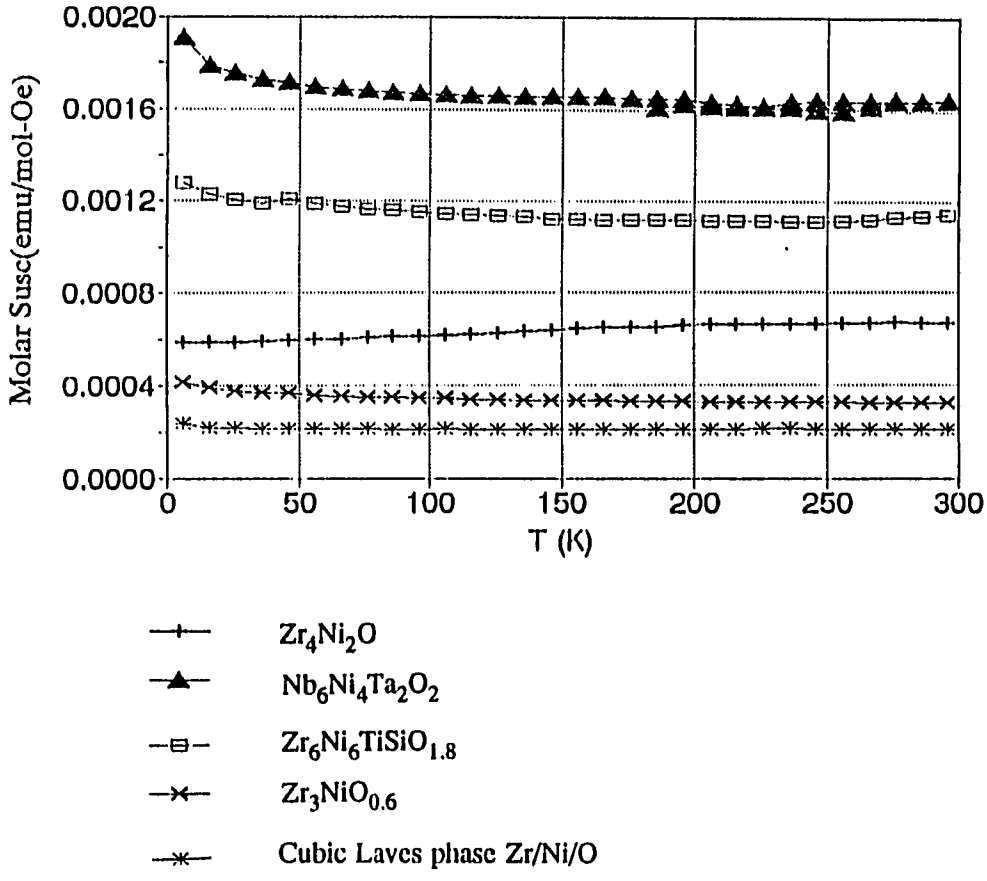

Figure 4.7 Summary of magnetic properties of phases studied in this research.

Band Calculations

Band calculations were done in an effort to explain the role of oxygen in the Zr_4Ni_2O phase, and determine if calculations could predict a preferred ordering of oxygen. Calculations were performed also on the compound Nb_6Ni_6O in an attempt to correlate the oxygen ordering with the metal ratios. The calculations were of the extended Hückel type using the tight binding method. The programs were described previously in the second chapter on Experimental Techniques. Density of states (DOS) diagrams and crystal orbital overlap population (COOP) curves were obtained, in addition to Fermi energies, total energies, orbital populations, and overlap populations of specific interactions. The atomic parameters used for the calculations are listed in Table 4.5. Calculations were done on the primitive cell of the large face center cubic cell. The k-points used for the calculation were chosen automatically by the program. The number of k-points used affects the accuracy of the results, and also determines the computer time required. Ten k-points were used for these calculations.

Table 4.5 Atomic parameters used for extended Hückel calculations

Atom	Orbital	H_{ii}, eV	ζ_1[a]	ζ_2[a]	c_1[b]	c_2[b]
Zr[c]	4d	-8.65	3.84	1.505	0.6213	0.5798
	5s	-7.78	1.82			
	5p	-4.96	1.78			
Ni[d]	3d	-12.99	5.75	2.20	0.5817	0.5800
	4s	-8.86	1.925			
	4p	-4.90	1.925			
O[e]	2s	-32.3	2.275			
	2p	-14.8	2.275			

[a] Exponent in the double ζ function for d orbitals
[b] Coefficients to exponential terms
[c] Parameters taken from [85]
[d] Parameters taken from[86]
[e] Parameters taken from [87]

The calculations carried out did not give clear answers to the questions asked. A clear preference for ordering of oxygen was not observed in Zr_4Ni_2O, as would be indicated by a lowering of the total energy of the system. To explain the subtle energy differences between oxygen occupying the different crystallographic sites, the possibility that the calculations might be sensitive to the starting parameters was considered. Consequently, a charge iterative procedure was performed to obtain new H_{ii}, ionization potential, values for zirconium and nickel. These new parameters are listed in Table 4.6 and were used to repeat several of the band calculations performed previously. However, again there was no clear preference calculated for ordering of the oxygen. The charge iteration was done only for zirconium and nickel. The oxygen parameters were kept the same. The iteration was done on the binary Zr_2Ni, which has the Al_2Cu type structure, with the assumption the parameters of the intermetallic would be very similar to those of the oxide. That this is a fair assumption can be inferred from the fact that the initial values were obtained from calculations on ZrCl for zirconium and on $Ni(CO)_4$ for nickel. Performing the charge iteration on Zr_2Ni saved time as well, since it has a much smaller unit cell than the oxide. Eleven cycles were necessary for the parameters to converge to the values listed in the table.

Table 4.6 Atomic parameters obtained from charge iteration on Zr_2Ni

Atom	Orbital	H_{ii}, eV
Zr[a]	4d	-6.72
	5s	-7.06
	5p	-3.68
Ni[b]	3d	-8.43
	4s	-6.76
	4p	-3.03

[a] A, B, C parameters for $H_{ii} = Aq^2 + Bq + C$ taken from [88]
[b] A, B, C parameters taken from [89]

General features of the DOS plots of Zr_4Ni_2O can be seen in Figures 4.8 and 4.9. Figure 4.8 (a) shows the DOS plot using the initial H_{ii} values listed in Table 4.5. Figure 4.8 (b) shows the same plot using the H_{ii} values obtained from the charge iteration, listed in Table 4.6. The most obvious result of the charge iteration procedure is the shift of all the levels to higher energies, except those for oxygen, for which parameters were not changed. The narrow band below -15 eV is principally oxygen 2p in character. Figure 4.8 (a) shows a contracted band between -14 and -12 eV, and a broad band from -12 eV and up. These bands can be assigned as being principally the nickel d band and zirconium d band, respectively. The d bands for late transition metals are more contracted than are those for early transition metals. In Figure 4.8 (b) the nickel d band is more contracted and is centered at about -9 eV, overlapping with the zirconium d band. The zirconium d band has the same general shape both with and without the charge iteration, but it is shifted to higher energies in (b). The broad, shallow Zr s and Ni s bands are in this region also. The projection of the individual atoms on the total DOS is shown in Figure 4.9 for the results from the charge iteration. Figure 4.9 (a) shows the projection of the Zr1 atoms on the total DOS. These are the zirconium atoms which make up the network of face-sharing octahedra. The oxygen atoms center an alternating set of these octahedra, and the mixing of zirconium with the oxygen p band is seen at low energy. The broad zirconium d band is seen at higher energy. Figure 4.9 (b) similarly shows the broad d band of zirconium in the icosahedral environment. Figure 4.9 (c) shows the narrow nickel d band, with nickel character extending up through the conduction band to higher energy. These general features are the same for both DOS plots in Figure 4.8. In both, the Fermi level is in the middle of the conduction band. The shifting of ionization potentials results in a shift of the calculated Fermi Energy from -9.386 eV to -7.205 eV. Another consequence of the charge iterative procedure was a change in orbital populations calculated for each atom. These changes are shown in Table 4.7, below. This shows the result of raising the ionization potentials of the metal

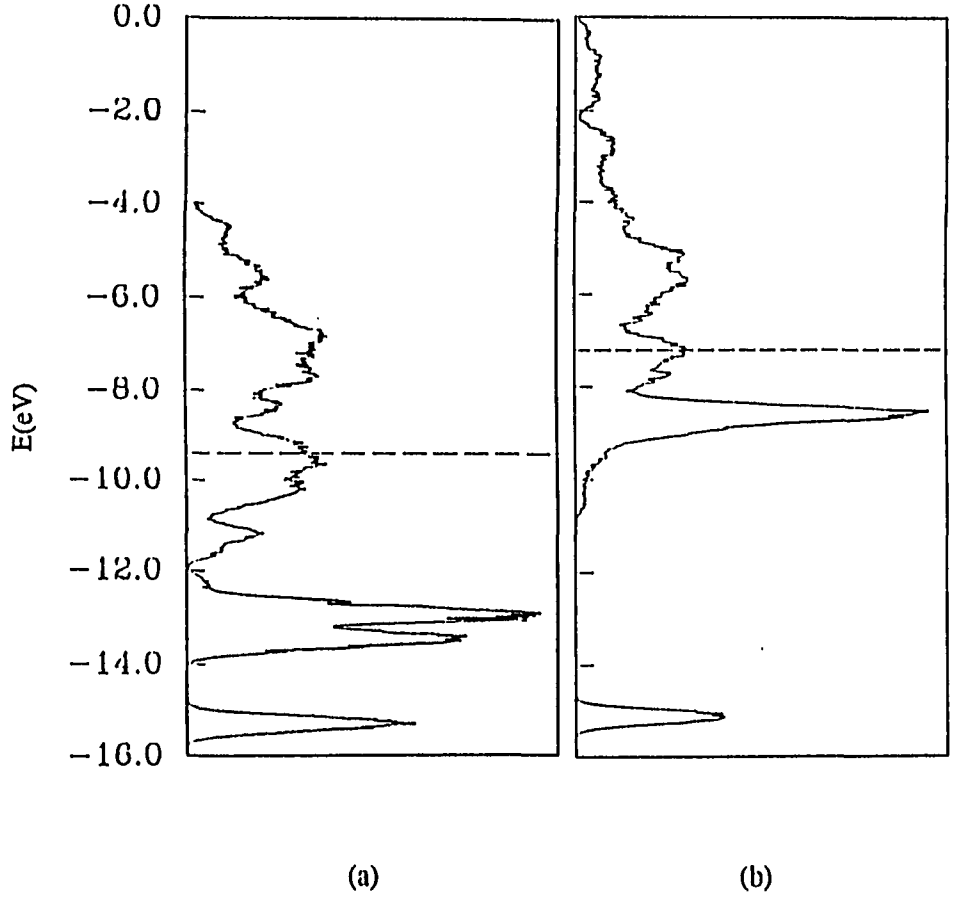

Figure 4.8 Total density of states plots for Zr_4Ni_2O. Fermi energy indicated by dashed line. (a) DOS before charge iteration. (b) DOS after charge iteration.

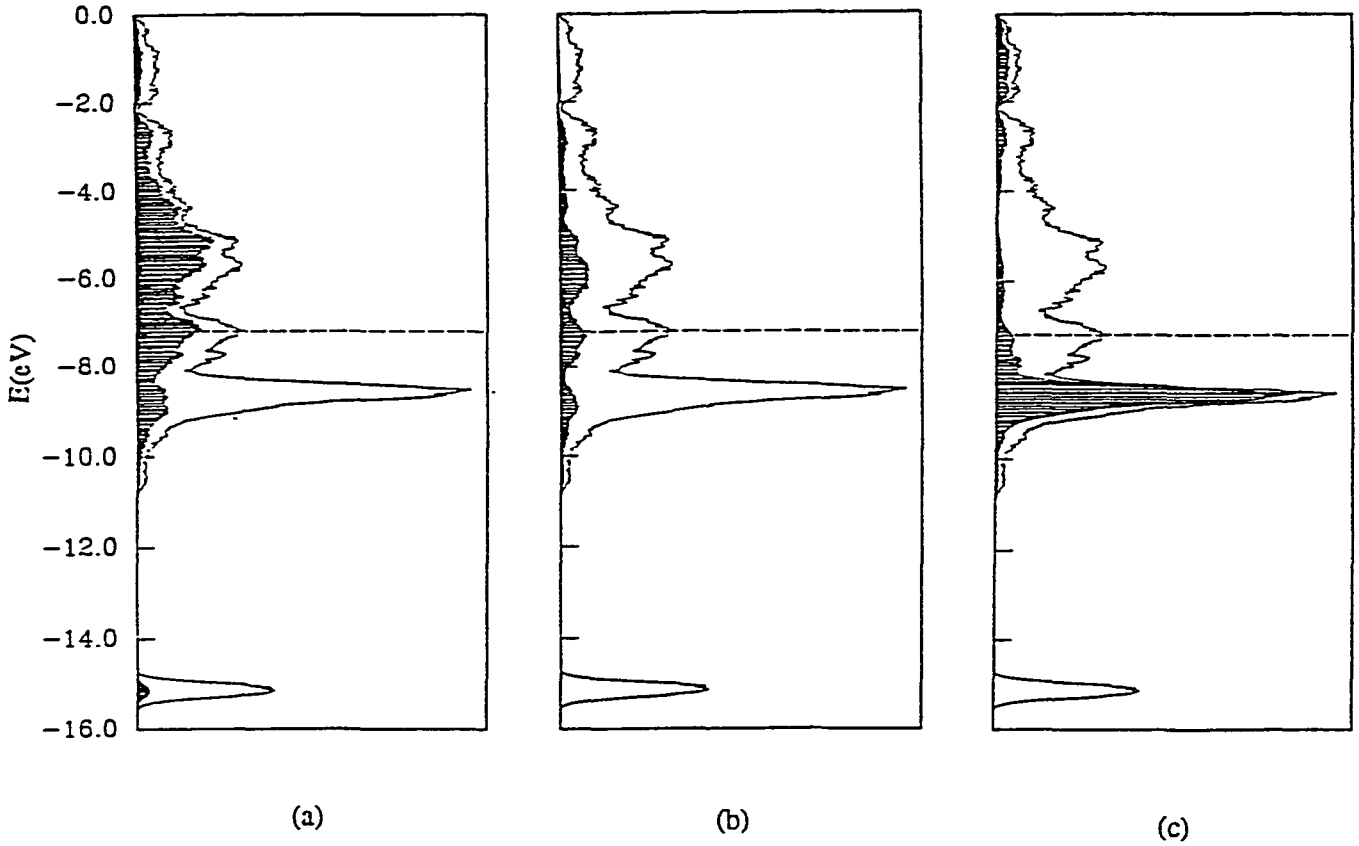

Figure 4.9 Projection of individual atomic contributions on total DOS for Zr_4Ni_2O.
(a) Projection of Zr1 on total DOS (b) Projection of Zr2 on total DOS (c) Projection of Ni on total DOS

atoms to nearly the same level. There is less charge transfer between zirconium and nickel, or less ionic character, indicative of metal - metal bonding and more realistic for intermetallic compounds, as for example, nickel changes from $Ni^{-0.7}$ when the initial parameters are used, to $Ni^{-0.3}$ using the parameters obtained from the charge iteration. The Zr2 becomes negatively charged. Oxygen builds up a higher charge, as these orbitals are kept at low energy even as the metal orbitals rise as a result of the charge iteration.

Table 4.7 Calculated orbital populations

Atom	Initial parameters	Charge iteration parameters
Zr1	3.1	3.3
Ni	10.7	10.3
Zr2	4.0	4.3
O	7.1	7.4

For comparison of results a consistent set of parameters is needed. The results reported here are those obtained using the parameters from the charge iteration procedure. In all of the calculations, the Zr1 atoms were placed on the "idealized" atom position [84], making all octahedral sites equal in size to avoid biasing the results and favoring a site for oxygen occupancy dependent on size factors. The nickel position was shifted to be between the observed atom position and the "idealized" atom position. The approach taken to this problem was to determine the effect the ordering of oxygen would have in the density of states and the total energy in the Zr_4Ni_2O phase. Figure 4.10 (a) shows the total density of states for the hypothetical oxygen-free Zr_4Ni_2 with the Ti_2Ni type structure. One can see in Figure 4.10 (b) the effect adding oxygen has to the DOS curve. The nickel band is unaffected by the addition of oxygen, as expected, since there are no nickel - oxygen interactions. Small changes in the DOS are seen at -7 and -9 eV, as zirconium metal

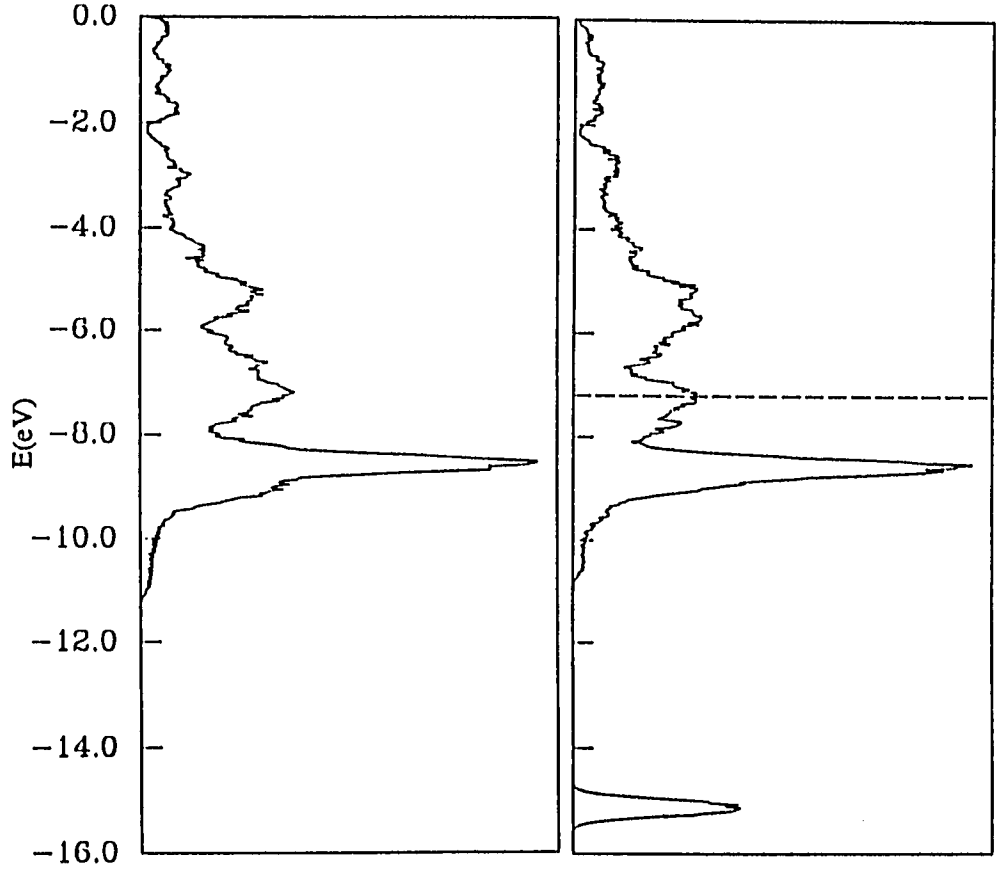

Figure 4.10 Effect on DOS of adding oxygen to the system
(a) DOS plot for hypothetical Zr_4Ni_2
(b) DOS plot for Zr_4Ni_2O.

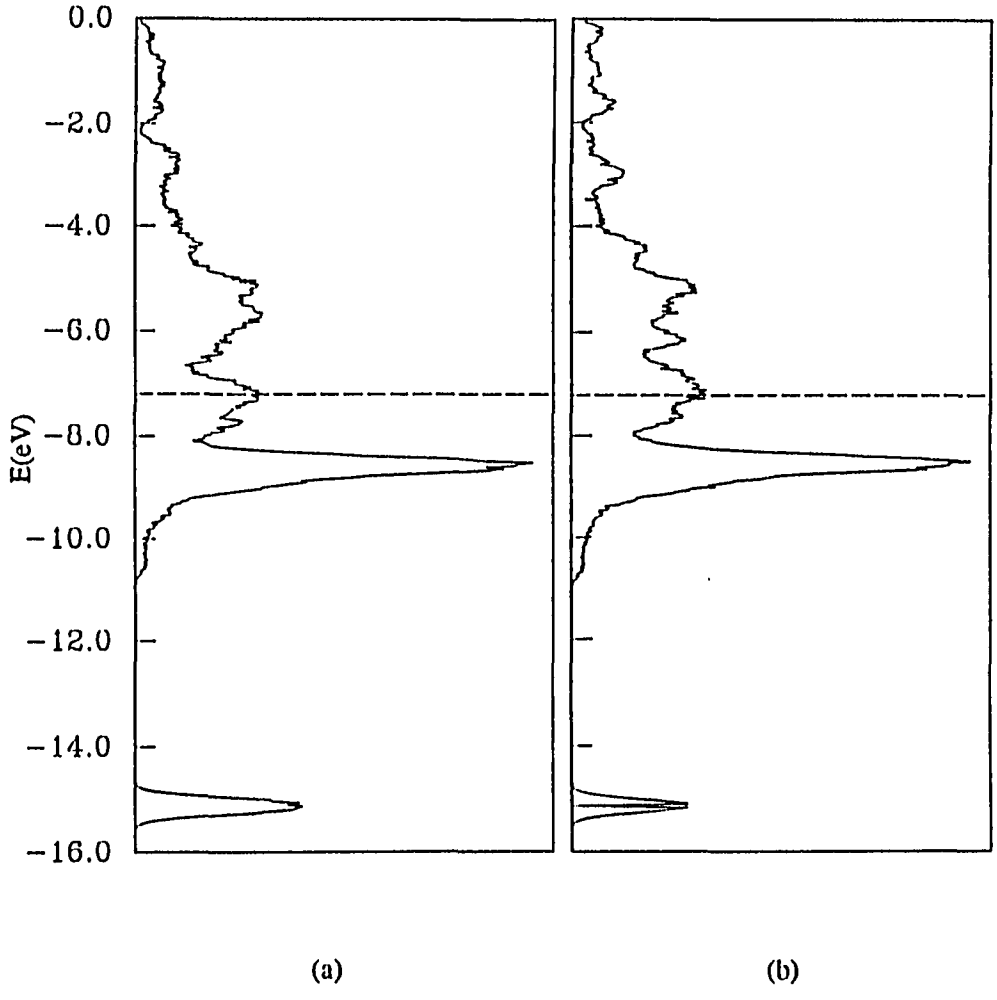

Figure 4.11 Effect on DOS of oxygen occupying different crystallographic sites.
(a) DOS when oxygen occupies 16*c* site, as observed in Zr_4Ni_2O.
(b) DOS when oxygen occupies 8*a* site, as in hypothetical $Zr_4Ni_2O_{1/2}$.

becomes involved in zirconium - oxygen bond formation. Figure 4.11 compares the effect on the DOS of adding oxygen to the sixteen - fold site, as is observed by the single crystal refinement, and adding oxygen to the other possible octahedral site, an eight - fold site. Little difference is observed between the two plots. The Fermi energies and total energies for each of these calculations are shown in Table 4.8. The bottom row of Table 4.8 is the total energy gain per oxygen atom added to the system. The formation of Zr_4Ni_2O from Zr_4Ni_2 decreases the total energy of the system from -1225.62 eV to -1775.43 eV, or by -549.81 eV. There are four oxygen atoms in the primitive unit cell, so the energy change per oxygen atom is one-fourth the total change, or -137.45 eV. By comparing the change per oxygen atom, the results of adding different amounts of oxygen can be compared. The table shows the two results differ by only 0.31 eV per oxygen. The calculated preferred ordering is in favor of the observed result, but it is doubtful the difference is significant within the errors of the calculations associated with the approximations of the extended Hückel method.

Table 4.8 Fermi energy and total energy of calculated phases (eV)

	Zr_4Ni_2	$Zr_4Ni_2O_{1/2}$	Zr_4Ni_2O
Fermi energy, E_F	-7.242	-7.212	-7.205
Total energy, E_T	-1225.62	-1499.91	-1775.43
ΔE_T/oxygen		-137.14	-137.45

The results of the single crystal refinement of Nb_6Ni_6O show the oxygen can occupy the eight - fold site in the structure. Not only is the oxygen occupancy different in this compound from Zr_4Ni_2O, but the metal/metal ratio is also different. An attempt was made to determine if there was a correlation between the differences in the oxygen and metal orderings. Calculations were done on the compound Nb_6Ni_6O, using for niobium the zirconium parameters from the charge iteration.

Figure 4.12 illustrates how changing the metal framework from the hypothetical Nb_8Ni_4 to the also hypothetical Nb_6Ni_6 effects the DOS. The nickel d band is broadened slightly, as might be expected from additional nickel atoms. Figure 4.13 is the result of the calculations for the observed Nb_6Ni_6O and the hypothetical $Nb_6Ni_6O_2$. Table 4.9 lists the energies associated with each of these phases. Again, there is little difference observed in the DOS plots. The changes in energy per oxygen atom are such that the observed phase is again favored, but by only 0.15 eV. In addition to the uncertainty within the calculations, another caution to the interpretation of these numbers must be added. The calculations do not allow for nonstoichiometry, or partial filling of the sites. If only half of the sixteen - fold sites are occupied by oxygen, the stoichiometry is the same as for the the observed phase, Nb_6Ni_6O. The program does not allow random partial occupancy of any sites. Electron counts can be varied, but the sites must be either completely filled or empty. For this calculation, then, two of the four oxygen sites were filled, and the other two were empty. The total energy for this phase was -1789.01 eV, resulting in a stabilization of -136.82 eV per oxygen atom. This is only 0.04 eV difference with the calculated energy for the observed structure. If these results show anything, it may be that the important consideration is not which site is occupied, but rather the amount of oxygen the system requires for maximum stabilization.

Crystal orbital overlap population (COOP) curves were calculated for the interactions in Zr_4Ni_2O. The calculated overlap populations are tabulated in Table 4.10. Nickel - nickel overlap population was very low, about one one-thousandth, and is not included in the table. There are twenty - four symmetry related Zr2 - Zr1 interactions in the unit call. In fact, there are twenty - four symmetry related interactions for each of the combinations listed. The sum of the overlap populations of the symmetry related bonds are plotted in the COOP curves. The program would not yield the sum of all the overlap populations in one curve, so the interactions were broken down into smaller groups. Figure 4.14 (a) contains the sum of all Zr2 - Zr1 and Zr2 - Ni overlap

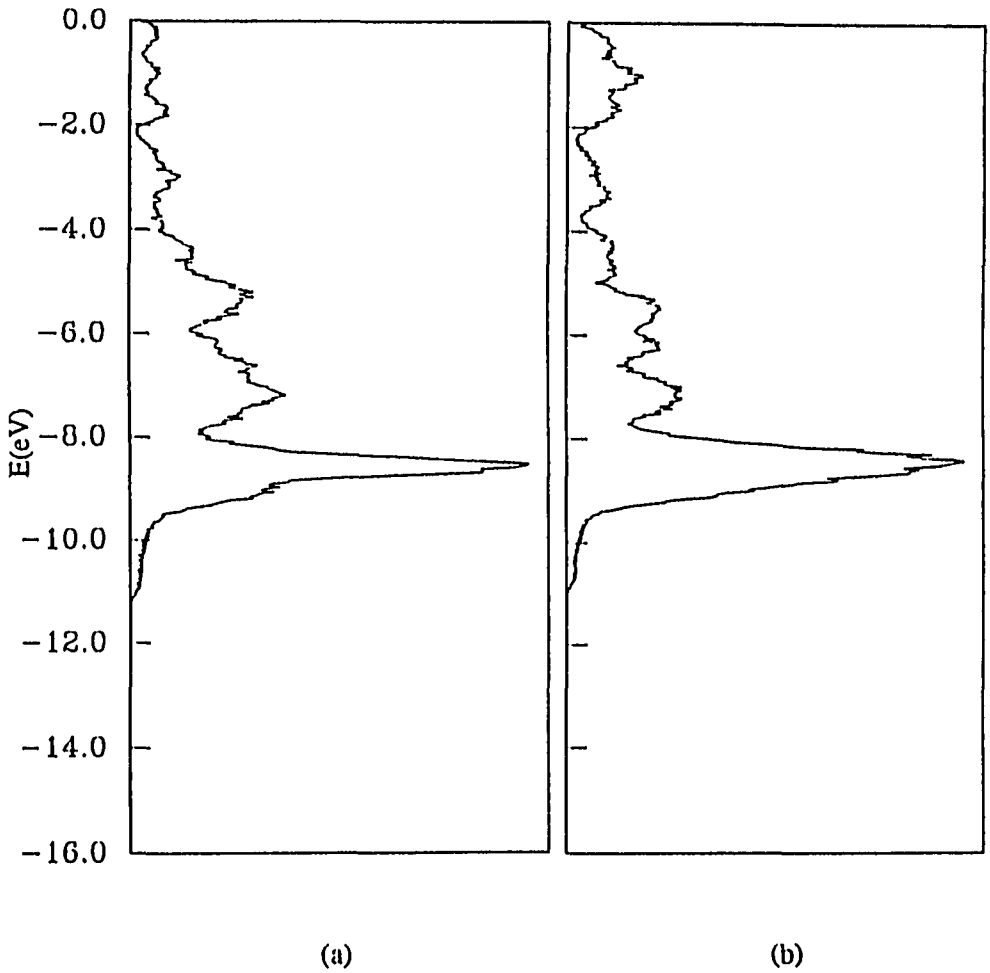

Figure 4.12 Effect on DOS of changing metal/metal ratio in Ti_2Ni type structure.
(a) DOS for Nb_8Ni_4
(b) DOS for Nb_6Ni_6

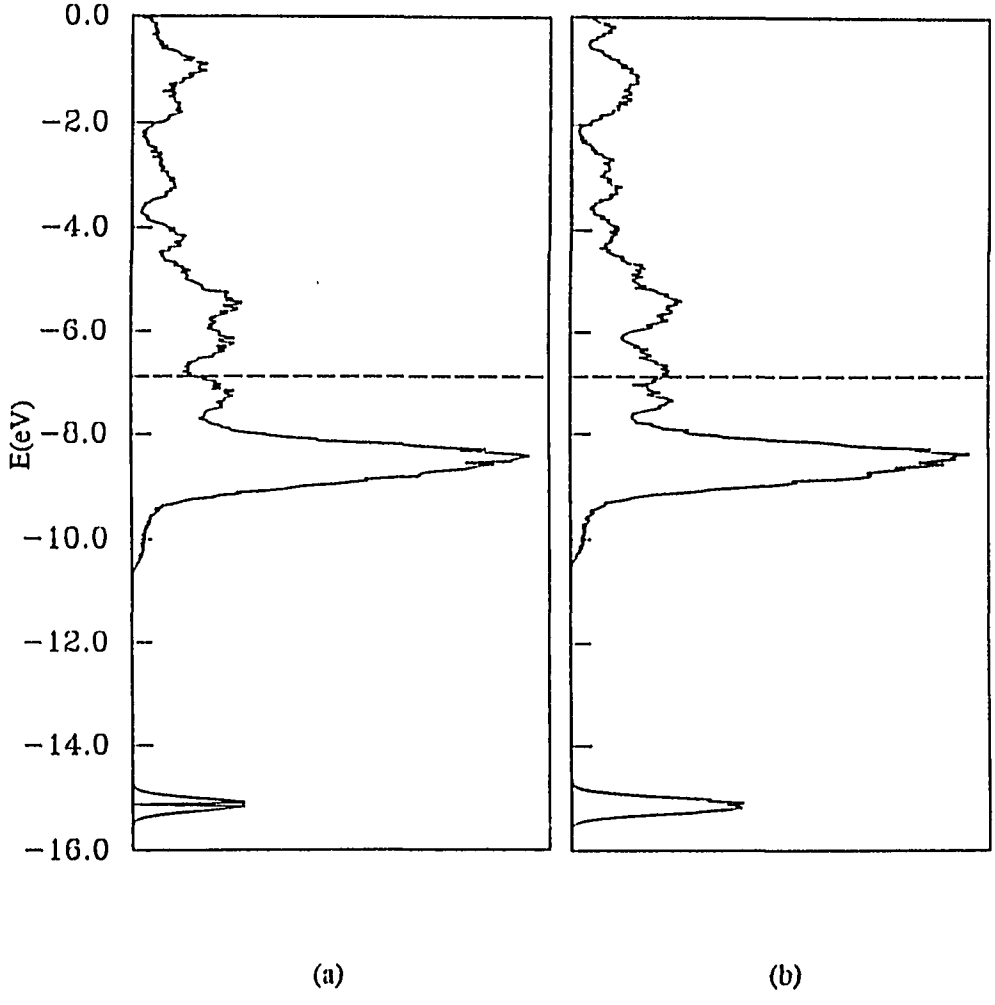

Figure 4.13 Effect on DOS of oxygen occupying different crystallographic sites.
(a) DOS when oxygen occupies the 8*a* site, as observed in Nb_6Ni_6O.
(b) DOS when oxygen occupies the 16*c* site, as in hypothetical $Nb_6Ni_6O_2$.

Table 4.9 Fermi energy and total energy of calculated phases (eV)

	Nb_6Ni_6	Nb_6Ni_6O	$Nb_6Ni_6O_2$
Fermi energy, E_F	-7.087	-7.027	-6.817
Total energy, E_T	-1515.37	-1789.10	-2062.22
ΔE_T/oxygen		-136.86	-136.71

Table 4.10 Overlap populations for Zr_4Ni_2O

Atomic interaction	Overlap population	Interatomic distance (Å)
Zr2 - Zr1	0.1646	3.12
Zr1 - Ni	0.1347	2.76
Zr1 - O	0.1089	2.27
Zr2 - Ni	0.1014	2.67
Zr1 - Zr1	0.0980	3.21
Zr1 - Ni	0.0412	3.10

populations. Figure 4.14 (b) contains the sum of the Zr1 - Zr1 and the short Zr1 - Ni overlap populations. Each of these COOP curves show empty bonding orbitals above the Fermi level. The only indication of antibonding character at the Fermi level is in the COOP curve for Zr1 - O interactions, in Figure 4.14 (c). The calculation of empty bonding levels was the motivation for the synthesis of more electron - rich compounds than Zr_4Ni_2O, substituting niobium for zirconium, or copper for nickel.

Discussion

The Ti_2Ni type structure has been described in terms of two interpenetrating three-dimensional networks made of idealized octahedra and tetrahedra [84]. Table 4.2 lists the idealized positions that

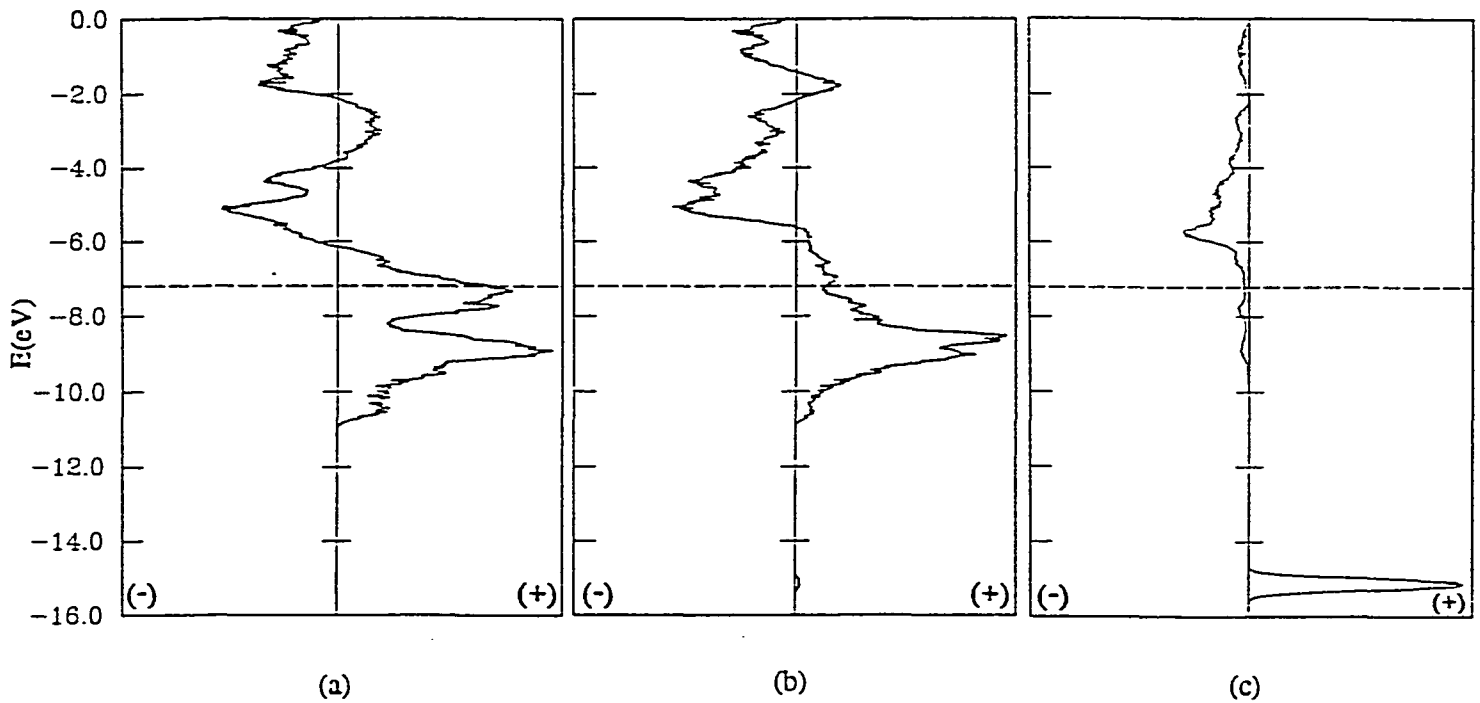

Figure 4.14 COOP curves for Zr_4Ni_2O. Fermi level indicated by dashed line. Bonding interactions indicated by (+), and antibonding by (-). (a) Sum of Zr2 - Zr1 and Zr2 - Ni overlap populations. (b) Sum of Zr1 - Zr1 and Zr1 - Ni overlap populations. (c) Sum of Zr1 - O overlap populations.

would give regular polyhedra. A network of octahedra is formed by the metal atoms on the 48*f* site. Figure 4.4 shows this network of octahedra, with oygen occupying the 16*c* site. With the idealized parameters, M1 is at (x,0,0) with $x = 0.1875$, and all the face sharing octahedra are exactly the same size. When x deviates from this position the octahedra centered at an 8*a* site maintain ideal octahedral symmetry, but the other octahedra, centered at 16*c* site, lose their four fold symmetry, and become distorted octahedra, or more precisely, trigonal antiprisms. The direction of the deviation of x from ideality is related to the oxygen occupancy. The octahedra, regular or distorted, centered by oxygen are expanded. When oxygen occupies the 8*a* site, at the origin, the expansion of the regular octahedron corresponds to an increased value for x (compare Nb_6Ni_6O, with $x = 0.1996$, and ideal $x = 0.1875$). Occupancy of the 16*c* site causes expansion of the distorted octahedra, or trigonal antiprisms, and a corresponding decrease in x (compare $x = 0.1852$ in Zr_4Ni_2O and $x = 0.1867$ in $Nb_6Ni_4Ta_2O_2$, with ideal $x = 0.1875$). The expansion of the oxygen - centered octahedra can be interpreted as resulting from the filled antibonding metal - oxygen orbitals, as seen in Figure 4.14 (c) for Zr_4Ni_2O. Oxygen occupancy is not the full story, however. In the case of the binary Ti_2Ni [79], with no oxygen, $x = 0.189$, and is also expanded from the ideal framework. Likewise, in $Zr_6Ni_4Ti_2O_{0.6}$, where oxygen is in both sites, x increases. Only one reference suggests the simultaneous occupation of both 8*a* and 16*c* sites in $Nb_8Zn_4C_3$ [71], noting the C-C separation would be comparable to the spacing between octahedral sites in the filled - Mn_5Si_3 type structures. The stoichiometry of this phase was determined by elemental analysis on a heterogeneous sample. The coordination number of an interstitial atom in the Mn_5Si_3 structure is 6 + 2. The interstitial atoms in a Ti_2Ni structure with all octahedral sites filled would have coordination numbers of 6 + 2 and 6 + 4. Refinement results of $Zr_6Ni_4Ti_2O_{0.6}$ are the first indication of partial occupancy of both sites. All previous reports in which interstitial atomic parameters are refined indicate occupancy of either the 8*a* or 16*c* site, but not both.

Interpenetrating the octahedral network is another network made of corner-sharing stella quadrangula. See Figure 4.5. An ideal stella quadrangula is defined as consisting "of four regular tetrahedra, each sharing one face with a central, fifth tetrahedron, which is also regular (or four regular tetrahedra each sharing three edges, one with each of its three neighbors)." [84] In these compounds the central tetrahedron is always Ni, on the 32*e* site, and the other atoms are the metals on the 16*d* site, which cap the faces of the Ni_4 tetrahedra. None of these tetrahedra are centered by interstitial atoms. The fractional coordinate of x for the metal atom at 32*e* has been converted from the value in the source to the alternate but equivalent value corresponding to the conventional positions. The atom position for Ni at 32*e*, (x, x, x), shifts from the ideal $x = 0.8250$ to the observed $x = 0.8311$ to $x = 0.8396$. The effect of increasing the x parameter is to enlarge the central nickel tetrahedron. A look at the distances in Table 4.4 shows these units are far from regular stella quadrangula. In all cases the central Ni_4 tetrahedron is expanded ($d_{Ni\text{-}Ni} > d_{Ni\text{-}M2}$). Zr_4Ni_2O shows the largest departure from ideality. For the ideal structural arrangement of this compound, $d_{Ni\text{-}Ni}$ = 2.5873 Å. The observed distance is much larger, $d_{Ni\text{-}Ni}$ = 3.0910 Å. The distance between the nickel atoms and the zirconium atoms in the octahedral network consequently decreases considerably from the ideal. Compare the observed $d_{Zr1\text{-}Ni}$ = 2.783 Å with the ideal $d_{Zr1\text{-}Ni}$ = 3.0224 Å in Zr_4Ni_2O. This bond lengthening within the Ni_4 tetrahedron suggests Ni-Ni interactions are weakening, relative to Zr-Ni interactions. It is tempting to suggest this is supported by the calculated overlap populations, where nickel - nickel overlap was more than an order of magnitude lower than the other interactions. The zirconium - nickel overlap populations, on the other hand, were quite significant (see Table 4.10). However, comparisons between overlap populations must be done with care. The overlap population between atoms A and B is defined as being proportional to $c_{iA}c_{jB}S_{ij}$, where c is the orbital coefficient, and S is the overlap integral. Overlap populations of Ni-Ni interactions can only be compared to other Ni-Ni interactions, and even then only when

distances are the same, since S is a function of distance. Then, if there is a difference in the overlap populations is it related to chemical interactions driven by symmetry rather than by distance. But if these Zr-Ni interactions are strong, as mentioned above, this suggests that the visual description of the structure in terms of two interpenetrating networks does not accurately portray the chemical interaction between the two networks. Rogl [90] perhaps recognized this, and described the structure in terms of the packing of the icosahedral units around the M2 atoms at the 16*d* sites. Figure 4.5 only shows the six nickel atoms around M2. Table 4.4 lists the coordination also to six M1 atoms, and they arrange in a distorted icosahedral coordination. The Zr1 - Zr2 and Zr1 - Ni interactions are exactly the bonding connections between the two networks. Note the highest orbital overlap populations in Table 4.10 involve interactions *between* the two interpenetrating networks, rather than within a network.

The inherent beauty of this structure has not been overlooked by others. Calculations of periodic minimum surfaces for W_3Fe_3C of this structure type divide the structure into two interpenetrating networks, and suggest the mode for wearing of this high speed steel [91]. Two flaws appear in this article. First, W_3Fe_3C is not responsible for the characteristic properties of high speed steel [70]. Second, periodic minimum surfaces cannot be generated for certain space groups, $Fd\bar{3}m$ among them [92]. However, periodic equi-potential surfaces and periodic zero potential surfaces can be generated for this space group. The potential surfaces of appropriate Coulombic fields are very similar in shape to minimal surfaces, but can be correlated to the spatial distribution of the electrons, and hence correlated to physical properties. For the Ti_2Ni structure the potential surface resides between the two interpenetrating networks. One can assume that the weakest bound electrons are located close to the potential surface. In a metal, these are the conduction electrons. This view of potential surfaces in no way contradicts the finding here of significant interaction between the two structural networks.

It is interesting to note some structural similarities with other phases here. A two-dimensional analogue to the three-dimensional network of face-sharing zirconium octahedra is seen in the kappa phase [80] and the new $Zr_6Ni_6TiSiO_{1.8}$ structure [81]. In each case, rings of twelve face-sharing octahedra form. In the case of all three of these structures, icosahedral units fill the void spaces and link the octahedral networks.

The results of this study can be rationalized in a system by system manner. In the Nb/Ni/O system the two phases Nb_4Ni_2O and Nb_6Ni_6O occur. This occurance was not observed in the Zr/Ni/O system. This may be explained by looking at the phase diagrams of the intermetallic Zr/Ni and Nb/Ni systems. In the Nb/Ni binary system there are only two compounds, $NbNi_3$ and Nb_7Ni_6, which compete with formation of the ternary oxide. In neither case is the Nb:Ni ratio 1:1 or 2:1. The binary intermetallics in the Zr/Ni system, especially ZrNi, compete more favorably with the formation of the ternary oxide. The oxygen occupancy in the Nb_4Ni_2O phase has not been determined experimentally, but is based on the assumption that the oxygen occupancy in this phase is the same as for $Nb_6Ni_4Ta_2O_2$. The two phases Nb_6Ni_6O and Nb_4Ni_2O show different Nb/Ni ratios and different oxygen content. The band calculations on Nb_6Ni_6O suggest the ordering of the oxygen may not be as important as the total amount of oxygen present. Figure 4.15 (a) outlines the possibility of adding different amounts of oxygen to metal frameworks with different Nb/Ni ratios. With oxygen acting as an electron sink, the core with more free valence electrons in the conduction band will favor adding more oxygen atoms. Assuming a filled d^{10} configuration, Nb_8Ni_4 contains 80 free valence electrons per primitive unit cell, and Nb_6Ni_6 has 60 electrons. Thus Nb_8Ni_4 will add two oxygen atoms per formula unit to form $Nb_8Ni_4O_2$ and Nb_6Ni_6 will add only one to form Nb_6Ni_6O.

The same conclusion is reached if the oxygen ordering is assumed to determine the metal ratios, rather than the metals determining oxygen ordering as described above. In this case, the two

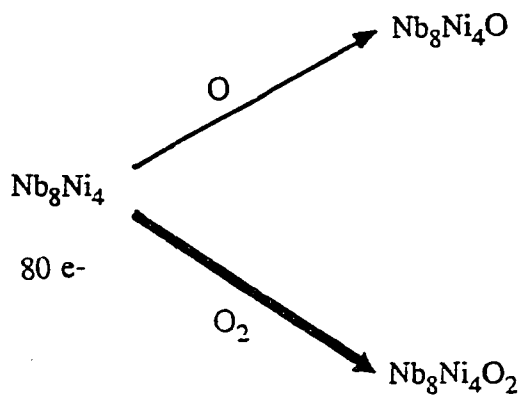

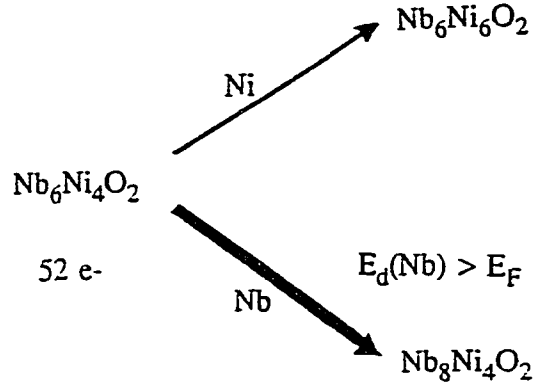

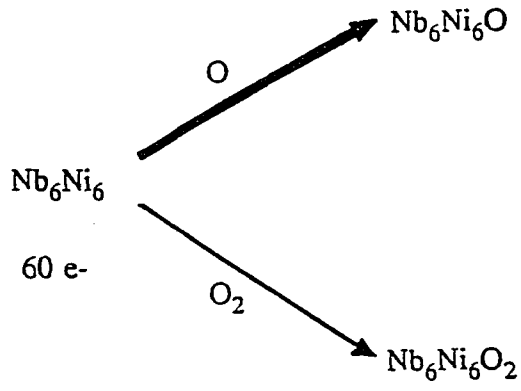

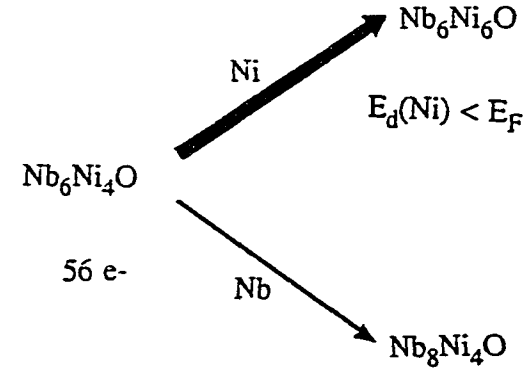

(a) (b)

Figure 4.15 (a) Addition of oxygen to hypothetical metal framework follows path shown by bold arrows.
(b) Addition of capping metal atoms to core compounds follows path shown by bold arrows.

core compounds with different oxygen content, Nb_6Ni_4O and $Nb_6Ni_4O_2$, can add either niobium or nickel to the 16*d* site (Figure 4.15 (b)). Nb_6Ni_4O has 56 free electrons in its conduction band, and $Nb_6Ni_4O_2$ has 52. Since Nb_6Ni_4O is more electron rich it will more readily add nickel, whose atomic orbitals lie lower in energy than the Fermi level and will act as electron acceptors, than gain electrons by adding niobium. $Nb_6Ni_4O_2$, with fewer free electrons will favor the addition of niobium, whose orbitals lie above the Fermi energy and will act as electron donors to form $Nb_8Ni_4O_2$, or Nb_4Ni_2O. While this explanation is internally consistent, it does not explain the formation of phases like Mo_6Co_6C and $Mo_6Co_6C_2$ where both possible orderings of interstitials are observed for a single metal ratio. A $Nb_6Ni_6O_2$ phase may also exist, but the corresponding shift in lattice parameters would be minimal, and would require sufficient diffraction data for structural analysis. However, the formation of this phase is unlikely. When additional oxygen was added in the synthesis NbO and Ni formed as minor phases.

The formation of only $Nb_6Ni_4Ta_2O_2$, and no other tantalum containing compounds, can be explained on the basis of work on mixed niobium/tantalum sulfides performed previously in this lab [19,20]. In these sulfides, the formation of certain phases depends on the relative strengths of metal -sulfur bonds and metal - metal bonds. The same interplay between metal - oxygen and metal - metal bonds exists in these oxide phases. Generally speaking, Ta-O bonds are stronger than Nb-O bonds, by electronegativity arguments. Also, Ta-M bonding among transition metals is generally stronger than Nb-M bonds in a given structure, because of greater d-orbital expansion and overlap of 5d transition metals. In the Ti_2Ni type structure one must consider the balance between the M-O and the M-M bonding. It was found that Nb_4Ni_2O forms. In this structure, the oxygen is surrounded by niobium in the 48*f* site, forming Nb_6O octahedra. The other niobium atom sees only other metal atoms, icosahedrally coordinated to six nickel and six niobium atoms. When tantalum replaces niobium in the 16*d* site, oxygen still sees only niobium, but now tantalum can increase the

metal-metal interactions in the structure. If, however, tantalum were to replace the other niobium atoms, the stronger Ta-O bonds would come *at the expense* of the Ta-M bond strength, shifting the balance of metal - oxygen versus metal - metal bond strength, and the phase becomes unstable with respect to formation of the binary phases.

One can consider the role of oxygen in stabilizing the Ti_2Ni type structure in the Zr_4Ni_2O phase. Oxygen is also necessary for the formation of the Hf_4Ni_2O phase [73], but is not necessary for Ti_2Ni. A principle difference between titanium on the one hand, and zirconium and hafnium on the other, is the orbital expansion of the d orbitals for zirconium and hafnium and the corresponding increase in metal - metal bond strength. The binary intermetallic phases that form are the arrangements of atoms that maximize the bonding energy between them, and thus minimize the Gibbs free energy. The phases in the Zr/Ni system are different than those in the Ti/Ni system because the bonding energies of zirconium and titanium are different. When oxygen is added to the Zr/Ni system and zirconium - oxygen bonds form, the zirconium - metal bonding decreases. This decrease in metal - metal bonding makes it more like the Ti/Ni system, and the filled Ti_2Ni phase is stabilized with respect to the binary phases. In the mixed Zr/Ti phase, $Zr_6Ni_4Ti_2O_{0.6}$, even less oxygen is required, as would be expected.

5. NEW ZIRCONIUM KAPPA PHASES

Introduction

The kappa phases are an interesting set of compounds. The kappa phase is of the general form $M_9M'_4X$, where M and M′ are transition metals, M being the more electropositive of the two. They exist for a wide variety of interstitial atoms, and for a wide combination of transition metals. Recently, superconductivity has been discovered in a kappa phase [21]. Interest has also been expressed in studying the catalytic properties of these compounds in processes where Chevrel phases have been studied. If a technological interest arises for these kappa phases, many of which have been known for quite some time, they may come under intense physical and chemical study. The work reported here demonstrates that through the use of modern techniques these compounds may each be found to be significantly more complicated than the formula suggests. Both the transition metal framework and the interstitial atoms demonstrate significant deviation from ideality. Specifically, the mixing of M and M′ on the metal atom sites can change the stoichiometry substantially from the $M_9M'_4X$ formula. Secondly, the formula, as written, does not reveal the presence of a second interstitial site, the occupation of which may have been undetected in the earlier work. The possibility exists for two different interstitial sites to be occupied by the same element, or by different elements, or for one site to be preferentially occupied in one compound and the other site to be occupied in another compound. The interstitial sites may also undergo substitution and/or exhibit partial occupancy or nonstoichiometry. Each of these are considered later in more detail, but this serves to illustrate that the findings of this study will be important in any future work on these kappa phases. Specifically, the presence of light interstitial elements must be considered, i.e. by performing the synthesis with both the intentional and unintentional presence of oxygen, for example, and noting changes in lattice parameters. In some cases, the formation of the

phase may be affected by the presence of the interstitial atoms. Chemical analysis, i.e. by EDS, is important for determining ranges of substitution in metal atoms, and in the interstitial atoms. Finally, the importance of the precision of single crystal diffraction studies cannot be overstated.

Many examples of the hexagonal kappa phase in ternary systems have been reported since their original discovery [93,94]. Table 5.1 shows the surprising variability and adaptability in the elements which fill the X position in the kappa phase. X can be one of several p-group elements or an iron group 3d transition metal.

Table 5.1 Known kappa phases ($M_9M'_4X$)[a]

M-M′-X	X	M-M′-X	X
Zr-Os-X	O	Ti-Fe-X	O
Zr-Re-X	B,O	Ti-Mn-X	O
Zr-Mo-X	B,O,Fe,Co,Ni[b],S[b]	Mo-Cu-X	Al/C
Zr-W-X	B,O,S[b],S/Ni[b]	Mo-Ni-X	Al/C
Zr-Nb-X	S[c]	Mo-Co-X	Al/C
Zr-Ta-X	S[c]	Mo-Fe-X	Al/C
Hf-Os-X	B,O,Si,P,S,Ge,As, Se,Fe,Co,Ni	Mo-Mn-X	Al/C
Hf-Re-X	B,O,Si,P,S,Ge,As, Se,Fe,Co,Ni	W-Ni-X	C
Hf-Mo-X	B,O,Si,P,S,Ge,As, Se,Fe,Co,Ni	W-Co-X	C
Hf-W-X	B,O,P,S,Ge,As,Se, Fe,Co,Ni	W-Fe-X	C, Al/C
Hf-Nb-X	S[c]	W-Mn-X	C, Al/C
Hf-Ta-X	S[c],Se[d],S/Se[d]	W-Cr-X	C

[a] Table adapted from [94]
[b] [80]
[c] [21]
[d] [95]

The above formulation is somewhat simplified in that it does not reveal the fact that the interstitial elements can occupy different interstitial sites. To take this into account the formula can be rewritten $M_9M'_4X_1X'_3$, where X is an interstitial atom on the 2*c* position, a trigonal prismatic site, and X′ is an interstitial atom on the 6*g* position, an octahedral site. It has been convenient up until now to consider just one interstitial site because all previous reports, with three exceptions, have indicated occupancy of only one site or the other, but not both. These exceptions are the carbides W-Fe-C and W-Co-C, where both sites are simultaneously occupied, but with 50% of the 2*c* site vacant [96,97]. Hf-Mo-S has also been reported with complete filling of the 2*c* site, but only partial filling (6-9%) of the 6*g* site by S [98]. The ternary Hf-Mo-Ge kappa phase is found to be a quaternary, Hf-Mo-Ge-O, with germanium on the 2*c* site, and oxygen on the 6*g* site, and vacancies on both sites [99]. Besides these three exceptions, the kappa phases are reported to have only one interstitial site occupied. The oxides are thought to contain oxygen in the octahedral site, and all other interstitial atoms, X, occupy the larger trigonal prismatic site. The results of this study demonstrate that simultaneous occupation of both sites is at least a common, and sometimes necessary, condition. The new zirconium-containing kappa phases, $Zr_9W_4SO_x$, $Zr_9Mo_4SO_x$, and $Zr_9W_4(S/Ni)O_3$, have been synthesized. The Zr_9W_4Ni phase has been determined to be oxygen stabilized. The lattice parameters of the new phases are reported, as well as the single crystal refinement of the nickel substituted sulfide. This last compound is an example of nickel substitution for sulfur in metal rich chalcogenides, a previously reported effect [27]. In addition, this compound shows the ability of the structure to fully occupy the octahedral interstitial sites with oxygen.

Before proceeding further with the chemistry of the kappa phase it is useful to look more closely at the structure of this phase. The unit cell is hexagonal ($P6_3/mmc$) with a *c*/*a* ratio nearly equal to one. Figure 5.1 shows in projection a layer network of face sharing octahedra. In terms of the $M_9M'_4X_1X'_3$ formula, this figure contains only the $M_9X'_3$ portion. The hexagonal unit cell is

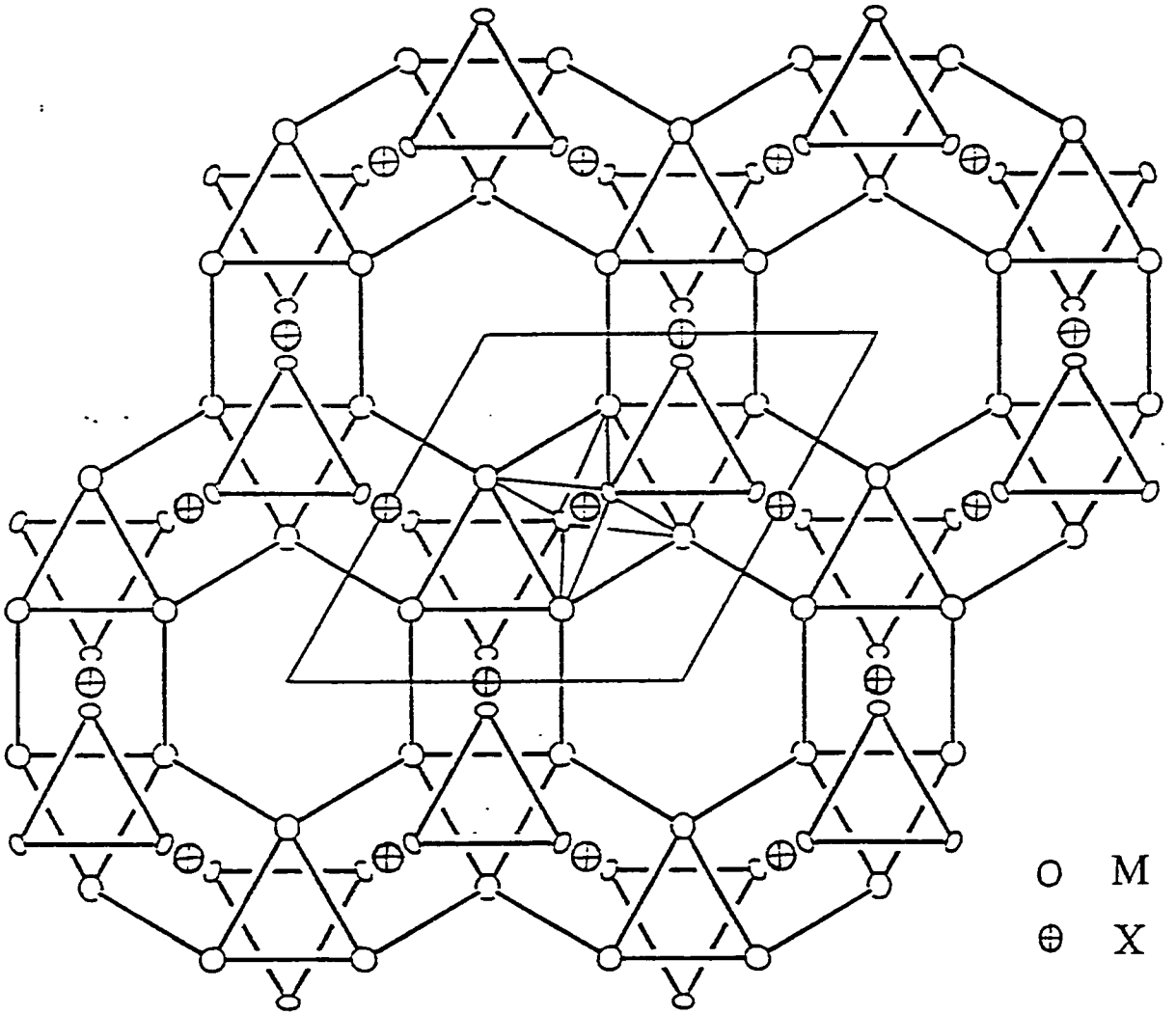

Figure 5.1 Projection of M_9X_3' portion of $M_9M_4'XX_3'$ kappa phase, showing network of face sharing octahedra. Central octahedron is outlined for clarity. Alternating octahedra are centered by interstitial atom X'.

outlined. The octahedron in the center of the unit cell is also outlined for clarity, and is centered by an X′ atom. This octahedron shares two opposite faces with octahedra which are seen in projection along their three fold axis. The face sharing octahedra form rings containing twelve octahedra. The octahedra are alternately centered and empty. In terms of a zirconium network of face sharing octahedra there is a surprising relation between the kappa phase and the Ti_2Ni-type structure. In the kappa phase a two-dimensional hexagonal layer forms from these octahedra, which are alternately filled and empty. In the cubic Ti_2Ni-type structure, these rings of face sharing octahedra form a three-dimensional network. In these cases, similar building blocks arrange to form strikingly different structures. Oxygen is essential to the formation of this network of octahedra in these kappa phases as well as in the Ti_2Ni-type phases containing zirconium.

The interstitial sites are more clearly seen viewing along the [110] direction. In Figure 5.2 trigonal prismatic sites and two crystallographically distinct octahedral sites are shown. The trigonal prisms are tricapped, although only one face is shown capped in the figure. The octahedra above and below the trigonal prism have their center at the 4*f* site and are vacant in all known cases. The octahedra which are occupied by interstitial atoms are those shown between the trigonal prisms. These form a zig-zag chain of corner-sharing octahedra along the *c*-axis. This network shown consists only of the metal M atoms.

Figure 5.3 is a projection of the complete structure. Icosahedral units fill the voids in the octahedral network. These icosahedra share faces to form a chain along the *c*-axis. The icosahedra are all centered by metal M′ atoms (Figure 5.4).

Such is the structure of the kappa phase. The variability in X and X′suggests the formation of this phase depends largely on the strength of the metal-metal interactions within the framework of this structure. In fact, the kappa phase may be considered a filled variant of the intermetallic compounds Mn_3Al_{10} and Co_4Al_{10}.

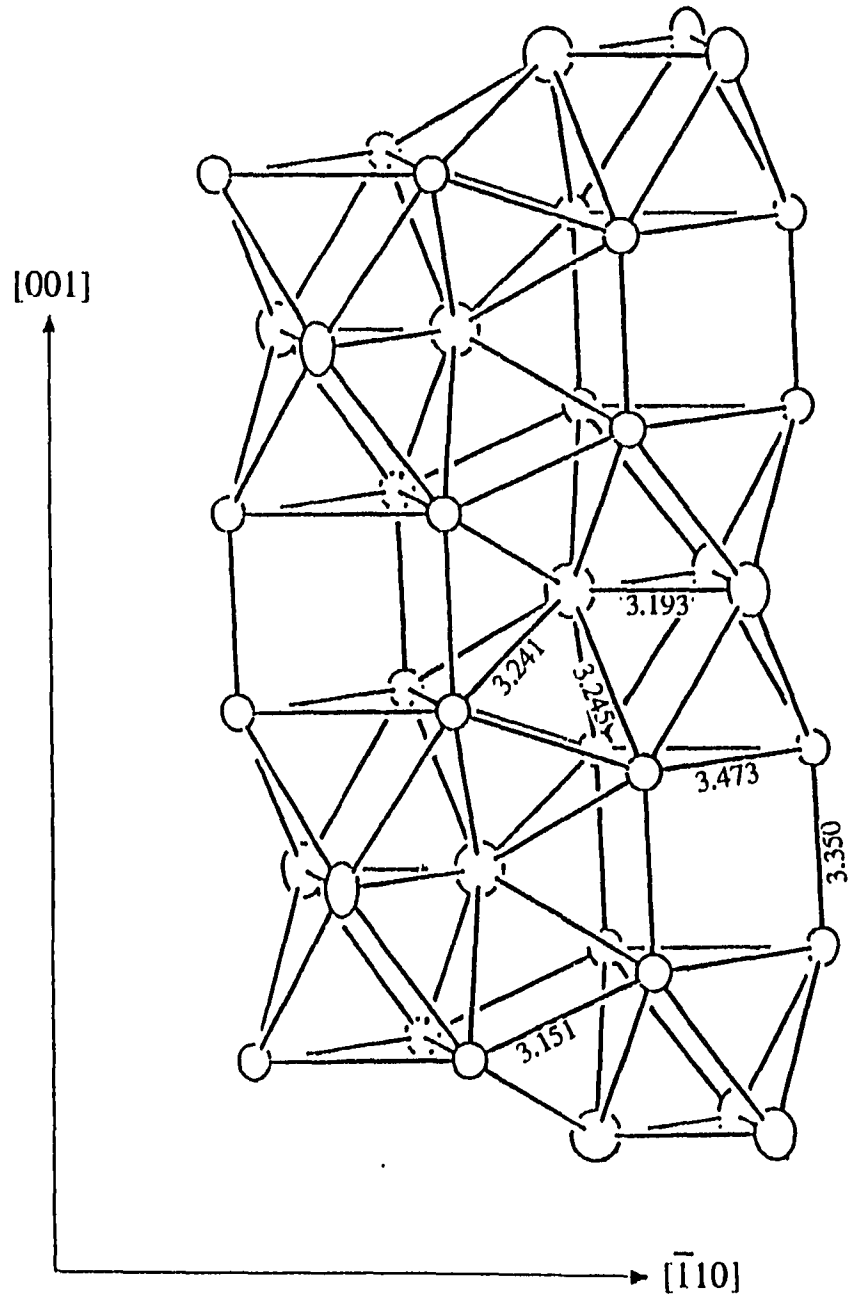

Figure 5.2 Portion of the kappa phase structure, showing only the metal atoms M, projected along a plane almost perpendicular to the (110) plane. Octahedral and trigonal prismatic interstitial sites clearly seen. Distances shown for $Zr_9W_4(S/Ni)O_3$.

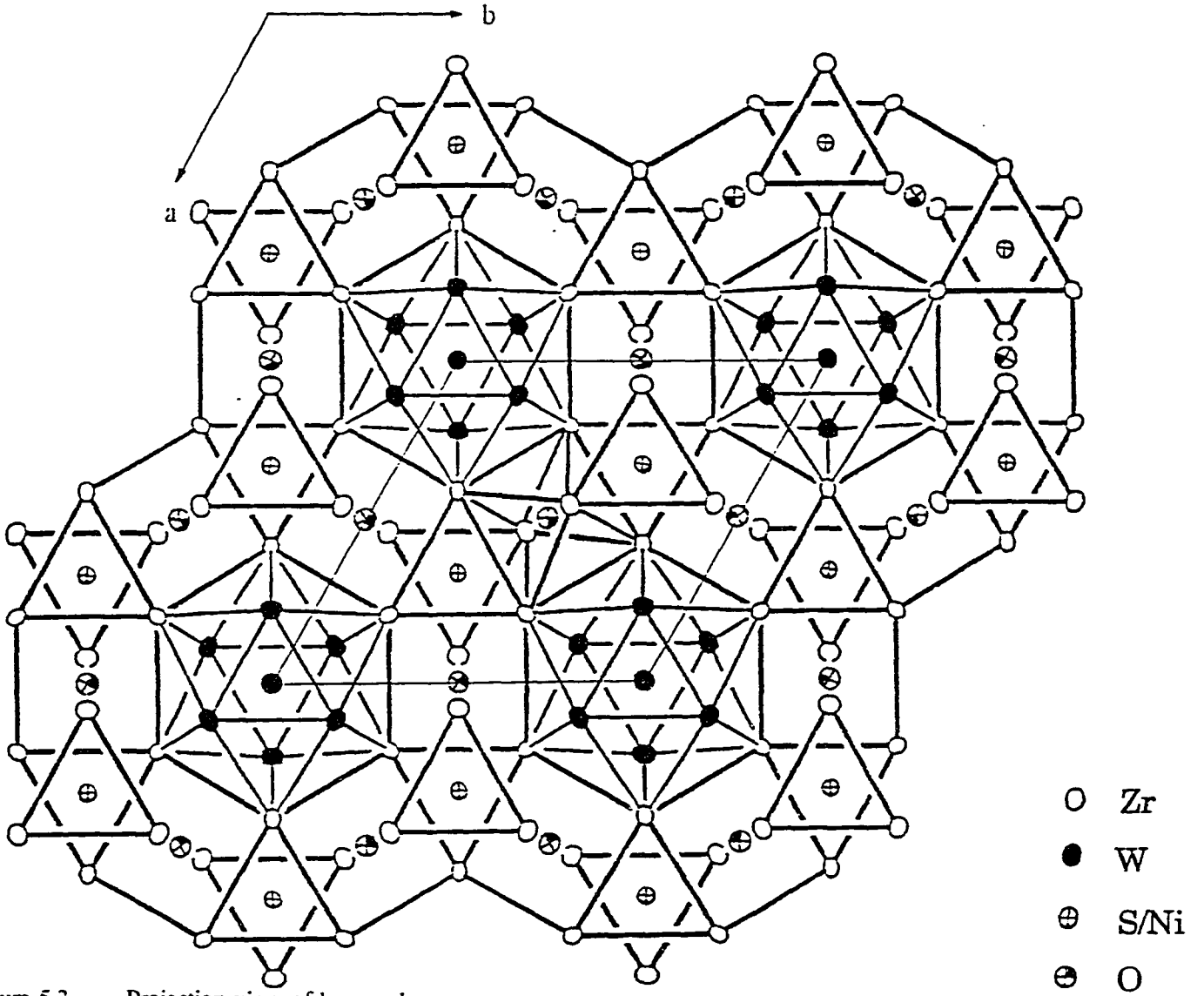

Figure 5.3 Projection view of kappa phase.

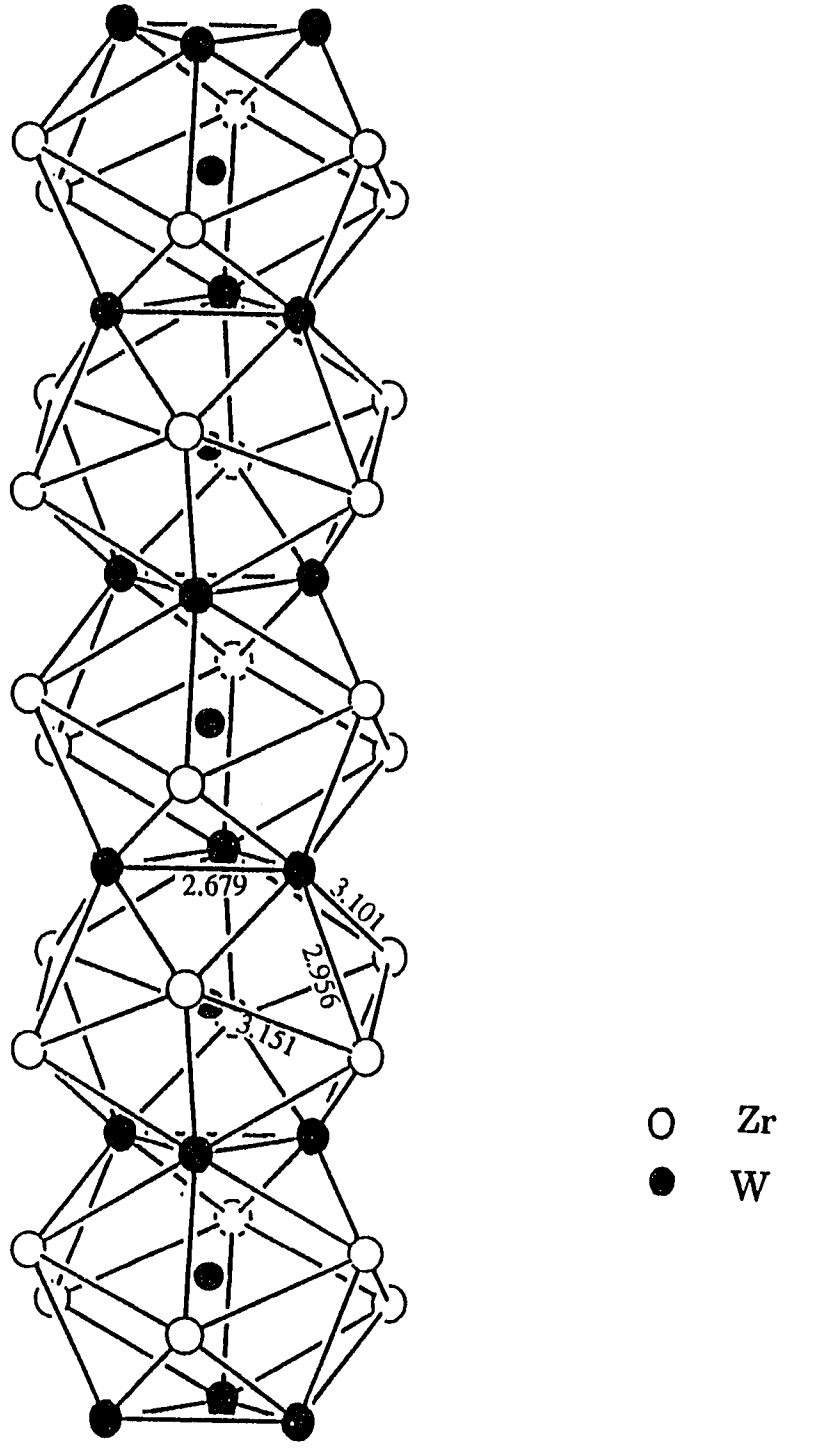

Figure 5.4 View of icosahedral chain along *c* axis. Distance shown for $Zr_9W_4(S,Ni)O_3$.

Experimental Details

The single crystal used for the refinement was picked from a multi-phase sample of zirconium, nickel, and sulfur which melted and reacted with the tungsten crucible at 1400°C. The stoichiometry of the sample was initially taken to be "Zr_3NiS". The product contained the kappa phase as a major phase, with Zr_3S_2 and another (unknown) phase present as minor phases. The crystal was small but regular shaped. Intensity data for this crystal were collected using a Rigaku AFC6R single crystal diffractometer and monochromated MoKα radiation, employing the ω-2θ scan technique up to 55° in 2θ. The observed intensities were corrected for Lorentz polarization and absorption effect. Table 5.2 contains the crystal data.

The bulk synthesis of all samples was carried out by initially combining elemental zirconium and sulfur powders in the mole ratio n(Zr)/n(S) of 9/1 and heating in an evacuated silica tube at 450°C until no visible traces of elemental sulfur remained. The temperature was raised to 800°C and held there for several days. The resulting zirconium sulfide was mixed with powders of the other metals and pressed into pellets. The pellets were arc-melted on a water cooled copper hearth in an argon atmosphere with a tungsten electrode. Each arc-melted sample was annealed in a tungsten crucible in an induction furnace at about 1200°C for 6-18 hours.

X-ray powder patterns were obtained with a vacuum Guinier camera FR552 (Enraf-Ninius, Delft, The Netherlands) and CuKα1 radiation, with silicon as an internal standard. The powder patterns were indexed by comparison to the kappa phases, and the lattice parameters were calculated by least-squares refinement.

Results and Discussion

The initial refinement of the single-crystal data led to the nominal formula Zr_9W_4S. Three corrections were necessary for the final refinement. Initially, the thermal parameters for the sulfur

Table 5.2 Crystal data for $Zr_9W_4(S/Ni)O_3$

Formula	$Zr_{9.22}W_{3.78}S_{0.67}Ni_{0.33}O_{3.00}$
Space group	$P6_3/mmc$ (#194)
a (Å)	8.688(7)
c (Å)	8.558(5)
V (Å^3)	559.4(7)
Z	2
d_{calc} (g/cm^3)	9.627
Crystal size (mm^3)	0.04x0.02x0.02
μ (MoKα) (cm^{-1})	480.79
Data collection instrument	Rigaku AFC6R
Radiation (monochromated in incident beam)	MoKα (λ=0.71069)
Octants measured	±*h*,*k*,±*l*
No. reflections measured	1904
No. unique data, total with $F_o^2 > 3\sigma(F_o^2)$	162
No. parameters refined	24
Trans. factors, max/min	1.000/0.560
Secondary ext. coeff. (10^{-7})	2.496
R[a], R_w[b], GOF[c]	0.026, 0.026, 0.975
Largest difference peak (e/Å^3)	+3.78
Largest negative peak (e/Å^3)	-2.17

[a] $R = \Sigma||F_o|-|F_c||/\Sigma|F_o|$

[b] $R_w = [\Sigma w(|F_o|-|F_c|)^2/ \Sigma w|F_o|^2]^{1/2}$; $w = 1/\sigma^2(|F_o|)$

[c] $GOF = (\Sigma(|F_o|-|F_c|)/ \sigma_i)/ (N_{obs\ refl} - N_{parameters})$

were unreasonably small. Placing nickel on that position gave equally unreasonable results. Placing mixed sulfur/nickel occupancy on the 2*c* site improved the results considerably. Kappa phases are known which contain either sulfur or nickel, as well as many other elements, but this is the first example of mixed occupancy of this site. EDS measurements also detect the presence of both sulfur and nickel in this phase. The atoms in this site are tricapped trigonal-prismatically coordinated to zirconium atoms. Nickel substitution of sulfur has been observed in the metal rich sulphides $Nb_6Ni_xS_{3-x}$, and $Nb_9Ni_{2-x}S_{3+x}$ [27], in which nickel substitutes for sulfur in highly coordinated capped trigonal-prismatic sites. Substitution of sulfur by nickel is consistent with the ability of sulfur to be involved in delocalized, metallic bonding.

An additional change was necessary, since the Fourier difference map calculated during refinement indicated the presence of an atom at the 6*g* position. As noted previously, other reports have indicated partial occupancy of the octahedral position by oxygen (up to 48% [99,100]). The result of the refinement in this work yielded total oxygen occupancy of this site. This is the first example of both the 2*c* and the 6*g* sites being fully occupied. The experimental steps for sample preparation offered several opportunities for inclusion of oxygen. As discussed in the introduction, techniques for solid state synthesis of early transition-metal sulfides are susceptible to oxygen inclusion. The determination of partial or complete oxygen occupancy in the known kappa phases is incomplete, and the results obtained here suggest that such occupation is in all cases a real possibility.

The final step in the refinement was to allow partial zirconium substitution of the tungsten on the 6*h* and 2*a* sites [98-103], as substantial M-M′ mixing has been observed in other phases. The variability in M-M′ mixing has been correlated with the variability observed in lattice parameters of these phases. Full details of the refinement results are in the following tables. Table 5.3 lists the atomic parameters, including percent mixing on those sites refined with mixed

occupancy. Anisotropic thermal parameters are in Table 5.4. Interatomic distances less that 3.7 Å are listed on Table 5.5.

A few of the interatomic distances are labelled in Figure 5.2 and Figure 5.4. The zirconium-zirconium distances within the trigonal prism range from 3.350 to 3.473 Å (Figure 5.2). This range is similar to the distances in the trigonal prism in Zr_3NiO, where $d_{Zr\text{-}Zr}$ = 3.325 - 3.682 Å. In both structures, these distances are much larger than the distance between the zirconium and the central atom, which is 2.612 Å in the kappa phase with mixed S/Ni occupancy, and 2.657 Å in Zr_3NiO, where just nickel occupies the central position. The octahedral arrangement of zirconium atoms is significantly distorted. Along one edge $d_{Zr1\text{-}Zr1}$ = 3.151 Å, while along the edge shared with the trigonal prism it is 3.473 Å. Consequently, the zirconium-oxygen distances are different, with $d_{Zr1\text{-}O}$ = 2.345 Å and $d_{Zr2\text{-}O}$ = 2.240 Å.

The possibility of filling the 4*f* site by placing oxygen in this octahedral site at (1/3, 2/3, 0.598) can be considered. The zirconium-oxygen distances would be between 2.26 and 2.39 Å. The short oxygen-oxygen distance would be only 2.60 Å, and with the oxygen in the 6*g* position the separation would be 2.64 Å. For the same reason as discussed in the Ti_2Ni type structures, full occupancy of both sites simultaneously is not expected.

A bulk sample of the $Zr_9W_4(S_{0.7}Ni_{0.3})O_3$ phase was prepared, and had the same lattice parameters as the minor phase from which the crystal was picked. Very little work on zirconium-containing kappa phases has been done. Only two previous reports for Zr-W-X kappa phases exist, so an attempt was made to synthesize both the Zr-W-S and Zr-W-Ni phases. In the synthesis of these phases, if the kappa phase was present after the arc melting step, as determined by X-ray powder diffraction films, the sample was then annealed. If the phase was not present after arc melting, it generally did not appear upon annealing. In preparing these new phases oxygen was not added in the starting material as a metal oxide, but oxygen was undoubtedly present as surface or

Table 5.3 Atomic parameters for $Zr_9W_4(S,Ni)O_3$

Atom	Site	*x*	*y*	*z*	Occupancy(%)	B_{eq}(Å)[a]
Zr1	12*k*	0.2001(2)	0.4002	0.0543(2)	100	0.4(1)
Zr2	6*h*	0.5442(2)	0.0883	1/4	100	0.5(2)
W1 Zr	6*h*	0.8928(1)	0.7857	1/4	94(2) 6	0.35(7)
W2 Zr	2*a*	0	0	0	95(2) 5	0.26(6)
S Ni	2*c*	1/3	2/3	1/4	67(6) 33	0.9(3)
O	6*g*	1/2	0	1/2	100	0.7(4)

[a] $B_{eq} = 8\pi^2/3\ \Sigma_i^3\Sigma_i^3 U_{ij} a_i^* a_j^* \vec{a}_i^* \vec{a}_j^*$

Table 5.4 Anisotropic thermal parameters for $Zr_9W_4(S,Ni)O_3$

Atom	U_{11}	U_{22}	U_{33}	U_{12}	U_{13}	U_{23}
Zr1	0.005(1)	0.008(1)	0.004(1)	0.004	0.002(2)	0.001
Zr2	0.005(1)	0.009(2)	0.006(1)	0.004	0	0
W1	0.0050(6)	0.0038(7)	0.0041(7)	0.0019	0	0
W2	0.004(1)	0.004	0.002(1)	0.002	0	0
S/Ni	0.012(5)	0.012	0.008(6)	0.006	0	0
O[a]	0.008(5)					

[a] Isotropic thermal parameter refined for oxygen

Table 5.5 Interatomic Distances for $Zr_9W_4(S/Ni)O_3$.Values listed for distances less than 3.7 Å.

Zr1	- O	2.345(2) x 2	W1	- W2	2.679(2) x 2
	- S/Ni	2.612(2) x 1		- W1	2.793(4) x 2
	- W1	2.956(2) x 1		- Zr2	2.951(3) x 2
	- W2	3.047(3) x 1		- Zr1	2.956(2) x 2
	- W1	3.101(3) x 2		- Zr1	3.101(3) x 4
	- Zr1	3.151(3) x 2			
	- Zr2	3.241(3) x 2			
	- Zr2	3.245(2) x 2	W2	- W1	2.679(2) x 6
	- Zr1	3.350(4) x 1		- Zr1	3.047(3) x 6
	- Zr1	3.473(5) x 2			
			S/Ni	- Zr1	2.612(2) x 6
Zr2	- O	2.240(2) x 2		- Zr2	3.172(4) x 3
	- W1	2.951(3) x 2		- O	3.300(2) x 6
	- S/Ni	3.172(4) x 1			
	- Zr2	3.193(6) x 2	O	- Zr2	2.240(2) x 2
	- Zr1	3.241(3) x 4		- Zr1	2.345(2) x 4
	- Zr1	3.245(2) x 4		- S/Ni	3.300(2) x 2

low level bulk oxide in the zirconium. The zirconium used was in a powder form, and was stored on a shelf rather than in a dry box. Thus, while the presence of oxygen is certain, the amount of oxygen is undetermined. By this method $Zr_9W_4SO_x$ was prepared. Zr_9W_4Ni did not form, even when oxygen was intentionally added, as ZrO_2 or NiO, in the starting material. Thus, there is not a continuous range of solid solubility between the two endmembers $Zr_9W_4SO_x$ and $Zr_9W_4NiO_x$, since the nickel endmember does not form. A few more experiments were done to investigate the extent of nickel substitution for sulfur. The four molar ratios n(S)/n(Ni) 3/1, 2/1, 1/1, and 1/3 were used in the starting materials. The kappa phase formed when the n(S)/n(Ni) ratio was 3/1 and 2/1, but did not form when it was 1/1 or 1/3. The maximum extent of nickel substitution may be that found in the sample from which the crystal was picked. In all of these experiments there was a small (1-3%) mass loss in the arc melting step due to vaporization of sulfur and/or nickel. Consequently, in all these samples, minor phases present were elemental zirconium, tungsten, or W_2Zr.

The kappa phase Zr_9Mo_4Ni has been previously reported [97]. The preparation of this compound from the elements, by the arc melting method, was not successful. When the synthesis was tried again using NiO in the starting materials, the kappa phase was observed by X-ray powder diffraction. Thus it appears that complete oxygen occupancy of the 6*g* site may be necessary for the formation of the kappa phase. The importance of oxygen for the formation of the phase is dependent on the elements making up the metal framework, as well as the interstitial element X. Indeed, the role of the metal framework and the difference between tungsten and molybdenum is evident in the fact that the kappa phase forms for Zr/Mo/Ni/O, but not for Zr/W/Ni/O. The $Zr_9Mo_4SO_x$ phase was also synthesized, and since $Zr_9Mo_4NiO_x$ is also known, and sulfur/nickel substitution has been observed on the tungsten analogue, it might expected that a solid solution forms between these two. The lattice parameters for these new kappa phases are listed below in

Table 5.6.

By looking at the list of known kappa phases, many other possibilities of mixed interstitial sites can be considered. Examples, like $Zr_9W_4(S,Ni)O_3$, where another element only partially substitutes for the interstitial atom, or examples of complete solubility ranges might be found. In the former case, new understanding may be gained concerning the role of metal-metal bonding in this phase (i.e. W vs Mo in Zr-M-Ni). In the latter case, in which the identity of the interstitial atoms is of little consequence, the effect of orbital interactions and electron counts may be such that the Fermi level crosses a region of nonbonding bands. The properties to be found for mixed interstitial phases are not known and present a fertile area for future study. Exceptions to this are the recently discovered superconductivities in Hf-Nb-S, Zr-Nb-S, and Hf-Ta-Se [21,95]. In general, it can be stated that the single crystal and powder diffraction results obtained here strongly suggest that the known kappa phases (Table 5.1) could contain currently undetected interstitials and could exhibit currently undetermined variations in stoichiometry.

Table 5.6 Lattice parameters for new kappa phases

	a (Å)	c (Å)	V (Å^3)
$Zr_9Mo_4SO_x$	8.685(2)	8.571(2)	559.8(2)
$Zr_9W_4SO_x$	8.671(2)	8.607(3)	560.4(3)
$Zr_{9.2}W_{3.8}S_{0.67}Ni_{0.33}O_3$	8.688(4)	8.558(7)	559.4(7)

6. $Zr_6Ni_6TiSiO_x$: A NEW STRUCTURE TYPE WITH A MIXED EARLY-LATE TRANSITION METAL FRAMEWORK

Introduction

An interstitially stabilized intermetallic in a mixed early-late transition metal system has been found to crystallize in a new structure type. The new compound, $Zr_6Ni_6TiSiO_x$ (x=1.8), was synthesized by melting Zr, Ni, Si, and Ti_2O_3 in an arc furnace, followed by annealing in vacuum at 900 - 1150°C. The crystal structure was determined by refinement of single crystal x-ray diffraction data. The structure was refined in the centrosymmetric space group $P\bar{3}m1$, Z=2, with lattice parameters a = b = 8.2778(9) Å, and c = 7.444(1) Å (R=0.030, R_w=0.033). Oxygen atoms center zirconium trigonal antiprisms, which share faces to form a three dimensional network. The titanium and silicon atoms are coordinated by icosahedra of nickel, or zirconium and nickel atoms. A structural comparison with the kappa-phase will be discussed.

A substantial diversity of structures of binary compounds in mixed early-late transition metal systems, particularly in the Zr-Ni system, is described in the literature [47,104]. Typically, when an interstitial element reacts with a binary early-late transition metal compound to form a ternary compound, the compound crystallizes in a common structure type. In fact, only a limited number of structure types are known for phases of mixed early and late transition metals which are interstitially stabilized [46]. This work has described the importance of the presence of small amounts of oxygen in stabilizing phases in the Zr-Ni system which do not appear as true binary intermetallic compounds.

The ternary metal system, Zr-Ti-Ni, contains phases which do not occur in either of the binary systems Zr-Ni or Ti-Ni (i.e. the hexagonal Laves phase ZrTiNi [105,106], and the $BaPb_3$ type

structure $ZrTi_2Ni_9$ [107,108]). It is natural to expect that interstitials in this ternary system may stabilize new compounds, with respect to the ternary intermetallics and interstitially stabilized binary compounds. There are some examples of ternary, and quaternary, phases which form with the addition of an interstitial atom, such as oxygen in the case of a few kappa-phases (eg., $Zr_9W_4(S,Ni)O_{3)}$ [80,94,99]. In this section the structure of a new interstitially stabilized compound with the composition $Zr_6Ni_6TiSiO_{1.8}$ is reported.

Experimental Details

Samples were prepared from materials and by procedures described previously. All samples were arc melted three times on a water cooled copper plate with a thoriated nonconsumable tungsten electrode in an argon atmosphere. The arc melted buttons were subsequently crushed and pressed into pellets and annealed in evacuated silica tubes at 900 - 1150°C for 2-3 days. All samples contained ZrO_2 as a minor phase.

The single crystal used for the structural investigation was picked from a sample of a Zr-Ti-Ni alloy which reacted with the silica tube in the annealing process. Subsequent reactions included silicon and oxygen in the starting materials. All handling of materials was done in air. Details of crystal data are listed in Table 6.1.

Semiquantitative analysis by energy dispersive x-ray analysis (EDS) was carried out on a Cambridge S-200 scanning electron microscope with a Northern Tracor Micro Z-II x-ray detector. Surface analysis by x-ray photoelecron spectroscopy was performed on a Perkin Elmer 5500 multitechnique system.

A Quantum Design SQUID magnetometer was used to check for superconductivity and to measure magnetic behavior at a field of 3T over the temperature range 6 - 298 K.

Table 6.1 Crystal data for $Zr_6Ni_6TiSiO_x$

Formula	$Zr_{5.39}Ni_{6.00}Ti_{1.71}Si_{0.90}O_{1.80}$
Space group	$P\bar{3}m1(164)$
a Å	8.2778(9)
c Å	7.444(1)
V $Å^3$	441.7(1)
Z	2
d_{calc}, g/cm^3	7.366
Crystal size, mm^3	0.08x0.04x0.04
μ(MoKa), cm^{-1}	200.84
Data collection instrument	Rigaku AFC6R
Radiation (monochromated in incident beam)	MoK_α (λ = 0.71069 Å)
Temperature, °C	23±1
Scan method	2θ-ω
Octants measured	$\pm h \pm k l$
Data collection range, 2θ, deg	0-60
No. refl. measured	2897
No. unique data, total with $F_o^2 > 3\sigma(F_o^2)$	272
No. parameters refined	37
Trans. factors, max./min.	1.500
Secondary extinction coefficient	$2.0(8) \times 10^{-7}$
R[a], R_w[b], GOF[c]	0.030, 0.033, 1.006
Largest peak, $e/Å^3$	+1.44
Largest negative peak, $e/Å^3$	-1.89

[a] $R = \Sigma||F_o|-|F_c||/\Sigma|F_o|$

[b] $R_w = [\Sigma w(|F_o|-|F_c|)^2/ \Sigma w|F_o|^2]^{1/2}$; $w = 1/\sigma^2(|F_o|)$

[c] $GOF = (\Sigma(|F_o|-|F_c|)/ \sigma_i)/ (N_{obs\ refl} - N_{parameters})$

Results

The crystal was found to exhibit Laue symmetry $\bar{3}m1$, and the single crystal refinement was carried out in the centrosymmetric space group $P\bar{3}m1$. The refinement converged with the placement of the Zr, Ni, Ti, Si, and O(1) atoms at the proper sites. The refinement improved significantly when titanium was allowed to partially occupy the Zr(2) position, and also to partially occupy the Si position. At this point, a peak in the Fourier difference map suggested the presence of another oxygen atom, O(2). This atom was added to the refinement, and the multiplicities of both oxygen atoms were allowed to vary. The final positional parameters, equivalent B values, and occupancies of all sites are listed in Table 6.2. The refinement reported here was calculated using a $F_o^2 > 3\sigma(F_o^2)$ cutoff. An additional refinement using a 1σ cutoff resulted in R = 0.054 and R_w = 0.043 and no significant change in the thermal or positional parameters. The anisotropic thermal parameters of all non-oxygen atoms are in Table 6.3. Structure factor amplitudes, including unobserved reflections, are in the appendix.

A projection of the whole structure is shown in Figure 6.1. The structure can be described by viewing two connected, alternating layers, the projections of which are shown in Figures 6.2 and 6.3. The layers are labeled A and B, as shown in Figure 6.4. Figure 6.2 shows layer A, centered at z=1/2 and containing only the atoms within the range $z=1/2 \pm 1/3$. This layer consists of a network of face-sharing zirconium trigonal antiprisms which form buckled rings. This structural unit matches the description of the kappa phase (compare Figure 5.3). The bold lines mark the Zr-Zr connections that outline the rings. Titanium atoms in an icosahedral environment are in the center of the rings. A common feature in oxygen-stabilized intermetallics of zirconium is the presence of oxygen in the center of the zirconium trigonal antiprisms. The antiprisms in the buckled ring are centered by oxygen in two distinct crystallographic sites, one of which (O(2)) is only approximately one third occupied (this is the antiprism with the three-fold axis along the c-axis, as viewed in the

Table 6.2 Positional parameters for $Zr_6Ni_6TiSiO_x$

Atom	Site	x	y	z	B_{eq}[a]($Å^2$)	% occup
Ni(1)	6*i*	0.1129(2)	-0.1129	0.2553(3)	0.54(2)	100
Ni(2)	6*i*	0.1726(2)	-0.1726	0.9326(3)	0.54(2)	100
Zr(1)	6*i*	0.4598(1)	-0.4598	0.1953(2)	0.63(2)	100
Zr(2) Ti	6*i*	0.2073(1)	-0.2073	0.5688(2)	0.49(3)	79(2) 21(2)
Ti(1)	1*a*	0	0	0	0.4(2)	100
Ti(2)	1*b*	0	0	1/2	0.7(2)	100
Si Ti	2*d*	1/3	2/3	0.874(1)	0.4(2)	90(4) 10(4)
O(1)	3*f*	1/2	0	1/2	0.7(3)	96(4)
O(2)	2*d*	1/3	2/3	0.367(9)	0.4(8)	36(6)

[a] $B_{eq} = 8\pi^2/3\ \Sigma_i^3\Sigma_i^3 U_{ij} a_i^* a_j^* \vec{a}_i^* \vec{a}_j^*$

Table 6.3 Anisotropic thermal parameters for $Zr_6Ni_6TiSiO_x$

Atom	U_{11}	U_{22}	U_{33}	U_{12}	U_{13}	U_{23}
Ni(1)	0.0081(8)	0.0081	0.006(1)	0.0052(9)	-0.0004(4)	0.0004
Ni(2)	0.0077(7)	0.0077	0.006(1)	0.0044(8)	0.0001(4)	-0.0001
Zr(1)	0.0087(6)	0.0087	0.008(1)	0.0054(7)	-0.0004(3)	0.0004
Zr(2)	0.0051(7)	0.0051	0.007(1)	0.0015(7)	-0.0005(4)	0.0005
Ti(1)	0.005(2)	0.005	0.003(4)	0.003	0	0
Ti(2)	0.007(2)	0.007	0.013(4)	0.003	0	0
Si	0.003(2)	0.003	0.007(4)	0.002	0	0
O(1)	0.009(3)[a]					
O(2)	0.01(1)[a]					

[a]Isotropic thermal parameter refined for oxygen atoms

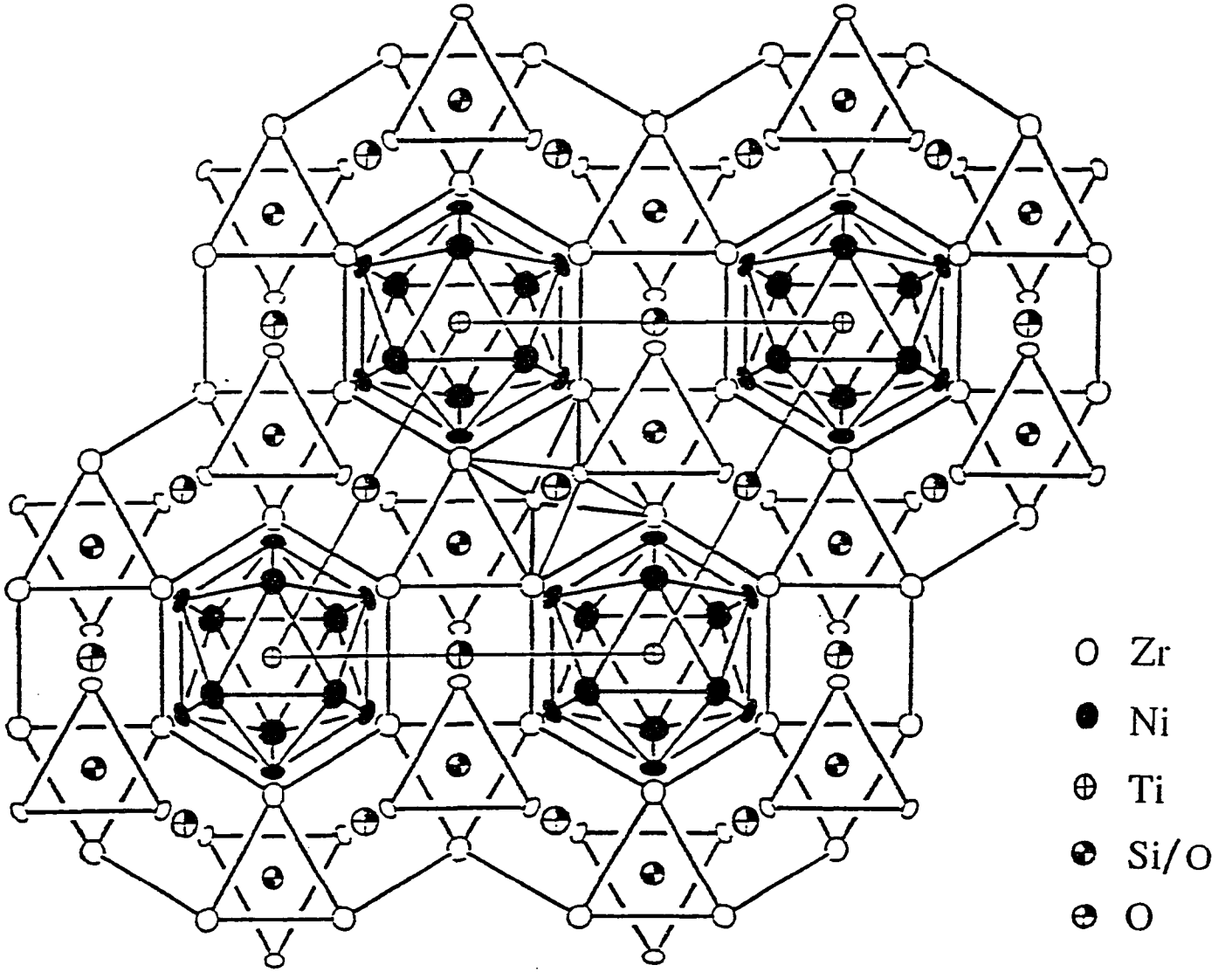

Figure 6.1 Projection along the *c* axis of the $Zr_6Ni_6TiSiO_x$ structure

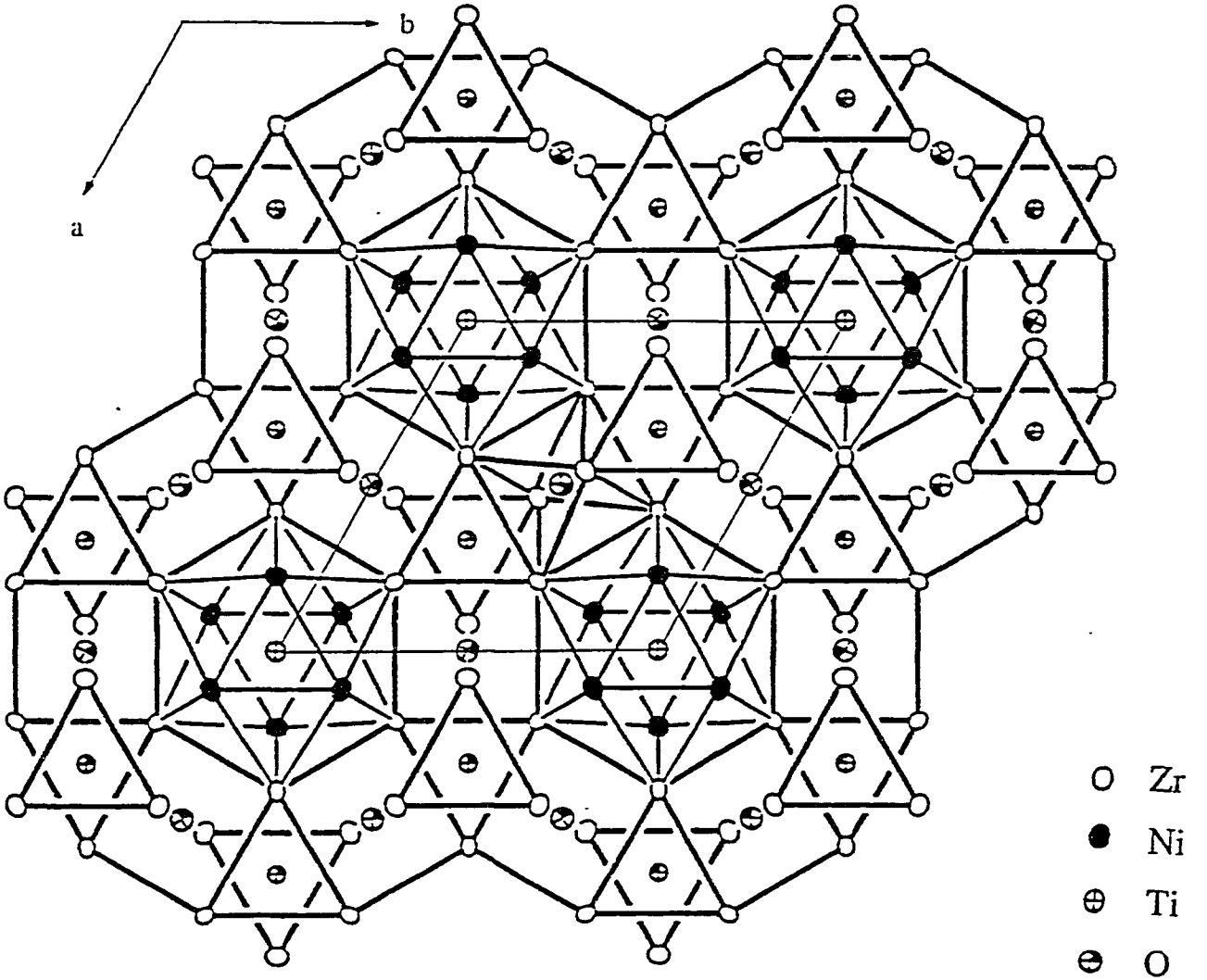

Figure 6.2 Projection of Layer A, showing atoms at positions with z=1/2 ± .33 (Ni(2), Ti(1), and Si not in this layer). Zr trigonal antiprism outlined at cell center.

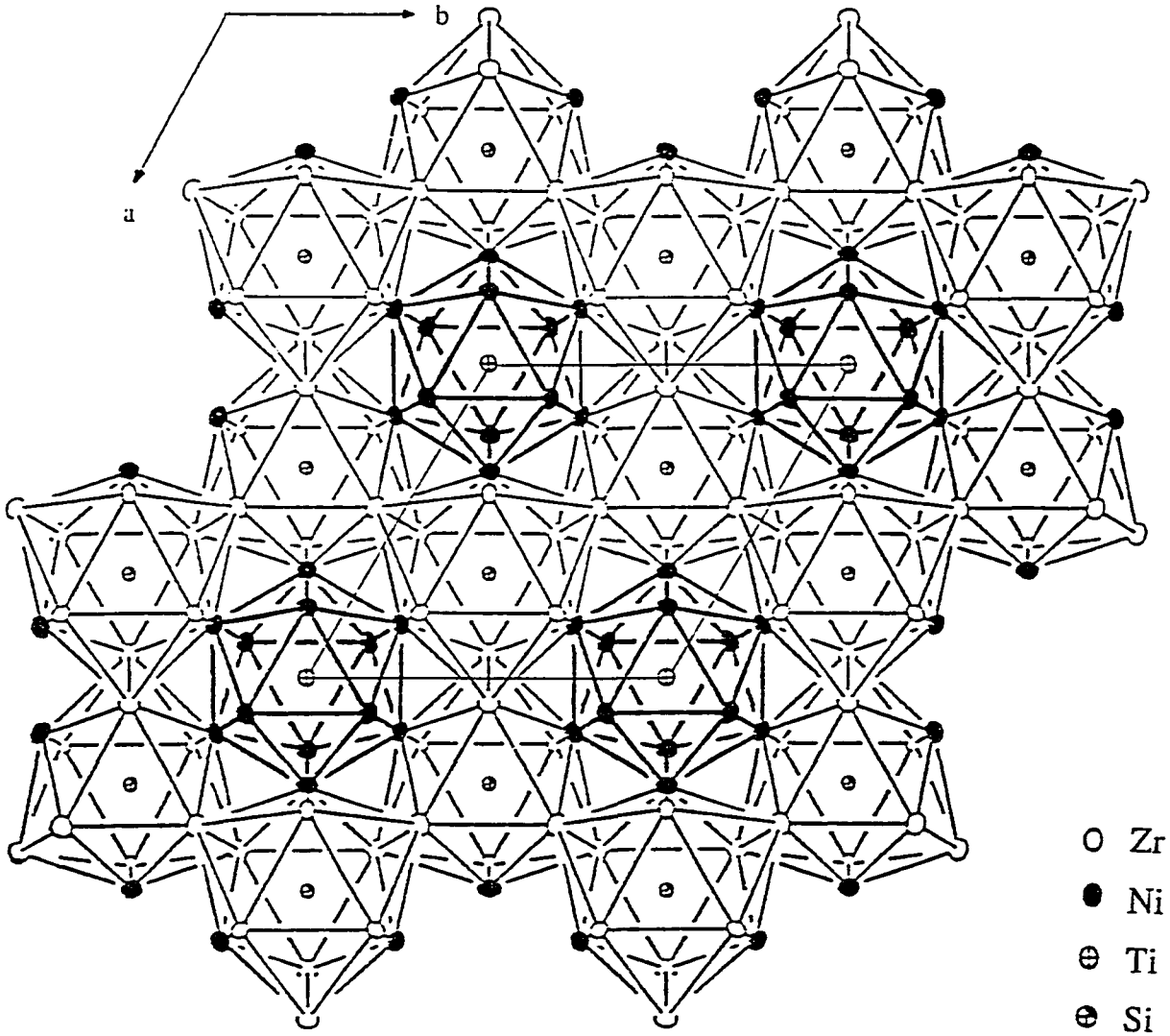

Figure 6.3 Projection of Layer B, showing atoms at positions with -1/2<z<1/2 (O(1), O(2), and Ti(2) at z=1/2 not in this layer).

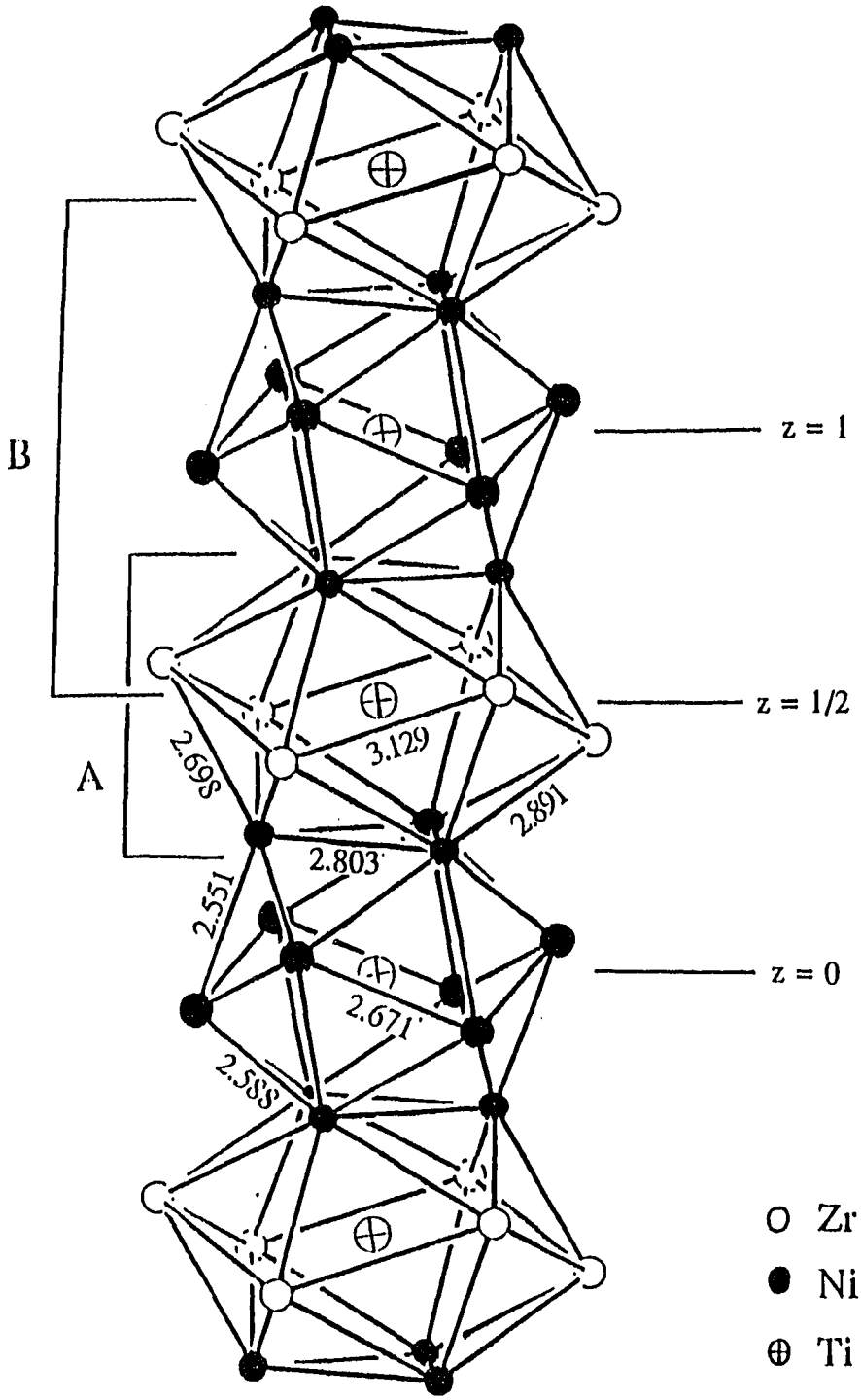

Figure 6.4 View along the c-axis. Icosahedral coordination of Ti atoms shown. Side view of regions included in Layers A and B, which are shown in projection in Figures 6.2 and 6.3, respectively.

projection in Figure 6.1). The antiprisms in the ring, then, form an alternating pattern of filled, and partially filled antiprisms. The Zr-O distances (2.22-2.35 Å) are typical of oxygen-centered zirconium antiprisms in intermetallic compounds ($d_{Zr\text{-}O}$=2.305-2.307 Å in Zr_3NiO [66] and 2.27 Å in Zr_4Ni_2O). The short O(1)-O(2) distance (2.59 Å) suggests that full occupancy of both sites would be energetically unfavorable, similar to the situation of filling adjacent octahedral sites in the Ti_2Ni type structures [72]. The icosahedron around the titanium atom consists of 6 zirconium and 6 nickel atoms. Distances in the Ni_6Zr_6 icosahedron are indicated in Figure 6.4. Figure 6.5 shows the distances within the zirconium network. All interatomic distances less than 3.6 Å are listed in Table 6.4.

Figure 6.3 shows the projection along c of layer B, centered at z=0 and including all atoms except those at z=±1/2. The bold outlines show the Ni_{12} icosahedra, centered by titanium at the unit cell origin. Figure 6.4 illustrates how this Ni_{12} icosahedron shares faces and stacks with the Ni_6Zr_6 icosahedron centered at z=1/2. The Ni_{12} unit is a fairly regular icosahedron, with a slight expansion at the top and bottom ($d_{Ni1\text{-}Ni1}$=2.80 Å, compared to $d_{Ni1\text{-}Ni2}$=2.55 Å or $d_{Ni2\text{-}Ni2}$=2.67 Å). This expansion is necessary to allow face-sharing chains to form with the larger and more irregular Ni_6Zr_6 icosahedron. The central titanium atom has very short titanium-nickel distances in all of these icosahedra (2.44-2.52 Å). They are shorter, in fact, than any of the nickel-nickel distances (2.55-2.80 Å). A calculation of Pauling bond orders [4] was carried out on this compound, and the short distances and high coordination give the titanium atoms an unusually high bond order in comparison to the other transition metal atoms. This short titanium-nickel distance, however, was also observed in Ti_2Ni and the filled-Ti_2Ni, Ti_4Ni_2O, structures ($d_{Ti\text{-}Ni}$=2.48 Å and 2.46 Å, respectively), in which Ti atoms also center icosahedra [79]. This may be surprising if one considers that the atomic radius of titanium is larger than that of nickel. It is not so surprising when the Lewis acid - base interaction is considered because strong titanium - nickel acid - base interactions

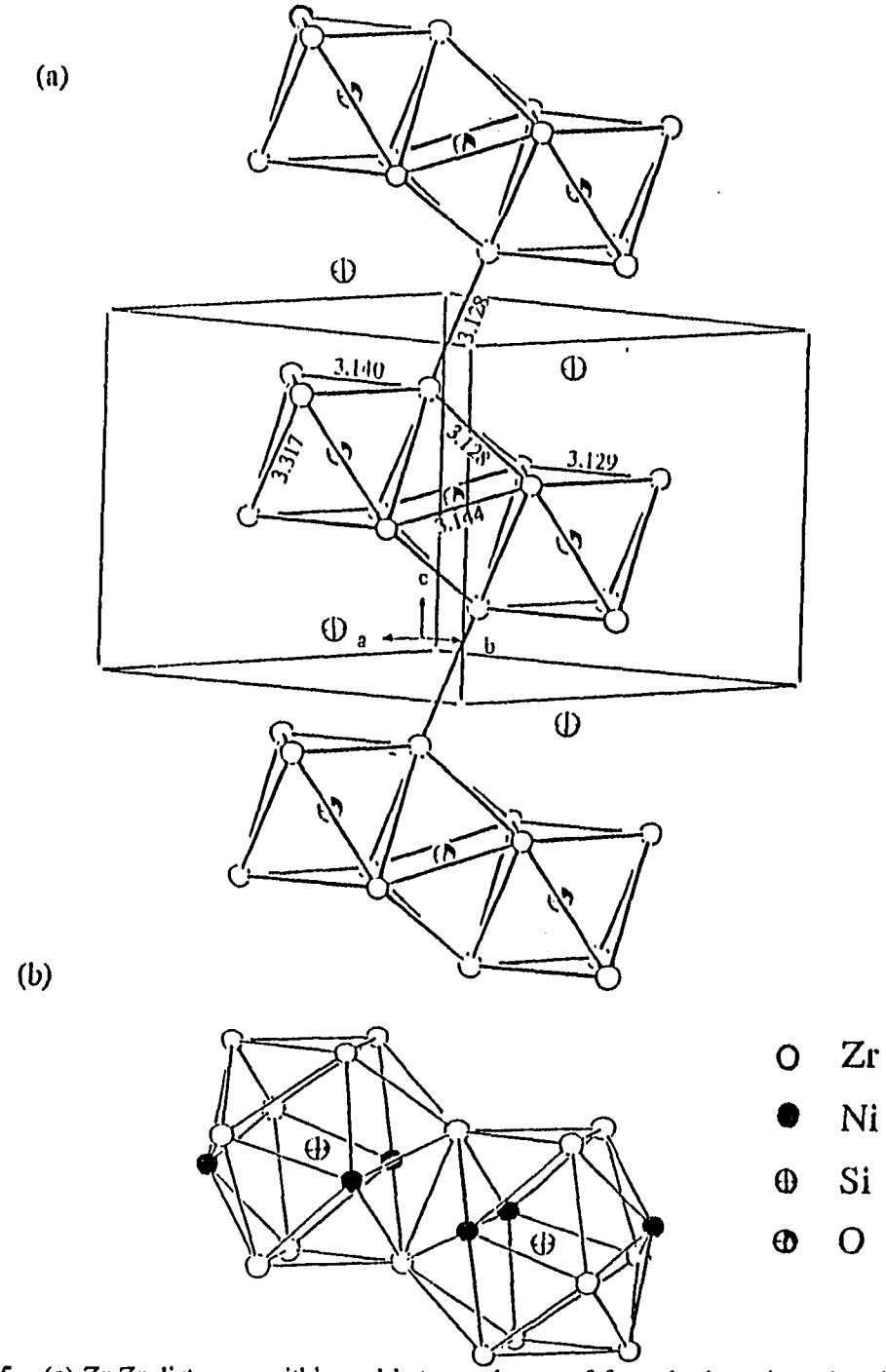

Figure 6.5 (a) Zr-Zr distances within and between layers of face-sharing trigonal antiprisms. (b) two edge-sharing silicon-centered icosahedra, which lie between the zirconium layers in (a).

Table 6.4 Interatomic distances in $Zr_6Ni_6TiSiO_x$ (Å) (distances less than 3.6 Å listed)

Zr(1) -	O(2)	2.22(4)	x 1	Zr(2) -	O(1)	2.2179(6)	x 2
	O(1)	2.340(1)	x 1		O(2)	2.35(4)	x 1
	Ni(1)	2.784(2)	x 2		Ni(1)	2.698(2)	x 1
	Ni(2)	2.860(1)	x 2		Ni(2)	2.754(2)	x 1
	Ni(2)	2.871(2)	x 2		Ni(1)	2.891(2)	x 2
	Si	3.001(6)	x 1		Si	2.903(6)	x 1
	Si	3.011(2)	x 1		Ti(2)	3.017(2)	x 1
	Zr(1)	3.128(3)	x 1		Zr(1)	3.128(2)	x 2
	Zr(2)	3.128(2)	x 2		Zr(2)	3.129(3)	x 2
	Zr(1)	3.140(3)	x 2		Zr(2)	3.144(2)	x 2
	Zr(2)	3.317(2)	x 2		Zr(1)	3.317(2)	x 2
Ni(1) -	Ti(2)	2.436(2)	x 1	Ni(2) -	Si	2.345(2)	x 1
	Ti(1)	2.496(2)	x 1		Ti(1)	2.525(2)	x 1
	Ni(2)	2.551(3)	x 1		Ni(1)	2.551(3)	x 1
	Ni(2)	2.588(2)	x 2		Ni(1)	2.588(2)	x 2
	Zr(2)	2.698(2)	x 1		Ni(2)	2.671(2)	x 2
	Zr(1)	2.784(2)	x 2		Zr(2)	2.754(2)	x 1
	Ni(1)	2.803(3)	x 2		Zr(1)	2.860(1)	x 2
	Zr(2)	2.891(2)	x 2		Zr(1)	2.871(2)	x 2
	O(2)	3.27(4)	x 1				
	O(1)	3.386(1)	x 2				
Ti(1) -	Ni(1)	2.496(2)	x 6	Ti(2) -	Ni(1)	2.436(2)	x 6
	Ni(2)	2.525(2)	x 6		Zr(2)	3.017(2)	x 6
Si -	Ni(2)	2.345(2)	x 3	O(1) -	Zr(2)	2.2179(6)	x 4
	Zr(2)	2.903(6)	x 3		Zr(1)	2.340(1)	x 2
	Zr(1)	3.001(6)	x 3		O(2)	2.52(2)	x 2
	Zr(1)	3.011(2)	x 3		Ni(1)	3.386(1)	x 4
				O(2) -	Zr(1)	2.22(4)	x 3
					Zr(2)	2.35(4)	x 3
					O(1)	2.52(2)	x 3
					Ni(1)	3.27(4)	x 3

are expected rather than strong nickel - nickel interactions, which were minimal in the results of the extended Hückel calculations of overlap populations for Zr_4Ni_2O. The titanium - nickel interactions in this case are certainly more important than the nickel - nickel interactions.

The projection in Figure 6.3 shows a Ni_{12} icosahedron sharing six vertices with six very distorted silicon-centered icosahedra. The distortion is seen in the very short Si-Ni distances (2.34 Å), compared with the Si-Zr distances (2.90-3.01 Å). These silicon-centered icosahedra form a network of edge-sharing icosahedra. Figure 6.5 (b) shows how two of these icosahedra share edges. Figure 6.5 (a) shows the location of the silicon between the layers of zirconium antiprisms. The trigonal antiprisms and icosahedra share faces. Thus, the structure consists of a metal framework of zirconium trigonal antiprisms and nickel icosahedra which arrange in this three-dimensional network. Titanium and silicon fill the icosahedral sites, and oxygen occupies trigonal antiprismatic sites.

The crystal structure refinement yields the atomic ratios Ni/Zr/Ti/Si of 6/5.4/1.7/0.9, to be compared with the idealized atomic ratios of 6/6/1/1. A small piece of the sample from which the crystal was extracted was studied by both EDS and XPS techniques. Surface analysis on a sample which was ion-beam etched in an argon atmosphere gave ratios of 6/5.8/1.6/0.5. Semiquantitative elemental analysis by EDS on a rough surface also resulted in a Ni/Zr ratio greater than one, with excess titanium, supporting the conclusion that titanium substitutes on the zirconium sites. The EDS experiment did not, however, indicate a deficiency in silicon. A bulk sample prepared with starting stoichiometry $Zr_6Ni_6TiSiO_2$, and containing ZrO_2 as a minor phase, had lattice parameters a = b = 8.334(2) Å and c = 7.483(2) Å. This lattice expansion from that reported for the sample from which the single crystal was selected is expected if less titanium substitutes for zirconium on the Zr(2) site, and suggests that there is a homogeneity range for this phase. The structure was not observed when nickel was substituted by iron or cobalt.

The sample was checked for superconductivity, but none was detected down to 6 K. Magnetic measurements from 6-297 K show the sample is paramagnetic. A correction was applied for the diamagnetism of the core electrons, and an approximately 5% impurity phase of ZrO_2 [111] (Figure 6.6). See also Figure 4.7.

Discussion

This new structure may usefully be compared to the kappa phases [94]. Kappa phases crystallize in the hexagonal space group $P6_3/mmc$. This new phase crystallizes in the trigonal space group $P\bar{3}m1$. Figure 6.7 compares the metal framework in the structures of these two phases, viewed perpendicular to the $[\bar{1}10]$ direction. The oxygen atoms are omitted in this figure. Figure 6.7 (a) is similar to Figure 6.5, showing the icosahedral coordination of silicon (B) between the two layers of zirconium trigonal antiprisms (A). Figure 6.7 (b) is a view of the kappa phase which also contains parallel layers of trigonal antiprisms made up of metal atom M at the top and bottom of the figure (A). A horizontal mirror plane contains the interstitial atom, X, and one face of the trigonal antiprism. It can be noticed that the parallel layers are connected by a middle "antiparallel" layer (A'). The interstitial atom has a tricapped trigonal-prismatic coordination. The new structure can be pictured as a modified kappa phase, where the distortion consists of expanding one trigonal face of the trigonal prism, as indicated by the arrows in Figure 6.7 (b), and moving the atoms to a position corresponding to the Ni atoms in Figure 6.7 (a). The interstitial atom then moves into this expanded region. A compression along the c-axis completes the distortion (a value of c/a=0.97-0.99 is typical for the kappa phases, compared to c/a=0.90 for the new structure).

The kappa phases are an intriguing class of compounds, in which the metal framework provides a host to many different interstitial elements. The general formula for the kappa-phase is $M_9M'_4X$, where X = B, C, Si, Ge, P, As, S, Se, Fe, Co, or Ni. Apparently, the strength of the

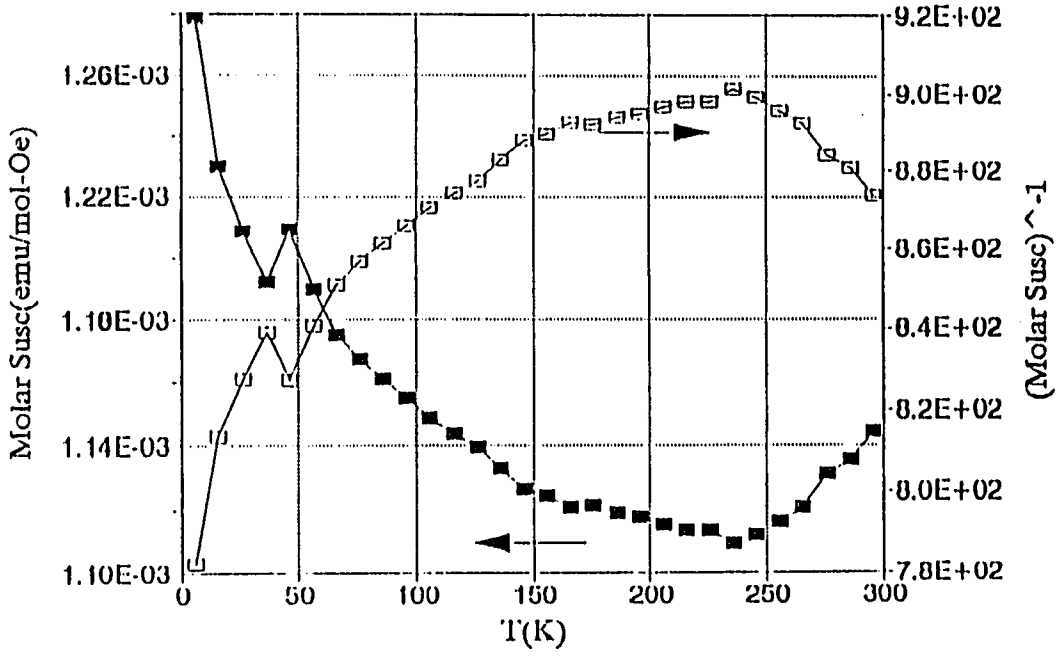

Figure 6.6 Magnetic susceptibility of $Zr_6Ni_6TiSiO_{1.8}$. The bump below 50 K is attributed to atmospheric oxygen.

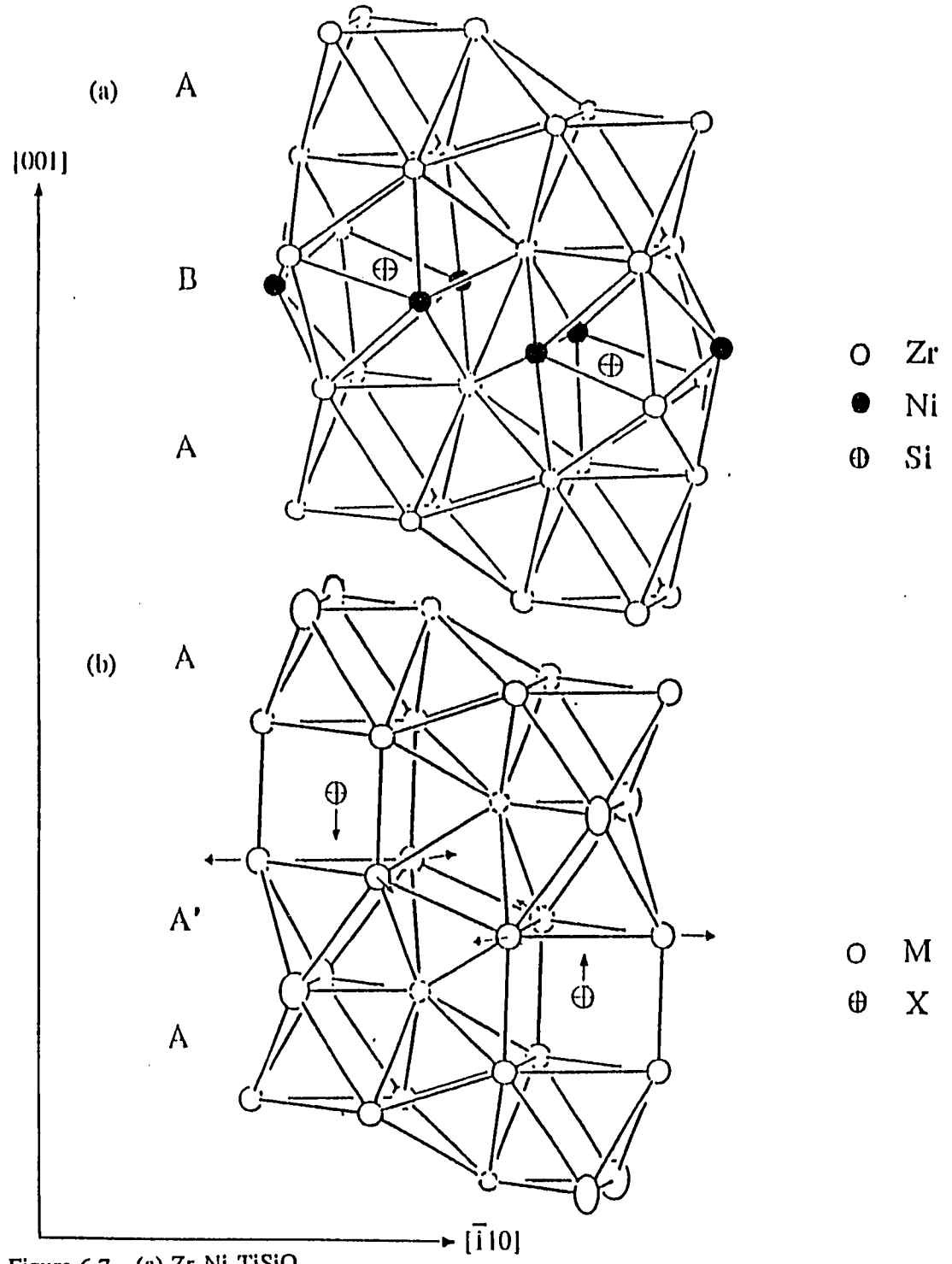

Figure 6.7 (a) $Zr_6Ni_6TiSiO_x$.
(b) Kappa-phase. Arrows show direction of distortion leading to the new structure.

metal-metal interactions in the framework allows for the variability in X. A similar argument suggests that this new phase might also form with a variety of interstitial elements. The kappa phase and the new phase both have a metal/non-metal ratio of 13/1, neglecting the oxygen. The difference between the two phases is the metal framework. The kappa phase contains two transition metals, while this new phase has a ternary framework with two early transition metals and a late transition metal.

It is very likely that this new phase will also accomodate a variety of interstitial atoms in the icosahedral site occupied by silicon. A tabulation of preferred coordination number for main group, and iron group transition metal elements, based on the results of the structural determination of compounds in 324 structure types, indicates gallium and aluminum prefer a twelve coordinated site over a coordination number of nine [109]. Many of the elements which are found in the tricapped trigonal prismatic interstitial site of the kappa phase, including B, Ge, As, Si, and P prefer a coordination number of nine. While this does not preclude the possibility of these elements forming in this new structure type (as in the case of silicon), it certainly gives an indication of what might be expected in attempts to synthesize new compounds of this structure type.

7. IDEAS FOR FUTURE WORK

Cubic Laves Phase: Zr/Ni/O

Reference has been made throughout of the existence of an interstitially stabilized cubic Laves phase in the zirconium - nickel system. Very little is actually reported for this phase, and as these phases appeared in the course of this research, a few comments are appropriate. The Laves phase is not known in the binary system. It was initially reported as a cubic $ZrNi_2$ [48], but was subsequently shown to form only when stabilized by an interstitial atom. Bsenko suggested it was stabilized by silicon [112]. Blažina and Ban report cubic $ZrNi_5$ can substitute oxygen for nickel, forming $ZrNi_{5-x}O_x$, for x = 0 to 1 [113]. $ZrNi_5$ crystallizes in the $AuBe_5$ type structure, which is related to the $MgCu_2$ structure by a group/subgroup relationship. The atoms in $MgCu_2$ both occupy special positions, 8*a* and 16*d* in $Fd\bar{3}m$. In the $AuBe_5$ structure the eight fold site is split into two four fold sites, with a lowering in symmetry to $F\bar{4}3m$. In the Laves phase AB_2, the larger A atoms are sixteen coordinated. The smaller B atoms are coordinated to twelve atoms. Because of the change in symmetry, the $AuBe_5$ type structure splits the A atoms position of the Laves phase, and the large sixteen coordinated sites are occupied by both A and B atoms. The solution of Blažina and Ban places zirconium and oxygen on these large four fold sites. This is a very large site for an oxygen atom. Their work was based on powder diffraction data, without full profile refinement, and should be checked. A solution to this may also help to understand the structure of the Laves phase. The lattice parameter for $ZrNi_4O$ is a = 6.680(5) Å. The lattice parameter of a cubic phase observed in the course of this work is a = 6.9158(4) Å.

The cubic phase was present in a sample also containing $Ni_{10}Zr_7$. This sample was examined by EDS, and identified as $Zr_{26}Ni_{70}O_4$. This corresponds to a formula $ZrNi_{3-x}O_x$, with x = 0.3. This is written assuming oxygen substitutes for nickel, not for zirconium. Clearly, the

difference in lattice parameters between those reported by Blažina and Ban and those reported here indicate more than just a range of oxygen substitution. This Zr/Ni ratio falls between the 1/2 ratio for a Laves phase and the 1/4 or 1/5 ratio for the $AuBe_5$ type. The Laves phases are tetrahedral close packed structures. The interstitial tetrahedral sites are too small for oxygen atoms, so substitution of oxygen on metal sites is assumed. No silicon was detected, so although it may also stabilize this cubic phase, it is not necessary. A single phase sample was prepared, and the magnetic measurements were taken (see Figure 4.7). A single crystal suitable for diffraction study was not found.

Hexagonal Laves Phase: Zr/Ti/Ni

The reports for the $MgZn_2$ type structure in the ternary Zr/Ti/Ni system are also incomplete. There are no Laves phases known in any of the binary systems, Zr/Ti, Zr/Ni, or Ti/Ni. It would be interesting to find this phase in a ternary system. There is indication that the hexagonal phase exists over a large region of homogeneity. One report gives the range of zirconium present as 21 to 30 atomic percent [106]. A 700°C isotherm of the Zr/Ti/Ni system shows the $MgZn_2$ phase extending from 14-34 atomic % Zr, 27-38 atomic % Ni, and 33-59 atomic % Ti [114].

This phase appeared in a sample which melted at 950°C, and contained a mixture of the $MgZn_2$ type phase and the filled Ti_2Ni type phase. EDS measurements gave the stoichiometry of this hexagonal phase as $Zr_{26}Ti_{32}Ni_{34}O_8$. A single crystal was picked from this mixture. The results are given below. Structure factor amplitudes, including unobserved reflections, are included in the appendix. The stoichiometry from the refinement is much different from that given by EDS, and those given from previous studies.

It is interesting to observe titanium substituting for nickel, in light of the results given for new filled Ti_2Ni phases, and $Zr_6Ni_6TiSiO_{1.8}$, where titanium substituted for zirconium atoms. The

Table 7.1 Crystal data for hexagonal Laves phase

Formula	$ZrNi_{1.45}Ti_{0.55}$
Space group	$P6_3/mmc$ (#194)
a (Å)	5.154(2)
c (Å)	8.376(3)
V (Å^3)	192.7(1)
Z	4
d_{calc} (g/cm^3)	7.06
μ (MoKα) (cm^{-1})	214.06
Data collection instrument	Rigaku AFC6R
Radiation (monochromated in incident beam)	MoKα (λ=0.71069)
Octants measured	$\pm h,\pm k,l$
No. reflections measured	1240
No. unique data, total with $F_o^2 > 3\sigma(F_o^2)$	142
No. parameters refined	12
Trans. factors, max/min	1.00/0.88
R[a], R_w[b], GOF[c]	0.028, 0.034, 1.03
Largest difference peak (e/Å^3)	1.17
Largest negative peak (e/Å^3)	-1.44

[a] $R = \Sigma||F_o|-|F_c||/\Sigma|F_o|$

[b] $R_w = [\Sigma w(|F_o|-|F_c|)^2/ \Sigma w|F_o|^2]^{1/2}$; $w = 1/\sigma^2(|F_o|)$

[c] $GOF = (\Sigma(|F_o|-|F_c|)/ \sigma_i)/ (N_{obs\ refl} - N_{parameters})$

Table 7.2 Atomic parameters for hexagonal Laves phase

Atom	*x*	*y*	*z*	$B_{eq}(Å^2)^a$	% Occupancy
Zr	0.3333	0.6667	0.0670(2)	0.99(5)	100
Ni1	0	0	0	1.0(1)	55(5)
Ti1					45
Ni2	0.8288(3)	0.6575	1/4	0.9(1)	80(5)
Ti2					20

[a] $B_{eq} = 8\pi^2/3\ \Sigma_i^3\Sigma_i^3 U_{ij} a_i^* a_j^* \vec{a}_i^* \vec{a}_j^*$

Table 7.3 Anisotropic thermal parameters for hexagonal Laves phase

Atom	U_{11}	U_{22}	U_{33}	U_{12}	U_{13}	U_{23}
Zr	0.0134(7)	0.0134	0.011(1)	0.007	0	0
Ni1	0.012(1)	0.012	0.014(2)	0.006	0	0
Ti1						
Ni2	0.0112(9)	0.013(1)	0.012(1)	0.007	0	0
Ti2						

Table 7.4 Interatomic distances less than 3.6Å

Zr -	Ni2	2.9987(9)	x 6	Ni2 -	Ni2	2.506(1) x 2
		3.0240(9)	x 3		Ni1	2.5926(7) x 2
	Ni1	3.028(1)	x 3		Ni2	2.648(1) x 2
	Zr	3.065(1)	x 1		Zr	2.9987(9) x 4
		3.181(1)	x 3			3.0240(9) x 2
Ni1 -	Ni2	2.5926(7)	x 6			
	Zr	3.028(1)	x 6			

two factors most frequently used in explaining the Laves phases are the relative sizes of the atoms, and the electron concentration. By size considerations, the titanium might be too small for the large sixteen coordinated site occupied by zirconium. The short titanium - nickel distances seen in this refinement are seen also in the filled Ti_2Ni type phases and $Zr_6Ni_6TiSiO_{1.8}$. Size considerations favor titanium substitution of nickel. By electron concentration considerations for transition metals which form the $MgZn_2$ phase, $ZrNi_{2-x}Ti_x$ would be favored for x ranging from 0.67 to 1.56 [115], assuming there is no substitution on zirconium. Clearly, many details remain unknown.

New Phase in Zr/W/Ni/O System

In trying to prepare a kappa phase of stoichiometry Zr_9W_4NiO, a sample was arc-melted and annealed at 1160°C for 10 hours. The powder pattern of the annealed sample contained lines identified as unreacted tungsten, and W_2Zr, and several more lines for another phase which has not been identified. The powder data is given below. The phase has a distinctive set of low angle lines not observed in any of the phases described previously. EDS measurements indicate titanium is present also.

New Phase in Zr/Ni/S System

Little work was actually performed in the sulfide system. Very likely, new and novel phases will be found in this ternary system. The results of this research show that even very small amounts of oxygen will favor formation of the new oxide phases. Therefore, work in the sulfide system will require great care in excluding all sources of oxygen throughout the synthetic process. As noted previously, the samples studied in this research were routinely handled in air. Thus, it may be necessary to eliminate steps like the arc-melting procedure, where the sample is momentarily exposed to air before and after melting, in favor of melting the samples in sealed metal tubes.

Table 7.5 Powder data for Zr/W/Ni/O sample

2θ	*d*	I/I_o	2θ	*d*	I/I_o
8.770	10.075	26.6	41.574	2.170	1.6
8.950	9.872	15.4	42.224	2.139	6.2
12.235	7.228	2.5	42.824	2.110	5.9
12.655	6.990	11.2	43.980	2.057	1.3
15.196	5.826	2.6	45.189	2.005	4.2
15.526	5.703	2.7	45.489	1.992	1.1
17.712	5.004	2.2	45.824	1.979	7.1
19.496	4.550	2.4	47.742[a]	1.904	18.1
20.188[a]	4.395	25.6	48.220	1.886	3.6
21.033	4.220	1.6	48.569	1.873	1.0
23.774	3.740	3.4	50.240	1.814	0.7
25.519	3.48	1.2	50.461	1.807	1.1
29.905	2.986	0.8	52.390[a]	1.745	12.6
32.728	2.734	7.4	54.183	1.691	1.4
32.936	2.717	3.0	54.869	1.672	2.2
33.268[a]	2.691	11.1	56.578	1.625	1.8
34.194	2.620	2.6	57.031	1.614	1.8
35.195	2.548	17.3	58.239[b]	1.583	22.1
35.390	2.534	1.0	58.497	1.576	2.6
35.771	2.508	2.7	59.417[a]	1.554	3.6
36.162	2.482	61.8	60.739	1.524	6.8
36.724	2.445	58.0	60.964	1.518	1.9
37.001	2.428	34.4	62.877	1.477	5.4
37.205	2.415	20.1	63.441[a]	1.465	44.5
37.282	2.410	13.0	64.623	1.441	9.5
37.447	2.400	11.0	66.037	1.414	48.2
37.787	2.379	15.2	66.918	1.397	3.7
38.674	2.326	36.0	67.343	1.389	11.2
38.909	2.313	39.6	67.583	1.385	3.6
39.223[a]	2.295	72.7	68.845	1.363	1.3
39.671	2.270	81.7	69.807[a]	1.346	32.5
40.275[b]	2.238	100.0			
41.042[a]	2.197	41.5			

[a] W_2Zr
[b] W

Vaporization Study of Nb_4Ni_2O

A sample of Nb_4Ni_2O was annealed at 1350°C for 8 hours, then 1100°C for 1 hour, and quenched. The sample showed the two phases Nb_4Ni_2O (a = 11.5917(5) Å) and Nb_6Ni_6O (a = 11.2344(7) Å), as well as NbO, which was also present as a minor phase in the initial sample. The quartz jacket had black vapor deposited film, probably nickel. It would be worthwhile to study the thermodynamics of the decomposition of Nb_4Ni_2O at high temperatures. The relation between these two phases may reveal much more about the filled Ti_2Ni structures in general.

REFERENCES

1. Moody, G.J.; Thomas, J.D.R. *J. Chem. Soc.* **1964**, *1964*, 1417.
2. Owens, J.P.; Conard, B.R.; Franzen, H.F. *Acta Cryst.* **1967**, *23*, 77.
3. Kapustinskii, A.F. *Quart. Rev. Chem. Soc.* **1956**, *10*, 283.
4. Pauling, L. *The Nature of the Chemical Bond.* 3rd ed. Cornell University Press, Ithaca, 1960.
5. Owens, J.P.; Franzen, H.F. *Acta Cryst.* **1974**, *B30*, 427.
6. Conard, B.R.; Franzen, H.F. *High Temp. Sci.* **1971**, *3*, 49.
7. Chen, H.-Y.; Franzen, H.F. *Acta Cryst.* **1972**, *B28*, 1399.
8. Franzen, H.F.; Graham, J. *Z. Kristallogr.* **1966**, *123*, 133.
9. Franzen, H.F.; Beineke, T.A.; Conard, B.R. *Acta Cryst.* **1968**, *B24*, 412.
10. Chen, H.-Y.; Tuenge, R.T.; Franzen, H.F. *Inorg. Chem.* **1973**, *12*, 552.
11. Franzen, H.F.; Smeggil, J.G. *Acta Cryst.* **1969**, *B25*, 1736.
12. Franzen, H.F.; Smeggil, J.G. *Acta Cryst.* **1970**, *B26*, 125.
13. Harbrecht, B. *J. Less-Common Met.* **1988**, *138*, 225.
14. Wada, H.; Onoda, M. *Mat. Res. Bull.* **1989**, *24*, 191.
15. Kim, S.-J.; Nanjundaswamy, K.S.; Hughbanks, T. *Inorg. Chem.* **1991**, *30*, 159.
16. Yao, X.; Franzen, H.F. *J. Solid State Chem.* **1991**, *86*, 88.
17. Yao, X.; Franzen, H.F. *J. Amer. Chem. Soc.* **1991**, *113*, 1426.
18. Yao, X.; Franzen, H.F. *Z. Anorg. Allg. Chem.* **1991**, *598/599*, 353.
19. Yao, X.; Miller, G.J.; Franzen, H.F. *J. Alloys Compd.* **1992**, *183*, 7.
20. Yao, X.; Marking, G.; Franzen, H.F. *Ber. Bunsenges. Phys. Chem.* **1992**, *96*, 1552.
21. Marking, G.A. Ph.D. Dissertation, Iowa State University, 1993.
22. Nanjundaswamy, K.S.; Hughbanks, T. *J. Solid State Chem.* **1992**, *98*, 278.

23. Franzen, H.F. *Prog. Solid St. Chem.* **1978**, *12*, 1.

24. Harbrecht, B.; Franzen, H.F. *J. Less-Common Met.* **1986**, *115*, 177.

25. Harbrecht, B. *J. Less-Common Met.* **1986**, *124*, 125.

26. Calhorda, M.J.; Hoffmann, R. *Inorg. Chem.* **1988**, *27*, 4679.

27. Harbrecht, B. *Z. Kristallogr.* **1988**, *182*, 118.

28. Harbrecht, B. *J. Less-Common Met.* **1988**, *141*, 59.

29. Conard, B.R. Ph.D. Dissertation, Iowa State University, 1969.

30. Franzen, H.F. *Anales de Fisica* **1990**, *B86*, 39.

31. Smeggil, J.G. Ph.D. Dissertation, Iowa State University, 1969.

32. *Binary Alloy Phase Diagrams, 2nd Ed.*; T.B. Massalski, Ed.; ASM International, Materials Park, 1970.

33. Laves, F. In *Theory of Alloy Phases*, Amer. Soc. Met., Cleveland, Ohio, 1956.

34. a)Slater, J.C. *J. Chem. Phys.* **1964**, *41*, 3199. b)Slater, J.C. *Quantum Theory of Molecules and Solids, Vol. 2*, McGraw-Hill Book Co., Inc., New York, 1963.

35. Goldschmidt, V.M. *Trans. Faraday Soc.* **1929**, *25*, 253.

36. Zachariasen, W.H. *Z. Kristallogr.* **1932**, *81*, 1.

37. Pauling, L. *Proc. Roy Soc. A.* **1927**, *114*, 181.

38. a)Shannon, R.D.; Prewitt, C.T. *Acta Cryst.* **1969**, *B25*, 928. b)Shannon, R.D. *Acta Cryst.* **1976**, *A32*, 752.

39. Nevitt, M.V.; Downey, J.W. *Trans. Met. Soc. AIME*, **1961**, *221*, 1014.

40. Cima, M.; Brewer, L. *Met. Trans. B* **1988**, *19B*, 893.

41. Brewer, L; Wengert, P.R. *Met. Trans.* **1973**, *4*, 83.

42. Brewer, L In *Alloying*, J.L. Walter; M.R. Jackson; C.T. Sims, Eds.; ASM International, Metals Park, 1988.

43. Hume-Rothery, W. *Prog. Mat. Sci.* **1968**, *13*, 229.

44. Johnston, R.L.; Hoffmann, R. *Z. Anorg. All. Chem.* **1992**, *616*, 105.

45. Hoistad, L.M.; Lee, S. *J. Am. Chem. Soc.* **1991**, *113*, 8216.

46. Leonard, S.R.; Snyder, B.S.; Brewer, L.; Stacy, A.M. *J. Solid State Chem.* **1991**, *92*, 39.

47. Bsenko, L. *J. Less-Common Met.* **1979**, *63*, 171.

48. Petkov, V.V.; Markiv, V.Ya.; Gorskiy, V.V. *Russ. Metallurgy*, **1972**, *2*, 188.

49. McGlynn, S.P.; Vanquickenborne, L.G.; Kinoshita, M.; Carroll, D.G. *Introduction to Applied Quantum Chemistry*, Holt, Rinehart and Winston, Inc., New York, 1972.

50. Basch, H.; Viste, A.; Gray, H.B. *Theoret. Chim. Acta* **1965**, *3*, 458.

51. Miller, G.J., Department of Chemistry, Iowa State University, Ames, IA, unpublished research, 1991.

52. Hoffmann,R. *J. Chem. Phys.* **1963**, *39*, 1397.

53. Ammeter, J.H.; Bürgi, H.-B.; Thibeault, J.C.; Hoffmann, R. *J. Am. Chem. Soc.* **1978**, *100*, 3686.

54. Whangbo, M.-H.; Hoffmann, R. *J. Chem. Phys.* **1978**, *68*, 5498.

55. Takusagowa, F., Ames Laboratory, Iowa State University, Ames, IA, unpublished research, 1981.

56. Ziebarth, R.P., Ames Laboratory, Iowa State University, Ames, IA, unpublished research, 1984.

57. Clark, C.M.; Smith, D.K.; Johnson, G.J. "A Fortran IV Program for Calculating X-Ray Powder diffraction Pattern-Version5," Department of Geosciences, Pennsylvania State University, University Park, 1973.

58. Johnson, C.K. "ORTEP-II, A Fortran Thermal-Ellipsoid Plot Program," Report ORNL-5138, Oak Ridge National Laboratory, Oak Ridge, 1976.

59. Werner, P.-E. "SCANPI Version 8 for IBM PC/AT," Arrhenius Laboratory, University of Stockholm, Sweden, 1990.

60. Malmros, G.; Werner, P.-E. *Acta Chem. Scand.* **1973**, *27*, 493.

61. Johansson, K.E.; Palm, T.; Werner, P.-E. *J. Phys. E:Sci. Instrum.* **1980**, *13*, 1289.

62. Sheldrick, G.M. In *Crystallographic Computing 3*, G.M. Sheldrick; C. Krüger; R. Goddard, Eds.; Oxford University Press, 1985.

63. TEXSAN: Single Crystal Structure Analysis Software, Version 5.0, Molecular Structure

Corporation, The Woodlands, 1989.

64. Krypyakevich, P.I.; Markiv, V.Ya; Burnashova, V.V. *Dopov. Akad. Nauk Ukr. RSR, Ser* A, **1970**, *32(6)*, 551.

65. Boller, H. *Monatsh für Chem* **1973**, *104*, 545.

66. Mackay, R.; Franzen, H.F. *J. Alloys Compd.* **1992**, *186*, L7.

67. *Pearson's Handbook of Crystallographic Data for Intermetallic Phases* 2nd ed., P. Villars and L.D.Calvert, Eds., Amer. Soc. Metals, Materials Park, 1991.

68. Westgren, A.; Phragmén, G. *Trans. Amer. Soc. Steel Treating*, **1928**, *13*, 539.

69. Nevitt, M.V. In *Intermetallic Compounds*, J.H. Westbrook, Ed.; John Wiley & Sons, Inc. 1967, 220-224.

70. Kuo, K. *Acta Met.* **1953**, *1*, 301.

71. Jeitschko, W.; Holleck, H.; Nowotny, H.; Benesovsky, F. *Monatsh. Chem.* **1964**, *95*, 1004.

72. Newsam, J.M.; Jacobson, A.J.; McCandlish, L.E.; Polizzotti, R.S. *J. Solid State Chem.* **1988**, *75*, 296.

73. Kotyk, M.; Stadelmaier, H.H. *Metallurgical Trans.* **1970**, *1*, 889.

74. Holleck, H.; Thümmler, F. *Monatsh. Chem.* **1967**, *98*, 133.

75. Nevitt, M.V.; Downey, J.W.; Morris, R.A.*Trans. Met. Soc. AIME* **1960**, *218*, 1019.

76. Karlsson, N. *Nature*, **1951**, *168*, 538.

77. Bonhomme, F.; Selvam, P.; Yoshida, M.; Yvon, K.; Fischer, P. *J. Alloys Comps.* **1992**, *178*, 167.

78. Rupp, B.; Fischer, P. *J. Less-Common Met.* **1988**, *144*, 275.

79. Mueller, M.H..; Knott, H.W. *Trans. Met. Soc. AIME* **1963**, *227*, 674.

80. Mackay, R.; Franzen, H.F. *Z. Anorg. Allg. Chem.* **1992**, *616*, 154.

81. Mackay, R.; Franzen, H.F. *Chem. Mater.* accepted for publication.

82. Hamilton, W.C. *Acta Cryst.* **1965**, *18*, 502.

83. Stadelmaier, H.H.; Fiedler, M.-L. *Z. Metallkde.* **1975**, *66*, 224.

84. Hyde, B.G.; Andersson, S. *Inorganic Crystal Structures*, John Wiley & Sons, Inc. N.Y. 1989.

85. Basch, H.; Gray, H.B.; *Theor. Chim. Acta* **1966**, *4*, 367.

86. Richardson, J.W.; Nieuwport, W.C.; Powell, R.R.; Edgell, W.F. *J. Chem. Phys.* **1962**, *36*, 1057.

87. Hoffmann, R. *J. Chem. Phys.* **1963**, *39*, 1397.

88. Baranovskii, V.I.; Nikolskii, A.B. *Teor. Eksp. Khim.* **1967**, *3*, 527.

89. Herman, F.; Sillman, S. *Atomic Structure Calculations*, Prentice Hall, Englewood Cliffs, 1963.

90. Rogl, P.;Nowotny, *H.Monatsh. Chem.* **1976**, *108*, 1167.

91. Andersson, S.; Hyde, S.T.; von Schnering, H.G. *Z. Kristallogr.* **1984**, *168*, 1.

92. von Schnering, H.G.; Nesper, R. *Angew. Chem. (Int. Ed. Eng.)* **1987**, *27*, 1059.

93. Rautala, P.; Norton, J.T. *Trans. AIME*, **1952**, *194*, 1045.

94. Hårsta, A.; Rundqvist, S. *J. Solid State Chem.* **1987**, *70*, 210 and references therein.

95. Schewe-Miller, I. unpublished results, Ames Laboratory, Iowa State University, Ames, Iowa, 1993.

96. Hårsta, A.; Johansson, T.; Rundqvist, S.; Thomas, J.O. *Acta Chem. Scand. Ser. A*, **1977**, *31*, 260.

97. Rogl, P.; Nowotny, H.; Benesovsky, F. *Monatsh. Chem.* **1973**, *104*, 182.

98. Hårsta, A. *J. Solid State Chem.* **1985**, *57*, 362.

99. Hårsta, A. *J. Solid State Chem.* **1985**, *57*, 373.

100. Hårsta, A. *Acta Chem. Scand. Ser.A* **1981**, *35*, 43.

101. Hårsta, A. *Acta Chem. Scand. Ser.A* **1982**, *36*, 535.

102. Rogl, P.; Rupp, B.; Wiesinger, G.; Schefer, J.; Fischer, P. *J. Less-Common Met.* **1985**, *113*, 103.

103. Hårsta, A.; Rundqvist, S.; Thomas, J.O. *J. Solid State Chem.* **1983**, *49*, 118.

104. Kirkpatrick, M.E.; Larsen, W.L. *Trans. Amer. Soc. Metals*, **1961**, *54*, 580.

105. Semenenko, K.N.; Verbetskii, V.N.; Mitrokhin, S.V.; Burnasheva, V.V. *Russ. J. Inorg. Chem.*, **1980**, *25*, 961.

106. Molokanov, V.V.;Chebotnikov, V.N.;Kovneristyi, Yu.K. *Inorg. Mat.*, **1989**, *25*, 46.

107. van Vucht, J.H.N. *J. Less-Common Met.*, **1966**, *11*, 308.

108. Glimois, J.L.; Forey, R.; Guillen, R. J.L. Feron, *J. Less-Common Met.*, **1987**, *134*, 221.

109. Zhao, J.T. Ph.D. Dissertation, Universite de Geneve, 1991.

110. Rabe, K.M.; Phillips, J.C.; Villars, P.; Brown, I.D. *Phys. Rev. B* **1992**, *45*, 7650.

111. Selwood, P.W. *Magnetochemistry*, 2nd ed. Interscience Publishers, New York, 1956.

112. Bsenko, L. *J. Less-Common Met.* **1979**, *63*, 171.

113. Blažina, Ž.; Ban, Z. *J. Less-Common Met.* **1973**, *33*, 321.

114. Eremenko, V.N.; Semenova, E.L.; Tretyachenko, L.A. *Dopo. Akad. Nauk Ukr. RSR, Ser. A* **1988**, *50*, 76.

115. Haydock, R.; Johannes, R.L. *J. Phys. F: Metal Phys.* **1975**, *5*, 2055.

ACKNOWLEDGEMENTS

It has been a privilege working under the direction of Professor Hugo F. Franzen, and a pleasure working with the group members.

J.W. Anderegg was responsible for the ESCA studies. Dr. G.J. Miller was very helpful with the band calculations. Dr. J. Ostenson performed the magnetic measurements. Quantitative EDS was done by Dr. W. Straszheim. Qualitative EDS was done by G.L. Schimek. Shirley Standley provided secretarial assistance.

This work was performed at Ames Laboratory under contract no. W-7405-eng-82 with the U.S. Department of Energy. The United States government has assigned the DOE Report number IS-T 1647 to this thesis.

APPENDIX:

OBSERVED AND CALCULATED STRUCTURE FACTOR AMPLITUDES

Observed and calculated structure factor amplitudes (x10) for Zr_3NiO

k	l	Fo	Fc	sigF
^^^^^^^	h =	0	^^^^^^^	
0	2	275	146	24
0	4	2177	2191	36
0	6	2363	2391	40
0	10	1617	1630	39
2	1	224	44	29
2	3	2812	2789	44
2	5	1104	1081	27
2	6	374	354	30
2	7	1185	1188	32
2	9	727	681	31
2	11	494	440	38
4	0	1266	1209	26
4	1	1418	1418	27
4	2	2068	2049	35
4	3	577	591	23
4	4	638	669	32
4	5	1267	1290	30
4	6	569	548	29
4	7	580	574	27
4	8	1619	1633	36
4	9	504	469	34
4	10	555	539	34
6	0	595	573	26
6	1	1070	1100	29
6	2	2028	2070	36
6	3	1041	1040	29
6	4	1064	1100	30
6	5	1706	1671	34
6	6	741	755	39
6	8	1203	1189	36
6	10	539	443	34
8	0	1300	1331	32
8	1	324	333	40
8	2	1312	1273	33
8	3	652	671	30
8	5	656	656	31
8	6	399	429	38
8	8	923	964	43
10	0	1516	1532	36
10	1	1025	1036	36
10	3	397	305	39
10	4	658	637	34
10	5	1363	1420	38
10	6	1096	1097	40
12	2	956	994	43
12	3	991	1070	42
12	4	347	416	56
14	0	920	920	46
14	2	481	469	43
^^^^^^^	h =	1	^^^^^^^	
-13	-3	319	284	41
-11	-6	383	429	42
-11	-2	1073	1078	30
-9	-5	378	402	32
-9	-4	381	366	29
-9	-3	2006	1949	36
-9	0	618	627	24
-7	-8	534	497	30
-7	-6	1475	1496	30
-7	-4	762	744	24
-7	-1	572	577	20
-7	0	2329	2339	38
-5	-9	296	337	42
-5	-8	667	641	23
-5	-7	647	635	48
-5	-5	1173	1181	26
-5	-3	1566	1540	28
-5	-1	518	525	18
-3	-10	723	702	26
-3	-9	719	731	66
-3	-4	452	467	18
-3	-2	1195	1183	26
-3	-1	2265	2300	59
-1	-11	421	447	34
-1	-7	748	720	27
-1	-4	950	981	22
-1	-2	1914	1903	31
1	3	1790	1795	29
1	5	964	922	23
1	8	1451	1473	36
3	0	2429	2340	55
3	3	710	693	22
3	5	2191	2249	36
3	6	888	882	25
3	7	735	748	34
3	8	738	756	26
5	0	658	641	36
5	2	1108	1110	23
7	3	1100	1142	26
7	7	715	711	52
9	1	367	332	28
9	2	368	311	28
9	6	493	518	27
9	7	1059	1046	42
11	0	1084	1079	30
13	1	1043	988	32
^^^^^^^	h =	2	^^^^^^^	
-10	-6	922	915	58
-10	-4	539	511	25
-10	-1	883	867	41
-8	-6	354	314	58
-8	-2	1083	1097	56
-6	-5	1385	1387	66
-6	-4	871	850	28
-6	-3	810	802	24
-6	-1	860	867	26
-4	-9	446	409	30
-4	-7	510	486	24
-4	-6	499	496	23
-4	-5	1037	1038	27
-4	-3	441	457	25
-4	-2	1492	1477	60
-4	0	993	978	43
-2	-3	2046	2044	35
0	-6	1835	1877	32
0	0	3571	3572	55
0	4	1525	1550	28
0	10	1387	1378	32
2	5	839	826	42
2	7	1025	992	27
2	9	548	591	39
4	1	1054	1041	48
4	4	459	430	22
4	8	1300	1332	31
6	2	1535	1537	39
6	6	590	581	22
6	8	965	989	32
8	0	994	989	28
8	3	533	537	23
8	5	545	562	24
10	0	1285	1249	70
10	5	1185	1214	31
12	2	825	825	26
12	3	963	938	73
^^^^^^^	h =	3	^^^^^^^	
-9	-3	1384	1349	32
-9	0	465	490	35
-7	0	1588	1602	31
-5	-7	555	549	77
-5	-5	718	710	26
-5	-3	1115	1135	91
-5	-2	706	715	24
-3	-7	456	478	53
-3	-2	659	663	46
-3	-1	1249	1288	28
-3	0	1352	1355	28
-1	-8	1080	1081	34
-1	-7	383	418	34
-1	-5	749	721	45
-1	-3	1000	968	28
1	1	287	252	33
1	2	1163	1183	28
1	4	607	615	25
3	3	365	356	29
3	5	1411	1443	94
3	6	612	641	27
7	3	736	709	25
7	4	537	543	32
7	6	1099	1093	57
^^^^^^^	h =	4	^^^^^^^	
-4	-3	332	295	40
-4	-2	784	773	27
-4	-1	675	627	25
-2	-3	1186	1215	64
0	0	1841	1859	35
0	4	833	830	28
4	0	705	690	64

Observed and calculated structure factor amplitudes (X5) for Zr_4Ni_2O

k	l	Fo	Fc	sigF
^^^^^^^ h = 0 ^^^^^^^				
0	16	2781	2824	67
2	2	400	190	58
6	6	6587	6566	0
6	14	1121	1111	29
8	0	3175	3152	52
^^^^^^^ h = 1 ^^^^^^^				
1	5	5267	5223	80
1	11	1439	1369	39
1	15	579	513	81
7	7	996	1010	48
9	1	1029	1071	36
9	7	985	938	25
9	9	778	753	40
9	13	548	546	69
11	11	605	679	62
17	1	990	900	45
^^^^^^^ h = 2 ^^^^^^^				
2	6	1689	1642	56
4	2	3551	3586	55
8	2	4045	4063	64
8	4	1312	1332	31
8	6	1217	1191	30
8	8	1185	1198	35
10	2	2361	2341	44
14	0	549	612	51
16	2	611	516	61
^^^^^^^ h = 3 ^^^^^^^				
1	3	2032	2056	35
1	5	786	820	19
3	3	5639	5683	88
3	7	2175	2185	42
3	13	1174	1174	45
3	15	2061	2073	50
9	5	763	768	26
11	7	800	842	29
13	1	1837	1828	38
^^^^^^^ h = 4 ^^^^^^^				
0	4	5558	5520	85
2	4	1593	1575	32
4	4	3172	3165	56
4	10	629	670	67
6	2	762	757	21
6	10	2491	2456	42
8	0	1528	1532	31
8	14	691	632	55
16	0	1465	1419	34
16	4	1180	1178	39
^^^^^^^ h = 5 ^^^^^^^				
3	5	1729	1733	36
3	11	1051	1036	25
5	1	771	763	27
5	5	5300	5339	86
5	11	1807	1826	45
5	13	954	939	37
5	15	1300	1283	38
7	1	1037	1043	24
9	9	875	866	38
15	1	832	854	34
^^^^^^^ h = 6 ^^^^^^^				
0	2	895	869	27
2	6	1653	1590	39
2	10	1429	1440	35
4	6	1036	970	32
6	6	1428	1456	64
6	8	536	476	47
6	14	868	861	46
10	0	1791	1769	35
^^^^^^^ h = 7 ^^^^^^^				
1	1	1327	1332	35
3	1	1086	1141	24
3	9	541	547	42
5	3	1167	1146	38
5	5	2031	2041	41
5	7	1448	1502	41
7	3	1396	1484	41
7	7	543	591	84
9	9	802	772	56
11	11	971	965	42
13	3	2087	2139	41
^^^^^^^ h = 8 ^^^^^^^				
0	12	958	987	29
4	8	3953	3922	64
8	8	2218	2307	66
8	12	2284	2365	52
^^^^^^^ h = 9 ^^^^^^^				
1	5	1627	1582	33
1	11	695	675	35
3	3	4232	4260	67
3	13	1428	1394	32
5	13	747	761	36
7	7	1735	1738	54
9	3	1961	1941	44
9	9	2021	2063	73
11	3	524	489	83
^^^^^^^ h = 10 ^^^^^^^				
0	2	2033	2019	37
0	10	3334	3297	58
2	8	1313	1334	30
4	2	623	626	46
6	6	1181	1139	37
6	10	835	817	55
6	12	849	925	34
8	4	554	586	59
8	8	750	641	44
10	2	554	593	74
10	4	594	565	94
^^^^^^^ h = 11 ^^^^^^^				
1	5	2488	2507	43
3	11	1096	1144	38
5	11	2703	2695	54
7	1	1888	1901	38
9	5	924	918	33
^^^^^^^ h = 12 ^^^^^^^				
0	0	2885	2859	51
0	4	1768	1780	37
2	2	1268	1269	62
6	6	2588	2586	50
12	0	2482	2501	54
^^^^^^^ h = 13 ^^^^^^^				
5	7	546	519	51
7	7	722	664	49
^^^^^^^ h = 14 ^^^^^^^				
2	2	1871	1838	47
2	4	1566	1580	37
4	4	599	559	55
6	2	1068	1041	30
8	2	2342	2373	44

Observed and calculated structure factor amplitudes (X3) for $Zr_6Ni_4Ti_2O_{0.6}$

k	l	Fo	Fc	sigF
^^^^^^^	h =	0	^^^^^^^	
0	12	1933	1921	82
4	4	2603	2590	42
8	0	868	780	27
10	6	1313	1320	29
16	0	1345	1448	40
16	4	933	901	33
16	8	650	688	80
^^^^^^^	h =	1	^^^^^^^	
1	7	827	861	45
5	1	2976	2979	47
5	5	883	892	41
11	7	966	949	29
15	5	670	683	72
^^^^^^^	h =	2	^^^^^^^	
2	8	2509	2556	43
2	14	725	697	53
4	2	2010	2059	35
4	6	395	397	54
4	16	450	390	65
6	2	685	675	26
10	8	717	681	55
12	6	572	563	37
16	6	546	508	52
^^^^^^^	h =	3	^^^^^^^	
1	7	690	724	21
1	13	971	932	26
3	1	1020	989	32
3	3	3636	3489	60
3	9	2259	2260	42
3	13	901	871	36
3	15	962	991	99
^^^^^^^	h =	4	^^^^^^^	
0	0	1038	1029	28
2	4	1169	1197	43
4	4	554	576	50
6	6	557	557	53
8	2	783	818	23
10	4	714	697	35
12	12	567	553	61
^^^^^^^	h =	5	^^^^^^^	
3	3	708	694	66
5	5	2933	2972	57
5	15	654	659	53
7	7	689	747	36
9	9	683	667	42
11	5	1125	1107	70
11	13	558	553	88
^^^^^^^	h =	6	^^^^^^^	
6	0	3627	3693	58
6	2	501	496	38
10	2	373	320	58
10	4	1297	1308	29
12	6	1275	1285	59
16	6	752	727	86
^^^^^^^	h =	7	^^^^^^^	
3	3	1410	1375	34
3	5	684	712	28
3	7	1034	1055	30
3	13	1079	1086	27
5	5	1380	1354	37
7	1	1059	1048	32
9	7	801	755	66
13	5	558	519	46
13	7	852	833	78
^^^^^^^	h =	8	^^^^^^^	
4	8	1860	1831	42
6	2	547	585	43
8	8	1600	1651	70
8	12	1014	1082	39
12	0	759	728	31
^^^^^^^	h =	9	^^^^^^^	
1	5	553	613	55
5	5	502	509	48
7	1	549	516	31
7	3	387	381	46
7	13	582	538	45
9	3	1060	1078	32
9	9	773	849	76
^^^^^^^	h =	10	^^^^^^^	
2	0	1252	1213	30
2	2	1143	1164	33
4	10	897	843	85
8	4	554	540	38
10	0	1723	1780	46
14	0	676	645	72
^^^^^^^	h =	11	^^^^^^^	
1	1	653	659	39
5	1	1485	1471	34
5	3	401	400	60
7	3	534	542	45
11	1	545	435	56
11	5	1307	1311	39
^^^^^^^	h =	12	^^^^^^^	
0	12	1015	990	67
2	2	911	905	33
4	0	445	483	48
^^^^^^^	h =	13	^^^^^^^	
5	1	450	413	51
9	3	673	673	55
^^^^^^^	h =	14	^^^^^^^	
2	4	775	748	31
2	8	1215	1191	29

Observed and calculated structure factor amplitudes (X5) for Nb_6Ni_6O

k	l	Fo	Fc	sigF
^^^^^^^ h = 0 ^^^^^^^				
4	0	2268	2361	39
8	0	2050	2043	43
^^^^^^^ h = 1 ^^^^^^^				
1	1	678	580	33
5	1	5359	5341	82
11	1	834	811	43
^^^^^^^ h = 2 ^^^^^^^				
2	2	513	490	60
4	2	3175	3216	51
6	0	458	366	35
10	0	2281	2266	41
10	2	2480	2440	49
14	0	1036	1061	34
14	2	1525	1561	56
^^^^^^^ h = 3 ^^^^^^^				
3	1	1621	1708	34
3	3	5230	5240	83
5	1	456	480	43
7	1	1283	1253	29
7	3	2668	2697	48
9	3	3456	3464	59
13	1	1675	1656	46
^^^^^^^ h = 4 ^^^^^^^				
4	0	5833	5926	92
4	2	2168	2119	52
12	0	790	773	36
^^^^^^^ h = 5 ^^^^^^^				
3	3	1145	1123	61
5	1	1565	1556	39
5	3	1652	1666	61
5	5	5570	5538	92
7	3	1637	1636	44
9	5	1454	1458	41
11	1	2095	2037	41
13	1	858	948	70
^^^^^^^ h = 6 ^^^^^^^				
2	2	1612	1593	37
6	0	5443	5401	84
6	2	1233	1201	36
6	6	975	1004	61
8	2	1196	1186	28
8	6	1214	1217	36
10	0	2424	2379	44
10	6	758	825	53
^^^^^^^ h = 7 ^^^^^^^				
1	1	802	764	33
5	1	404	352	57
5	5	1974	1984	45
7	1	2774	2752	70
7	3	2221	2254	47
7	5	1074	1070	45
7	7	1491	1477	62
9	7	1562	1547	41
11	1	1185	1191	44
11	3	1600	1642	35
^^^^^^^ h = 8 ^^^^^^^				
2	2	4402	4378	70
4	2	1524	1486	33
8	0	856	833	45
8	2	1113	1127	37
8	4	2733	2772	53
8	8	2256	2241	78
10	4	1066	1072	32
12	0	2028	2073	45
^^^^^^^ h = 9 ^^^^^^^				
3	1	1200	1192	29
5	1	1733	1733	38
5	3	832	815	35
7	1	1059	1005	29
7	5	715	711	98
9	1	979	987	42
9	3	895	916	54
9	5	2275	2267	53
^^^^^^^ h = 10 ^^^^^^^				
4	2	594	542	71
4	4	1321	1349	49
6	2	827	786	33
6	4	2403	2415	44
8	2	879	903	34
8	6	936	947	35
10	0	3553	3573	64
^^^^^^^ h = 11 ^^^^^^^				
3	1	991	988	31
5	3	503	533	63
5	5	1881	1955	52
9	1	817	862	89
^^^^^^^ h = 12 ^^^^^^^				
0	0	2642	2622	53
2	2	2531	2463	52
4	4	620	546	96
6	2	2150	2191	44
^^^^^^^ h = 13 ^^^^^^^				
3	3	1162	1117	41

Observed and calculated structure factor amplitudes (X1) for $Nb_6Ni_4Ta_2O_2$

k	l	Fo	Fc	sigF	k	l	Fo	Fc	sigF	k	l	Fo	Fc	sigF
^^^^^^^	h =	0	^^^^^^^		-4	0	1415	1427	50	-9	-9	615	578	23
					4	4	822	809	60	-9	-7	316	328	17
2	6	183	188	13	4	8	151	141	19	-9	-3	412	399	12
6	10	653	657	15	4	14	187	166	29	-9	-1	216	195	22
										-7	-5	236	217	12
^^^^^^^	h =	1	^^^^^^^	^^^^^^^	h =	5	^^^^^^^			1	5	360	364	8
										5	3	193	191	10
-15	-5	431	429	9	-7	-13	349	350	9	9	5	327	335	14
-11	-3	226	231	13	-7	-3	462	460	9					
-7	-1	173	165	12	-5	-11	724	712	21	^^^^^^^	h =	10	^^^^^^^	
-5	-3	301	297	9	-5	-7	375	376	14					
-3	-13	530	542	10	-5	-3	454	439	13	-10	-6	422	414	15
-3	-3	686	694	26	-1	-5	232	246	20	-10	-4	304	335	15
-1	-11	506	526	14	1	7	358	360	12	-8	-6	176	182	27
1	3	156	150	9	5	5	1365	1336	95	-4	-6	487	483	9
3	9	178	157	17	5	13	247	251	21	-4	-4	278	281	11
3	15	244	225	14	11	1	476	470	10	0	-10	670	675	15
5	1	1341	1339	51						2	10	228	207	21
9	1	206	213	18	^^^^^^^	h =	6	^^^^^^^		6	6	476	465	20
^^^^^^^	h =	2	^^^^^^^		-6	-6	544	559	35	^^^^^^^	h =	11	^^^^^^^	
					-2	-14	374	380	10					
-10	0	417	435	14	2	10	487	479	9	-11	-3	253	250	14
-8	-10	349	353	10	6	0	1512	1529	60	-9	-3	159	145	24
-8	-2	1100	1086	30						-3	-3	181	172	18
-6	-6	637	631	22	^^^^^^^	h =	7	^^^^^^^		-1	-7	573	587	11
-4	-8	309	299	7						5	3	332	336	8
-2	-14	587	587	18	-7	-7	265	241	18					
-2	-6	778	776	28	-7	-3	232	238	16	^^^^^^^	h =	12	^^^^^^^	
-2	-4	871	866	32	-7	-1	539	533	16					
-2	-2	439	451	25	-5	-7	512	512	12	-8	-4	239	232	11
0	-2	134	34	17	-1	-9	402	405	9	0	-8	568	572	11
2	12	333	327	10	3	3	798	796	26	0	0	509	534	22
4	4	441	434	21	9	7	445	451	11	6	6	683	689	15
10	2	857	847	22	11	3	311	326	8					
					13	3	595	598	12	^^^^^^^	h =	13	^^^^^^^	
^^^^^^^	h =	3	^^^^^^^											
					^^^^^^^	h =	8	^^^^^^^		-3	-9	493	483	10
-5	-3	237	223	12						-1	-7	211	200	15
3	3	1224	1206	0	-8	-4	1203	1203	21	3	3	283	278	12
3	9	1188	1173	36	-8	-2	206	221	16					
					-2	-6	225	219	12	^^^^^^^	h =	14	^^^^^^^	
^^^^^^^	h =	4	^^^^^^^		0	-8	319	332	16					
					0	0	763	795	49	-2	-8	625	622	12
-14	-2	441	433	11	4	0	474	495	12					
-12	0	636	645	13	8	8	475	468	29	^^^^^^^	h =	15	^^^^^^^	
-8	-10	205	212	19										
-6	-6	363	356	10	^^^^^^^	h =	9	^^^^^^^		3	3	637	634	14
-6	-2	128	130	17										
-4	-12	388	385	12	-11	-1	327	322	9	^^^^^^^	h =	16	^^^^^^^	
										0	0	1015	1011	19

Observed and calculated structure factor amplitudes (x10) for $Zr_9W_4(S/Ni)O_3$

k	l	Fo	Fc	sigF
^^^^^^^	h =	0	^^^^^^^	
0	2	1571	1460	0
0	4	7364	7305	0
0	6	4407	4346	80
0	8	2632	2653	79
0	10	3746	3823	87
1	-5	771	652	67
2	3	3842	3839	61
2	9	1032	1066	65
3	-9	2654	2578	59
3	-6	3026	2997	56
3	-1	4808	5130	0
3	4	1263	1232	33
4	-2	2272	2343	48
5	2	4349	4452	71
6	-7	1762	1829	59
6	-6	2188	2186	60
6	-5	3503	3507	64
8	-4	969	848	0
9	2	1915	1844	64
^^^^^^^	h =	1	^^^^^^^	
-9	-3	746	570	85
-9	0	956	1016	0
-8	4	1060	1039	93
-7	2	1432	1449	40
-7	7	820	805	73
-5	4	935	956	56
-5	6	662	736	82
-4	3	1775	1794	38
-4	6	1401	1399	35
-3	8	1380	1363	45
-2	0	905	684	95
-2	4	1084	1108	41
-2	6	909	936	55
-2	8	1315	1307	51
-1	-4	2361	2296	45
-1	0	2451	2468	64
-1	8	1907	1895	44
0	-7	1190	1162	45
0	-3	2028	1969	41
0	2	606	472	78
1	-10	875	881	0
2	-10	774	775	81
3	-10	1247	1218	55
3	-9	1232	1185	50
4	-8	822	884	0
5	-7	1698	1694	52
5	8	890	877	66
6	-5	773	868	0
7	0	1997	1930	73
^^^^^^^	h =	2	^^^^^^^	
-9	-2	1775	1820	42
-9	0	1227	1201	62
-8	0	869	748	78
-8	2	2875	2914	73
-8	6	1423	1385	56
-6	0	2026	1906	82
-5	3	2639	2629	48
-4	0	3678	3548	95
-4	2	2250	2232	93
-2	-7	2479	2461	53
0	-10	1217	1289	83
0	-6	1325	1274	43
0	-4	1522	1521	34
0	-1	1225	1220	37
0	8	1994	2011	49
1	-2	4259	4222	66
1	0	1066	1094	40
1	6	1641	1632	36
2	-4	1836	1842	46
3	-4	1306	1378	39
3	8	1957	1987	42
5	-8	1298	1350	58
5	6	989	941	64
7	-5	1135	1184	93
^^^^^^^	h =	3	^^^^^^^	
-10	1	1464	1436	43
-9	0	977	960	0
-9	5	2035	2088	52
-8	-3	2194	2220	46
-8	-1	603	627	75
-8	4	1305	1214	40
-8	7	1644	1623	42
-7	0	3443	3441	65
-7	4	2218	2287	47
-7	8	984	931	83
-6	4	4620	4729	95
-6	8	2659	2643	72
-5	-5	770	664	49
-5	0	596	557	86
-5	2	709	718	49
-4	1	1836	1902	30
-4	2	952	951	33
-4	7	1382	1369	50
-4	8	854	778	60
-3	-2	2168	2137	50
-3	0	2595	2656	55
-3	10	2534	2536	55
0	-7	1985	1944	50
0	-5	5331	5262	84
0	-3	2186	2193	64
1	-5	1594	1576	34
2	-9	616	604	0
2	-7	1737	1753	40
3	-6	2966	3010	64
3	0	6488	6394	0
3	2	2051	2077	67
6	2	1610	1625	50
^^^^^^^	h =	4	^^^^^^^	
-9	3	1168	1178	79
-9	6	1561	1551	43
-8	4	1027	1071	76
-7	6	911	898	52
-6	8	2044	2053	53
-5	-5	998	978	47
-4	-10	1529	1535	49
-4	-9	657	782	0
-4	-6	2015	2001	46
-4	-1	1449	1474	37
0	5	1912	1934	64
1	-3	944	901	64
1	-2	648	649	58
2	-4	2048	2092	43
^^^^^^^	h =	5	^^^^^^^	
-10	-2	1629	1617	53
-10	0	2794	2599	0
-10	4	1174	1190	0
-9	2	1697	1672	40
-7	-3	1094	1103	42
-7	1	767	689	58
-6	-3	2213	2302	47
-6	-1	1218	1186	38
-6	4	923	950	52
-6	9	960	978	0
-5	0	1835	1851	60
-5	8	2004	2028	46
0	-6	1118	1155	48
1	-6	741	666	64
2	-7	749	705	99
2	-5	1480	1472	39
2	4	743	708	75
^^^^^^^	h =	6	^^^^^^^	
-10	1	1463	1394	42
-10	5	1576	1660	45
-9	-1	2357	2330	52
-9	3	2242	2207	49
-9	4	653	584	85
-7	-1	1029	979	62
-7	3	926	945	83
-6	-3	2029	2072	51
-6	-2	2406	2430	55
-6	1	3356	3394	62
1	-6	1631	1660	40
3	-6	1800	1843	48
4	-2	1390	1404	44
^^^^^^^	h =	7	^^^^^^^	
-9	-1	1332	1332	46
-9	3	1349	1306	46
-9	6	786	632	83
-7	-2	929	926	70
-7	0	1033	1001	76
-7	1	1850	1750	45
-7	6	1681	1720	45
0	5	2409	2365	64
1	-2	1323	1291	84
^^^^^^^	h =	8	^^^^^^^	
-10	3	933	868	0
-8	-3	2014	2034	49
1	-4	1174	1214	60
^^^^^^^	h =	9	^^^^^^^	
-10	0	1759	1664	60
-9	0	2977	3018	0
0	-4	2776	2858	0

Observed and calculated structure factor amplitudes (x5) for $Zr_6Ni_6TiSiO_{1.8}$

k	l	Fo	Fc	sigF	k	l	Fo	Fc	sigF	k	l	Fo	Fc	sigF
^^^^^^^	h =	0	^^^^^^^		7	-6	91	31	77*	0	-1	117	89	36
					7	-5	255	265	39	0	0	161	166	7
0	1	183	167	16	7	-4	294	291	23	0	4	531	522	18
0	2	168	148	35	8	-6	574	581	19	0	5	0	2	67*
0	3	786	789	22	8	-5	322	301	75	0	8	438	433	26
0	4	616	638	27	9	-3	263	303	34	1	-8	352	324	33
0	5	534	509	24	9	1	234	24	56	1	-3	0	37	47*
0	6	804	817	31	10	-1	273	244	53	1	2	0	27	44*
0	7	186	154	94*						1	9	0	67	76*
0	8	655	607	28	^^^^^^^	h =	1	^^^^^^^		2	-4	341	360	11
0	9	0	31	0*						3	-8	0	75	69*
0	10	0	73	0*	-9	-1	273	273	18	3	-5	153	155	46
1	-6	513	506	21	-9	3	394	377	15	3	-2	178	193	18
1	-3	1159	1164	20	-9	4	309	302	23	4	-6	240	260	28
1	-2	177	196	28	-8	1	253	215	31	4	-5	207	204	25
1	-1	81	3	34	-8	4	183	173	42	5	-7	461	460	12
1	5	583	590	16	-8	5	271	280	37	5	-6	330	321	28
1	6	117	29	70*	-8	6	0	47	60*	5	-5	232	224	29
1	10	334	316	56	-7	3	222	258	32	5	-4	394	389	12
2	-7	0	25	0*	-7	4	133	115	38	5	0	263	261	17
2	-6	945	920	35	-7	5	186	174	31	5	1	64	50	57*
2	-4	303	301	15	-7	7	158	128	50	5	3	221	203	22
2	-3	627	641	15	-6	1	556	549	12	7	2	151	83	35
2	10	444	452	22	-6	2	294	281	14	7	4	120	92	55
3	-10	0	62	83*	-6	3	530	529	12	8	-5	0	47	67*
3	-9	261	276	34	-6	8	164	204	38	9	-3	0	50	62*
3	-8	382	372	23	-5	-7	0	22	72*					
3	-6	319	337	28	-5	-1	433	444	10	^^^^^^^	h =	2	^^^^^^^	
3	-3	446	439	13	-5	1	297	285	14					
3	0	1025	1018	17	-5	4	289	266	14	-10	-3	32	71	68*
4	-9	0	173	0*	-4	-4	453	457	11	-10	-2	248	267	38
4	-8	20	67	77*	-4	4	256	247	14	-10	-1	0	71	65*
4	-7	229	202	27	-4	9	236	252	30	-10	2	236	224	25
4	-6	345	362	19	-3	8	410	393	33	-10	4	406	411	17
4	-3	665	672	23	-3	9	209	188	55	-9	0	207	189	23
4	-2	0	172	59*	-3	10	0	63	71*	-9	2	164	105	39
4	1	0	77	58*	-2	0	286	233	8	-9	3	210	206	31
5	-9	510	516	17	-2	1	92	59	48*	-9	4	0	16	61*
5	-8	163	147	54	-2	4	0	22	49*	-8	-2	443	447	15
5	-7	178	43	48	-2	6	265	235	32	-8	5	298	306	21
5	-3	150	81	45	-2	10	0	55	69*	-7	-1	444	436	19
6	-6	0	87	74*	-1	-10	0	46	84*	-7	2	0	26	59*
6	-5	0	76	71*	-1	-9	100	156	83*	-7	3	0	61	59*
6	-4	693	696	27	-1	-7	0	8	91*	-6	6	431	431	13
6	-2	557	544	19	-1	3	393	395	12	-6	8	308	299	25
6	0	76	91	58*	-1	8	217	270	44	-5	3	1185	1179	20
6	1	385	348	16	0	-9	59	65	80*	-5	6	475	486	12
6	3	337	374	18	0	-7	160	128	50	-5	9	173	111	43
6	4	318	328	20	0	-4	332	340	18	-4	1	400	392	17
6	5	856	835	21	0	-2	167	188	65	-4	2	489	492	15

k	l	Fo	Fc	sigF	k	l	Fo	Fc	sigF	k	l	Fo	Fc	sigF
-4	5	0	11	55*	-8	3	75	134	59*	3	2	524	515	12
-4	7	278	265	32	-8	4	296	286	16	4	-8	0	21	67*
-4	9	99	105	64*	-8	5	321	326	26	4	-7	216	194	60
-3	-6	141	128	38	-7	4	0	89	59*	4	-3	329	316	15
-3	-2	1391	1395	22	-7	6	292	294	17	5	-7	206	212	35
-3	-1	73	92	43*	-6	0	1413	1411	23	7	1	305	329	36
-3	2	353	368	9	-6	3	505	486	12					
-3	6	417	423	12	-5	0	130	142	22	^^^^^^^	h =	4	^^^^^^^	
-2	-10	451	455	22	-5	2	212	209	20					
-2	-8	141	36	75*	-4	-7	101	7	57*	-11	-3	144	50	54
-2	-5	848	855	19	-4	-3	93	62	61*	-11	0	86	20	52*
-2	-2	530	529	24	-4	1	555	561	13	-11	1	0	90	69*
-2	-1	24	153	51*	-4	3	170	153	21	-10	1	156	140	35
-2	5	0	34	64*	-4	7	500	484	13	-9	-4	0	38	61*
-2	6	601	579	18	-3	-7	124	48	68*	-9	-2	213	181	22
-2	9	466	478	34	-3	-5	1016	1014	28	-9	0	179	145	24
-1	-7	161	152	38	-3	-4	559	575	17	-9	5	55	16	62*
-1	-5	138	78	45	-3	-2	355	353	12	-8	-7	229	229	40
0	-8	199	65	45	-3	-1	1324	1345	21	-8	1	369	382	17
0	-7	661	619	37	-3	2	292	340	15	-8	3	136	190	43
0	-4	255	279	18	-3	3	0	50	70*	-8	5	389	384	14
0	-3	1757	1760	28	-3	5	423	415	15	-7	2	0	52	60*
0	-2	524	531	25	-2	-5	102	180	53*	-7	3	0	27	58*
0	-1	0	50	52*	-2	-3	330	323	10	-7	4	332	333	15
0	0	116	39	26	-2	0	215	228	12	-6	-4	697	704	16
0	9	464	470	24	-1	-10	0	11	70*	-6	1	471	472	12
1	-7	0	122	60*	-1	-9	449	414	15	-6	2	611	634	15
1	-1	510	519	11	-1	-8	99	120	71*	-6	5	267	271	26
1	7	509	497	26	-1	-5	286	245	28	-5	-7	239	249	25
2	-4	104	31	59*	-1	-4	0	78	46*	-5	-2	112	31	77*
3	-8	601	604	16	-1	-3	80	89	46*	-5	0	90	35	38
3	-7	191	168	32	0	-10	207	148	0*	-4	-5	377	370	16
3	-4	572	569	16	0	-9	232	240	34	-4	-4	324	325	17
3	-2	533	534	12	0	-8	423	426	19	-4	0	73	100	45*
4	-7	200	199	51	0	-7	95	91	70*	-4	4	453	459	15
4	-3	141	95	36	0	-6	588	580	17	-4	5	889	874	20
5	-7	64	60	62*	0	-4	1036	1038	20	-3	-1	41	32	49*
5	2	0	110	58*	0	-1	1520	1512	24	-3	0	60	31	36*
8	-3	190	219	34	1	-9	121	122	59	-2	-8	376	371	15
					1	-8	36	2	59*	-2	-6	250	248	30
^^^^^^^	h =	3	^^^^^^^		1	-5	335	318	13	-2	-3	211	217	14
					1	-2	185	184	34	-2	0	1499	1482	23
-10	-2	271	280	19	2	-8	325	315	16	-1	-6	186	187	29
-10	2	199	181	28	2	-7	138	160	58	-1	6	322	333	14
-10	3	132	173	81*	2	1	0	66	50*	0	-9	0	85	83*
-10	4	205	245	37	3	-9	231	193	37	0	-8	0	23	78*
-9	-6	250	230	36	3	-8	176	65	48	0	-7	218	37	39
-9	3	289	317	20	3	-7	264	271	38	0	-6	386	398	30
-9	5	356	365	30	3	-5	504	504	12	0	-3	99	177	55*
-8	0	202	211	20	3	-4	429	432	11	0	-2	120	136	54

k	l	Fo	Fc	sigF	k	l	Fo	Fc	sigF	k	l	Fo	Fc	sigF
0	1	646	639	16	-2	-4	201	187	21	-3	-6	265	272	23
1	-6	111	67	56*	-2	-3	510	514	12	-3	-1	327	320	25
1	-5	136	133	41	-2	-1	286	300	15	-2	-3	98	23	53*
1	-3	157	187	32	-1	-4	315	330	13	-1	-6	161	163	32
1	8	150	177	40	-1	3	0	42	54*	-1	-2	415	411	17
2	-8	497	509	14	0	-9	211	213	40	0	-8	52	71	84*
2	-7	103	26	58*	0	-8	454	447	20	0	-6	0	16	65*
3	-8	0	72	67*	0	-7	672	687	36	0	-2	648	659	17
3	-7	0	18	66*	0	-5	249	232	39	1	-5	90	3	56*
3	-6	356	351	14	0	-3	268	252	64	2	-1	537	541	13
4	-6	108	58	64*	0	1	743	722	23	2	0	83	90	45*
					1	-7	98	135	59*	2	7	537	559	13
^^^^^^^	h =	5	^^^^^^^		1	-5	199	169	43	4	2	333	338	15
					1	-4	152	207	32	5	1	47	66	58*
-11	0	110	68	42	2	-6	332	328	15					
-11	2	208	238	33	2	6	79	75	67*	^^^^^^^	h =	7	^^^^^^^	
-11	3	567	556	16	4	-6	59	14	63*					
-10	-5	413	420	21						-11	2	0	61	62*
-10	0	700	701	14	^^^^^^^	h =	6	^^^^^^^		-10	-1	79	76	60*
-10	1	200	185	33						-9	5	102	75	61*
-10	2	84	52	56*	-10	-4	239	252	27	-9	6	0	43	65*
-10	4	55	40	58*	-10	0	268	244	19	-7	-7	287	290	53
-9	-4	58	45	60*	-10	2	178	186	43	-7	-3	423	413	16
-9	3	226	263	24	-10	3	0	85	65*	-7	-2	126	54	70*
-8	-2	636	649	16	-10	4	38	88	58*	-7	-1	230	195	56
-8	1	480	490	19	-9	-4	242	209	23	-7	1	188	49	34
-8	3	650	665	15	-9	-2	263	261	21	-7	2	141	158	67
-8	4	525	519	14	-9	0	358	365	11	-7	6	405	409	24
-8	7	528	553	17	-9	2	104	52	59*	-6	6	245	244	37
-7	-8	396	381	15	-9	3	151	191	42	-5	-4	319	335	17
-7	-5	417	409	18	-9	4	442	450	14	-5	0	360	350	10
-7	-1	399	398	12	-8	-4	560	547	13	-5	5	0	32	56*
-6	8	128	148	55	-8	-2	490	496	13	-5	8	320	338	26
-5	-6	651	664	18	-8	-1	525	518	13	-4	-5	0	98	68*
-5	-5	238	211	46	-8	3	170	183	34	-4	-2	321	329	25
-5	-4	213	206	25	-8	4	449	461	13	-4	-1	78	93	58*
-5	-2	461	477	14	-8	5	426	438	13	-4	0	421	422	10
-5	0	327	305	12	-8	7	143	158	48	-4	1	227	230	19
-5	1	113	108	62*	-7	-6	0	91	56*	-3	-5	185	113	33
-5	2	1371	1400	24	-6	-8	0	20	74*	-2	-7	243	241	29
-5	4	531	544	21	-6	-7	305	321	51	-2	-4	332	337	14
-5	6	80	16	72*	-6	-3	0	20	69*	-2	-3	285	303	15
-4	-9	90	111	65*	-6	-1	1285	1253	23	-1	-7	134	63	58
-4	2	120	62	44	-6	7	202	259	37	-1	-4	145	102	40
-4	8	233	211	30	-4	-5	142	148	33	-1	-3	184	195	29
-4	9	288	283	37	-4	-2	129	154	67*	-1	-2	407	408	12
-3	-5	0	71	58*	-4	-1	110	42	50	-1	-1	0	56	58*
-3	5	674	697	14	-4	0	93	34	37	-1	0	61	37	52*
-2	-9	163	166	47	-4	4	109	80	62*	-1	1	48	34	54*
-2	-6	356	338	14	-4	6	237	256	21	-1	2	0	42	58*

k	l	Fo	Fc	sigF	k	l	Fo	Fc	sigF	k	l	Fo	Fc	sigF
0	-7	157	159	50	-9	-1	239	266	74	-7	-2	0	89	71*
0	-5	480	459	23	-9	0	578	548	16	-7	1	113	152	68*
0	-4	0	148	73*	-9	2	257	192	33	-6	1	272	249	19
0	-3	224	167	31	-8	-1	71	82	59*	-5	-3	185	162	44
0	0	312	307	14	-8	2	100	10	58*	-5	-2	174	233	45
2	6	0	59	67*	-8	3	72	144	60*	-4	3	97	123	70*
					-7	-5	85	88	61*	-3	-2	661	663	16
^^^^^^^ h = 8 ^^^^^^^					-7	-1	111	152	63*					
					-7	4	72	49	55*					
-11	0	118	57	69*	-6	-1	399	403	14					
-9	-2	227	207	41	-6	1	481	483	14					
-9	0	173	151	25	-6	5	123	142	62*					
-9	4	141	156	57	-5	-3	396	406	14					
-9	5	116	199	66*	-4	-5	133	19	50					
-8	-4	498	497	17	-4	-1	182	200	38					
-8	-3	146	117	76*	-4	1	96	141	59*					
-8	-2	460	429	17	-4	2	438	438	13					
-8	0	278	272	41	-4	6	0	102	61*					
-8	1	340	337	20	-3	6	315	313	17					
-8	2	728	733	21	-2	-3	0	99	62*					
-8	3	477	490	17	-2	-2	359	370	15					
-8	4	109	92	61*	-2	-1	316	316	16					
-8	5	237	158	47	0	-4	236	252	65					
-8	6	434	436	46	0	-3	58	28	84*					
-7	-3	225	229	25	0	4	272	259	33					
-7	-2	0	16	57*	1	-3	91	33	68*					
-7	0	499	487	10										
-6	-6	154	49	38	^^^^^^^ h = 10 ^^^^^^^									
-6	-3	180	164	34										
-6	6	114	47	59*	-10	0	48	177	65*					
-5	-6	301	281	36	-9	-2	257	263	34					
-5	-1	257	219	17	-9	0	211	196	22					
-5	2	46	104	60*	-9	2	113	84	71*					
-5	5	174	232	36	-6	-5	0	69	68*					
-4	-4	0	34	69*	-6	-3	184	179	34					
-4	-2	345	387	15	-5	-3	365	372	14					
-4	0	192	189	24	-4	-5	0	23	76*					
-3	-6	501	497	13	-4	-1	72	108	63*					
-1	-6	71	44	65*	-3	-4	127	148	55					
-1	-5	307	301	23	-3	-3	114	100	60*					
-1	-3	306	319	32	-3	0	203	134	28					
-1	-1	80	66	57*	-2	0	117	114	45					
0	1	279	205	32	-2	1	644	622	15					
2	-4	384	415	18	0	-1	478	515	20					
^^^^^^^ h = 9 ^^^^^^^					^^^^^^^ h = 11 ^^^^^^^									
-10	-1	91	74	62*	-8	-2	126	127	61					
-10	1	0	39	67*	-8	-1	501	495	15					
-9	-2	344	321	43	-8	1	196	167	60					

* indicates unobserved reflection

Observed and calculated structure factor amplitudes (x10) for $ZrNi_{1.5}Ti_{0.5}$

k	l	Fo	Fc	sigF	k	l	Fo	Fc	sigF	k	l	Fo	Fc	sigF
^^^^^^^	h =	0	^^^^^^^		-1	2	116	160	29*	-2	8	83	153	71*
					-1	3	1269	1254	24	-1	-8	555	557	14
0	2	186	136	20	-1	4	541	525	13	-1	-6	24	101	62*
0	4	1375	1361	23	-1	6	475	446	14	-1	-2	1490	1422	62
0	6	1246	1240	24	-1	10	204	180	34*	-1	6	111	101	51*
0	8	138	223	81*	0	-9	442	431	29	-1	8	556	557	32
0	10	533	544	24	0	-7	343	329	16	0	-9	201	160	81*
1	-9	414	431	14	0	-5	355	347	16	0	-4	153	131	34*
1	-6	435	446	16	0	3	1284	1254	20	0	7	434	445	13
1	-5	349	347	11	0	8	531	548	24	1	-9	334	339	22
1	-1	100	14	50*	0	10	196	180	59*	1	-8	491	507	14
1	0	89	13	25*	1	-2	1426	1422	31	1	-7	237	235	35
1	8	532	548	15	2	-9	323	339	18	1	-6	296	296	15
2	-9	179	160	39*	2	-7	235	235	21	1	-5	341	320	31
2	-6	868	856	21	2	-6	287	296	30	1	-4	470	476	20
2	0	704	739	12	2	-5	325	320	14	2	-8	169	143	42*
3	-7	66	61	59*	2	-4	468	476	13	2	-6	827	806	20
3	-6	157	81	33*	3	-8	363	386	17	2	-4	800	790	34
3	-5	94	77	52*	3	-3	749	723	32	2	6	807	806	20
3	-3	99	92	68*	4	-5	97	51	75*	3	-4	199	213	32
3	-2	1062	1072	21	4	-4	0	61	89*	3	-2	0	27	56*
4	-7	293	303	24	4	-2	719	691	38	3	2	20	27	55*
4	-6	552	579	16	4	-1	0	63	62*					
5	-3	462	470	29	4	4	0	61	65*	^^^^^^^	h =	3	^^^^^^^	
5	4	336	314	17										
					^^^^^^^	h =	2	^^^^^^^		-6	0	455	461	19
^^^^^^^	h =	1	^^^^^^^							-5	-6	282	295	36
					-6	-1	549	540	16	-5	-5	141	166	48*
-5	-4	103	61	64*	-6	1	525	540	40	-5	-3	642	645	42
-5	-3	103	58	58*	-5	0	82	68	45*	-5	-1	0	31	66*
-5	-2	683	691	18	-5	5	207	166	71*	-5	1	70	31	52*
-5	2	645	691	17	-4	8	212	143	33	-5	3	649	645	25
-5	3	251	58	51*	-3	-8	504	507	15	-5	5	283	166	67*
-5	5	185	51	39*	-3	-3	898	875	24	-5	6	312	295	18
-4	3	720	723	33	-3	-1	0	64	51*	-4	-7	216	215	32
-4	8	401	386	16	-3	0	69	96	36*	-4	-6	314	305	16
-3	-2	214	209	33	-3	1	111	64	29*	-4	-5	261	244	18
-3	2	242	209	13	-3	7	238	235	36	-4	-4	321	310	14
-3	4	485	476	13	-2	-8	132	153	79*	-4	-2	68	88	58*
-3	5	303	320	28	-2	-5	1278	1271	25	-4	-1	73	25	48*
-3	7	239	235	20	-2	-4	97	131	78*	-4	0	96	19	37*
-3	8	478	507	31	-2	-3	0	128	51*	-4	1	0	25	52*
-3	9	340	339	29	-2	-2	546	558	36	-4	2	126	88	40*
-2	-4	14	121	47*	-2	-1	1313	1351	31	-4	6	311	305	28
-2	0	1085	1078	40	-2	1	1337	1351	40	-4	7	191	215	42*
-2	4	94	121	51*	-2	2	557	558	13	-3	-8	490	477	24
-1	-7	346	329	16	-2	3	128	128	31*	-3	-4	133	107	35*
-1	-4	530	525	13	-2	5	1268	1271	26	-3	0	768	774	13
-1	-2	164	160	16	-2	6	873	856	20	-3	1	78	102	53*
-1	1	62	14	39*	-2	7	437	445	14	-3	6	35	81	61*

k	l	Fo	Fc	sigF
-2	-6	292	296	20
-2	-3	926	875	38
-2	-1	0	64	53*
-2	0	114	96	39*
-2	1	0	64	50*
-2	3	871	875	30
-1	-9	348	339	17
-1	-8	479	507	14
-1	-6	293	296	15
-1	-5	329	320	13
-1	-4	484	476	12
-1	-3	916	875	29
-1	-2	209	209	46*
-1	2	206	209	40*
0	-8	495	477	26
0	-7	95	61	58*
0	-5	0	77	60*
0	-4	110	107	57*
0	-3	128	92	63*
0	-2	1060	1072	29
0	1	124	102	33*
1	-8	385	386	16
1	-6	330	305	16
1	-5	233	244	21
1	-4	323	310	20
1	2	47	88	58*
2	-6	291	295	24
2	-4	255	213	19
2	-2	81	27	62*
2	4	231	213	21
3	-2	577	565	21
3	2	614	565	19

^^^^^^^ h = 4 ^^^^^^^

k	l	Fo	Fc	sigF
-6	-3	0	32	81*
-6	-2	216	219	62*
-6	-1	551	540	29
-6	0	311	301	13
-6	2	240	219	22
-5	2	676	691	29
-5	3	159	58	40*
-4	-5	835	835	28
-4	-4	0	75	62*
-4	-3	0	59	61*
-4	-2	299	320	15
-4	-1	770	792	22
-4	1	802	792	17
-4	2	296	320	15
-4	3	59	59	60*
-4	4	122	75	40*
-4	5	849	835	39
-3	-7	212	215	33
-3	-6	320	305	16
-3	-5	219	244	45*
-3	-4	324	310	18
-3	-1	76	25	57*
-3	0	67	19	42*
-3	1	0	25	63*
-3	2	111	88	62*
-3	3	746	723	38
-3	7	235	215	22
-2	-4	827	790	38
-2	-2	0	63	57*
-2	0	1648	1743	25
-2	2	136	63	39*
-1	-8	379	386	19
-1	-5	256	244	24
-1	-4	334	310	27
-1	-3	718	723	31
0	-6	590	579	17
0	0	435	434	17
1	-5	0	51	89*
1	-1	0	63	56*
1	0	527	523	13
1	1	59	63	77*
1	4	0	61	79*

^^^^^^^ h = 5 ^^^^^^^

k	l	Fo	Fc	sigF
-6	0	0	23	57*
-5	-4	308	314	29
-5	-2	205	170	24
-5	0	84	95	53*
-5	1	0	57	68*
-5	2	0	170	64*
-5	3	468	470	19
-3	-6	293	295	19
-3	-3	639	645	18
-3	-2	113	27	60*
-3	-1	0	31	69*
-3	1	0	31	61*
-3	3	637	645	18
-3	5	188	166	71*
-2	-4	261	213	19
-2	0	124	68	43*
-1	-5	72	51	57*
-1	-1	25	63	62*
-1	0	509	523	15
-1	3	0	58	69*
-1	1	0	57	68*

^^^^^^^ h = 6 ^^^^^^^

k	l	Fo	Fc	sigF
-5	0	0	23	61*
-4	-3	111	32	58*
-4	-2	213	219	55*
-4	0	261	301	41
-4	2	233	219	23
-4	3	68	32	66*
-2	-3	0	32	81*
-2	-1	548	540	15

* indicates unobserved reflection